Fundamental Principles of Semiconductor/Electrolyte Junctions

27

Sofiya Hlynchuk, Mitchell Lancaster, Molly MacInnes, Robert Vasquez, and Stephen Maldonado

Contents

Abstract

This chapter describes the equilibrium and non-equilibrium characteristics of semiconductor electrodes immersed in electrolyte solutions. The intent is to build the reader's intuition on how to use and design semiconductor photoelectrodes for effecting purposeful chemistry. The text illustrates how the kinetic details of charge transfer processes affect the concentrations of charge carriers in the semiconductor, thereby influencing experimental observables (e.g., current, potential). A brief historical summary of major ideas in the field is presented to help readers appreciate the development of models for heterogeneous charge transfer at semiconductor/solution interfaces. The Marcus and Gerischer formalisms are described, including predictions that have been verified and those that are still to be evaluated. These topics are intended to provide more explicit descriptions of key features of semiconductor photoelectrode responses that may not be intuitive and to distill key concepts to contextualize knowledge gaps and opportunities in the field.

Keywords

Marcus-Gerischer · Charge-transfer theory · Rate constants · Reorganization energy · Photoelectrochemistry

27.1 Introduction

Understanding the operation of a semiconductor photoelectrode encompasses many different topics including materials science, device physics, thermodynamics, and reaction kinetics. Through dedicated efforts by numerous groups across these disciplines, several of the fundamental aspects underpinning photoelectrochemical systems have been identified and described [1–7]. The majority of this book details and relays the most recent and exciting experimental advances in using semiconductor/electrolyte interfaces to

S. Hlynchuk · M. Lancaster · M. MacInnes · R. Vasquez
Department of Chemistry, 930 N University, Ann Arbor, MI, USA
e-mail: hlynsofi@umich.edu; mlanc@umich.edu; mmacinne@umich.edu; robtvasq@umich.edu

S. Maldonado (✉)
Department of Chemistry, 930 N University, Ann Arbor, MI, USA

Program in Applied Physics, 930 N University, Ann Arbor, MI, USA
e-mail: smald@umich.edu

D. W. Bahnemann, A. O. T. Patrocinio (eds.), *Springer Handbook of Inorganic Photochemistry*, Springer Handbooks,
https://doi.org/10.1007/978-3-030-63713-2_27

drive electrochemical transformations using sunlight as an input power source. This chapter provides the basis to understand and appreciate those works by presenting a physical chemistry perspective on how a semiconductor electrode functions both in the dark and under illumination.

The objectives of this chapter are twofold. First, the text describes the equilibrium and nonequilibrium characteristics of semiconductor electrodes immersed in electrolyte solutions. The intent is to build the reader's intuition on how to use and design semiconductor photoelectrodes for effecting purposeful chemistry. The text illustrates how the kinetic details of charge transfer processes affect the concentrations of charge carriers in the semiconductor, thereby influencing experimental observables (e.g., current, potential). Specifically, the conditions where the heterogeneous rate constants for electron and hole transfer (k_{et} and k_{ht}, respectively) influence the efficiency of optical-to-electrical energy conversion are described, including commentary on aspects that complicate and/or prevent ideal behavior. Second, a description of the fundamental factors that define the magnitudes of k_{et} and k_{ht} is provided for elementary, outer-sphere redox reactions. A brief historical summary of major ideas in the field is presented to help readers appreciate the development of models for heterogeneous charge transfer at semiconductor/solution interfaces. A further description of the Marcus and Gerischer formalisms, including predictions that have been verified and those that are still to be evaluated, is presented. Overall, the intention of the text is to avoid merely rehashing points raised in the numerous books and reviews on semiconductor heterojunction devices [8–10] and the plethora of excellent reviews on the topic of photoelectrochemistry itself [5, 7, 11–19]. Rather, the topics are intended to provide more explicit descriptions of key features of semiconductor photoelectrode responses that may not be intuitive and to distill key concepts so as to contextualize knowledge gaps and opportunities in the field. The individual topics and their cited references hopefully serve to stimulate and guide further reading, particularly for beginning practitioners.

27.2 Operation of a Semiconductor Electrode

27.2.1 Description of the Equilibrium State of a Semiconductor Immersed in Liquid Solution

The electronic structure of a solid is important to its behavior as a source/sink of electrons in electrochemical reactions. This chapter presupposes the reader has some familiarity with the basic concepts of what defines and distinguishes insulators, semiconductors, and conductors. The origins of bands and the details of band structure in solids generally has been reviewed in many excellent texts [9, 20–23], and beginning readers are encouraged to consult the extensive materials science literature. For the purposes of this chapter, the concept of bands in charge transfer at semiconductor/solution interfaces is key.

The band structure of a semiconductor material principally arises from two factors: the overlap of the discrete orbitals of the constituent atoms and the Pauli exclusion principle which dictates that each electron must have unique quantum numbers [22]. These aspects result in sets of closely spaced sets of orbitals that form a continuum of states or bands. There are two specific bands that control the electrical conductivity and electrochemical behavior of a semiconductor. The following terminology will be useful in this chapter. The band (mostly) filled with valence electrons that is highest in energy is known as the valence band. The highest filled energy level in the valence band is specifically known as the valence band edge energy ($\mathbf{E_{vb}}$). The band lowest in energy that is (mostly) devoid of valence electrons is referred to as the conduction band. The lowest empty energy level of the conduction band is known as the conduction band edge energy ($\mathbf{E_{cb}}$). The energetic separation between these two energies is denoted as the band gap energy (E_g).

The average energy of valence electrons in a semiconductor at equilibrium is described by the Fermi level, $\mathbf{E_F}$ [23]. Formally, the Fermi level is the energy at which the probability of finding an electron is 0.5 [23]. For an intrinsic (i.e., undoped) semiconductor, the Fermi level energy would be nearly in the middle of the band gap [10]. The Fermi level can be moved towards either band by introducing impurities that add either delocalized electrons or electron vacancies (i.e., holes) into the material. Such dopants can greatly affect the electrical conductivity, with doped semiconductors featuring an excess of mobile electrons exhibiting n-type character and semiconductors possessing an excess of mobile holes exhibiting p-type character. The law of mass action holds that the product of the concentrations of mobile electrons and holes are fixed,

$$n_i^2 = np \tag{27.1}$$

where n and p are the electron and hole concentrations, respectively, and n_i is a material specific parameter that describes the concentration of mobile charge carriers in the undoped semiconductor. This value is itself a function of E_g as well as the properties of the valence and conduction bands.

Unlike in pure conductors, in semiconductors the concentration of charge carriers is not necessarily uniform within the entire material. In fact, when a semiconductor is contacted by another material with a different Fermi level energy, the semiconductor will not be equipotential throughout its volume. This condition occurs often when a macroscopic semiconductor equilibrates with a liquid solution containing dissolved redox active species and is the focus of this chapter.

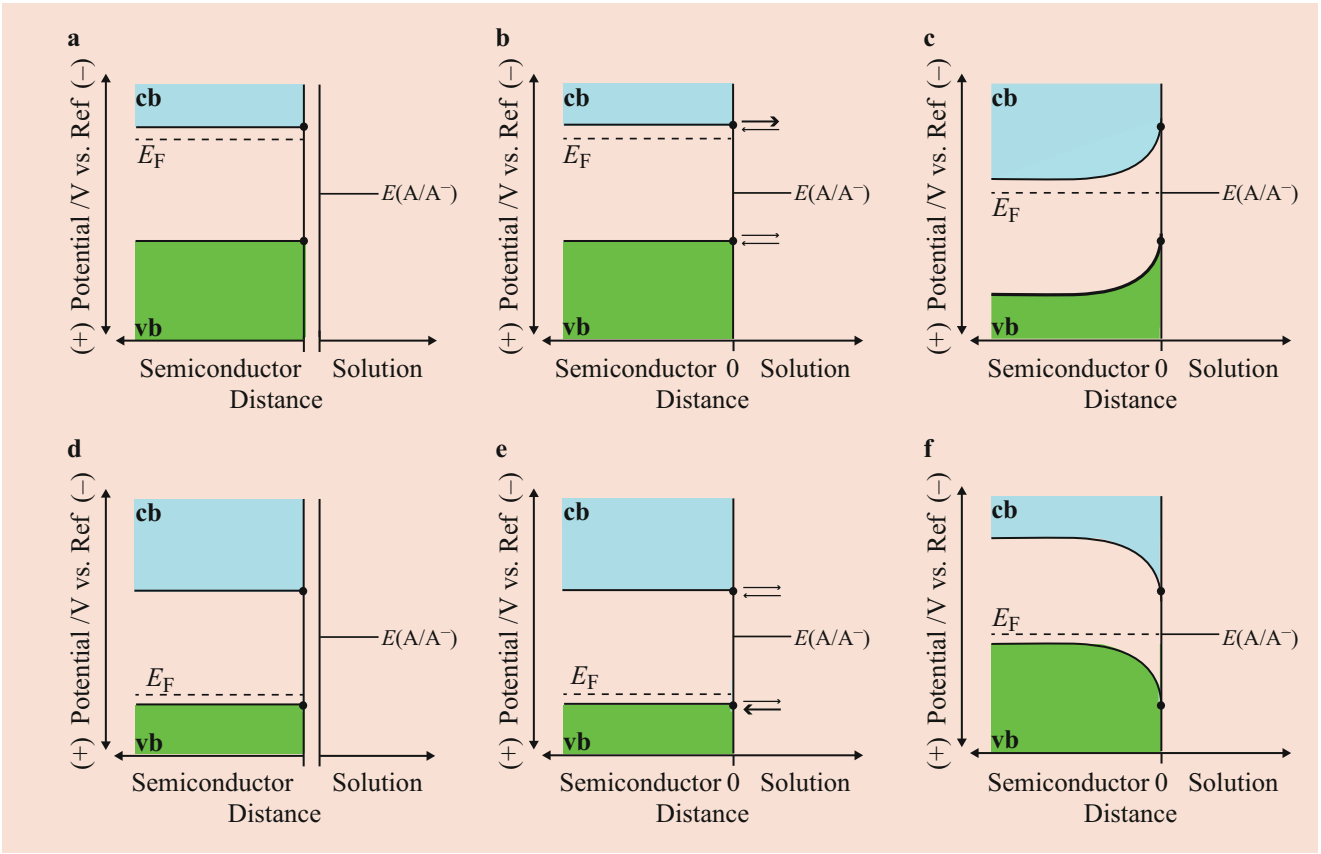

Fig. 27.1 Schematic depictions of the energy band diagrams for (top) n- and (bottom) p-type semiconductors immersed in liquid solutions at three separate times: (**a**, **d**) prior to immersion of the semiconductor in a solution containing a dissolved redox couple, A/A^-; (**b**, **e**) at the moment of immersion, where the arrows describe the possible charge-carrier transfer reactions available to attain equilibrium (the line thickness indicates which process is likely the most relevant); (**c**, **f**) after equilibrium is attained at the semiconductor/solution interface

Figure 27.1 depicts energy band diagrams of doped semiconductors prior to and after immersion in a liquid electrolyte containing both components of a single redox couple (A and A^-). In these diagrams, the electrochemical potential of electrons (referenced to an arbitrary potential) are plotted on the y-axis, with more negative potential values at higher positions. Conversely, the x-axis denotes a physical position, with the interiors of the semiconductor and liquid electrolyte denoted by the left-most and right-most values, respectively. In these band diagrams, the vertical separation between the conduction band edge and $\mathbf{E_F}$ reflects the value of n and p at each x-position through the following Boltzmann relations [10, 23],

$$\mathbf{E_F}(x) = \mathbf{E_{cb}} + k_B T \ln\left(\frac{n(x)}{N_{cb}}\right) \tag{27.2a}$$

$$\mathbf{E_F}(x) = \mathbf{E_{vb}} - k_B T \ln\left(\frac{p(x)}{N_{vb}}\right) \tag{27.2b}$$

where k_B is Boltzmann's constant, T is the system temperature, N_{cb} is the effective density of states at the conduction band edge, and N_{vb} is the effective density of states at the valence band edge. Equation 27.2 stem from the concept that knowing the concentration of a charge carrier is synonymous with knowing its average energy [23]. Importantly, large vertical gaps between $\mathbf{E_F}$ and $\mathbf{E_{cb}}$ in energy band diagrams imply low n values and large vertical gaps between $\mathbf{E_F}$ and $\mathbf{E_{vb}}$ denote low p values at that x value. Figure 27.1a depicts an n-type semiconductor and an electrolyte solution prior to contact. In this case, the value of n is determined by the dopant density and the value of p follows from Eq. 27.1.

In photoelectrochemical systems, the quantities $\mathbf{E_{cb}}$, $\mathbf{E_{vb}}$, and $\mathbf{E_F}$ are more readily understood as electrochemical potentials (referenced to the same arbitrary potential) rather than as energies. The following relation connects the two concepts,

$$\mathbf{E} = -qE \tag{27.3}$$

where q is the unsigned charge of an electron. Although the strict, rigorous application of the Fermi level concept to the energetics of a solution has been questioned in the past [6, 24], it is convenient to define the Nernstian redox potential of the dissolved A/A^- redox couple, $E(A/A^-)$, as the Fermi level of charge carriers in solution [25],

$$E(\mathrm{A}/\mathrm{A}^-) = E^{0'}(\mathrm{A}/\mathrm{A}^-) + \frac{k_\mathrm{B}T}{q}\ln\left(\frac{[\mathrm{A}]}{[\mathrm{A}^-]}\right) \qquad (27.4)$$

where $E^{0'}(\mathrm{A}/\mathrm{A}^-)$ is the formal electrochemical potential of the redox couple (referenced to an arbitrary potential) and [A] & [A^-] are the concentrations of A and A^- in solution. E_F of the n-type semiconductor in Fig. 27.1a is shown as uniformly more negative than $E(\mathrm{A}/\mathrm{A}^-)$. Accordingly, upon first contact, electrons will flow from the semiconductor into solution to reduce A into A^-. In the ideal case, heterogeneous charge transfer between the semiconductor and liquid electrolyte occurs at the band edge potentials at the interface (Fig. 27.1b). In this scenario, the dominant process would be transfer of electrons from the semiconductor at E_cb. Since the density of electron accepting states at E_F in solution is much larger for [A] $>10^{-6}$ M than the density of states at E_F in the semiconductor bandgap (where there are no states), the resultant charge transfer will perturb the value of E_F in the semiconductor more significantly than $E(\mathrm{A}/\mathrm{A}^-)$ in solution. Electron transfer will continue until the values of E_F and $E(\mathrm{A}/\mathrm{A}^-)$ on both sides of the semiconductor/electrolyte interface are equal, i.e., the average electrochemical potential of electrons is constant throughout both materials (Fig. 27.1c). Consequently, net electron transfer from the semiconductor into solution [26] will continue to take place until E_F is equal to $E(\mathrm{A}/\mathrm{A}^-)$ [27]. It is important to note that the specific value of k_et, so long as it is sufficiently large to permit charge transfer, is not germane in determining the equilibrium condition. Additionally, the excess negative charge now residing in solution is located specifically at the semiconductor/solution interface over depths $<10^{-8}$ m for typical electrolyte solutions with ionic strengths >0.1 M. The ions in this thin layer of solution, commonly referred to as the "double layer" [28], next to the electrode organize in alternating layers parallel to the plane of the electrode.

As depicted, the amount of charge needed to reach equilibrium exceeds the available electron density at the semiconductor surface and requires electron density from deeper within the semiconductor. The near surface region of the semiconductor accordingly becomes deficient in electron density. The electron density is at a minimum at the semiconductor/solution interface and gets progressively larger further into the semiconductor. At sufficient depth away from the interface, the electron density reflects the original doping level. However, since the electron density in an n-type semiconductor prior to reaching equilibrium is equal to the concentration of ionized dopant atoms, a key premise is that the dopant atoms near the interface are the source of electrons that transfer into solution, i.e., the dopant atoms (rather than the semiconductor atoms) are specifically ionized [29]. Accordingly, the near surface region becomes net positively charged with *fixed* charges. The depth over which net electrons are lost is referred to as the width of the depletion region, W. Notably, the amount of positive charges at any point in the depletion width is constant ($=qN_\mathrm{d}$) for semiconductors with uniform doping. The magnitude of W depends both on the amount of charge that was lost in order to reach the equilibrium condition and the concentration of dopants in the semiconductor (where higher dopant concentrations lead to shorter W). For many semiconductor/solution contacts, W can range from 10^{-8} to 10^{-6} m. Within the depletion width, the net positive charge leads to a potential difference ($\sim 10^{-1}$ V) between the interior and surface of the semiconductor. The potential difference results in the possibility of large electric fields at the semiconductor interface that direct electrons away from the semiconductor/ solution interface and back towards the bulk of the semiconductor.

A similar equilibration process occurs for a p-type semiconductor immersed into the same electrolyte solution in the dark (Fig. 27.1d), with some notable differences. Upon first contact, transfer of holes from the valence band edge is the primary process that oxidizes A^- to A in solution since holes are the majority charge carrier (Fig. 27.1e). E_F in the semiconductor will again be moved more significantly than the solution potential to reach the equilibrium condition. As before, a depletion width with a potential drop will result within the near-surface region of the semiconductor. However, in this case, the loss of holes results in a net negative charge across the depletion width, generating a potential drop and electric field (Fig. 27.1f) with the opposite sign as compared to Fig. 27.1c. Accordingly, there is now an additional electrostatic barrier that moves holes away from the interface.

In the energy band diagrams in Fig. 27.1c and f, the conduction and valence band edges are purposely drawn as curved across the depletion width. This "band bending" reflects the fact that the semiconductor itself is no longer equipotential. Rather, at every position within the semiconductor where there is a fixed net charge, there is an additional electrostatic term. To be clear, this electrostatic component does not appreciably change the total work necessary to pull an electron from the semiconductor conduction band edge out to vacuum since this is a material-specific property (i.e., the electron affinity of the semiconductor [20, 22]). Rather, this electrostatic term affects how any additional charges added to the semiconductor will move.

Thorough descriptions of the structure of the double layer in solution and the depletion width in the semiconductor are outside the scope of this chapter. One important aspect to note here is at equilibrium, the total charge held in the depletion region and in the double layer are equivalent but over very different volumes. Accordingly, an electron moving from the semiconductor bulk towards the interface is repelled from the interface because the entire net negative charge of the double layer is not fully screened inside the semiconductor depletion width. At the interface, none of the charge is screened,

resulting in the maximum field strength. The specific potential at any point within the depletion width of the semiconductor is a function of position. The potential difference between the potential at a point inside the semiconductor far away from the surface and the potential at a point at the interface ($\Delta E(x)$) is a quadratic function of position [5],

$$\Delta E(x) = -\left(\frac{qN_d}{2\epsilon_0\epsilon}\right)(W-x)^2 \qquad (27.5)$$

where N_d is the dopant density, ε_0 is the permittivity of free space, and ε is the relative dielectric constant. The potential drop across the entire depletion region, V_{bi}, is often referred to as the potential "built in" at the interface (i.e., $V_{bi} = \Delta E(x = 0)$) and is readily apparent from Eq. 27.5. For the case of an n-type semiconductor, the "upward" bending of the bands represents the potential barrier that keeps electrons away from the interface. For the case of a p-type semiconductor, the "downward" bending of the bands similarly illustrates the potential barrier that favors moving holes away from the interface. Notably, in both cases, the "bent" bands also represent the electrostatic attraction that favors movement of the minority carriers *towards* the surface. Hence, the internal potential drop within a semiconductor that is contacted by a solution can be an effective means to separate charge carriers and selectively drive (photo)electrochemical reactions. This aspect was the primary focus in many of the earliest studies of semiconductor/liquid junctions [30–33].

By definition, no further *net* change in the concentrations of species (n and p in the semiconductor; [A] and [A^-] in solution) occur as long as the semiconductor/solution interface remains at equilibrium. Conversely, any perturbation that moves the system away from equilibrium necessarily changes the concentrations of all these species. A key aspect of semiconductor electrochemistry is that specific perturbations can be used to effect desired chemical changes in solution. Although a change in any intensive property of the semiconductor/solution system will disrupt equilibrium, the two most useful changes to consider are either through the application of a bias or light.

27.2.2 Steady-State Condition of a Semiconductor Immersed in Liquid Solution Perturbed Away from Equilibrium by an Applied Potential

Energy Band Diagrams

For the purposes of this discussion, "ideal" semiconductors are defined as flat, macroscopic materials that are uniformly doped, possess large mobilities for both electrons and holes, and have no surface defects with energies within the bandgap that can act as sinks/traps for charge-carriers. In these materials, electron and hole motion can be treated as one-dimensional. Figure 27.2 illustrates qualitatively what happens when an ideal semiconductor is utilized as an electrode [34] immersed in the same solutions as Fig. 27.1 and a potential is applied to the semiconductor in the dark. In this case, the response of the system to this perturbation can be gauged by the net current that passes across the semiconductor/solution interface. To be clear, such an action requires the construction of a full electrochemical cell, i.e., the inclusion of at least one other (counter) electrode in solution. Although only two electrodes are needed to have a functional cell and just two are preferable for photoelectrochemical energy conversion systems, this discussion will assume a three electrode cell configuration is employed. The following representations in Fig. 27.2 also will assume that only the majority carriers transfer across the semiconductor/solution interface [35].

Figures 27.2a–c show respective energy band diagrams for different applied biases, ΔE_{app}. The corresponding current-potential response is shown in Fig. 27.2g. The current-potential convention shown in Fig. 27.2g is as follows. Cathodic currents (i.e., where electrons move from the semiconductor into solution to reduce A) are defined as positive and plotted upward on the y-axis. Anodic currents represent the inverse process and are shown as negative currents plotted downward on the y-axis. Separately, the x-axis is the electrochemical potential of the semiconductor, i.e., E_F, plotted with respect to an arbitrary reference potential. For convenience, potential values are more negative towards the right and more positive towards the left. This method of data presentation is commonly referred to as the "Texas"/"polarographic" convention [36]. The IUPAC convention for data presentation has the opposite definition for the sign of the current and plots potentials with more positive values on the left and more negative values on the right [36, 37].

By definition, the application of a potential involves altering the amount of charge carriers in/on the semiconductor [25]. Figure 27.2 illustrates specifically the cases when ΔE_{app} only alters the charge carrier concentrations in the depletion width in the semiconductor, i.e., no potential is dropped across the interface with the solution [38]. An additional assumption in Fig. 27.2 is that the rate constant for the minority charge carrier (i.e., k_{ht} for n-type and k_{et} for p-type semiconductors) is effectively zero. As shown in Fig. 27.2b, when ΔE_{app} is negative, E_F of the semiconductor moves to more negative potentials. Specifically, electron density is replenished in the depletion width, decreasing V_{bi} and "unbending" the valence and conduction bands. The diminution of the potential barrier for electrons means that it is now easier for electrons to move from bulk of the semiconductor towards the interface. As a result, a net current flows that represents electrons from the semiconductor reacting with A in solution to generate A^-, as indicated in Fig. 27.2g. This condition is colloquially referred to as "forward bias" of the

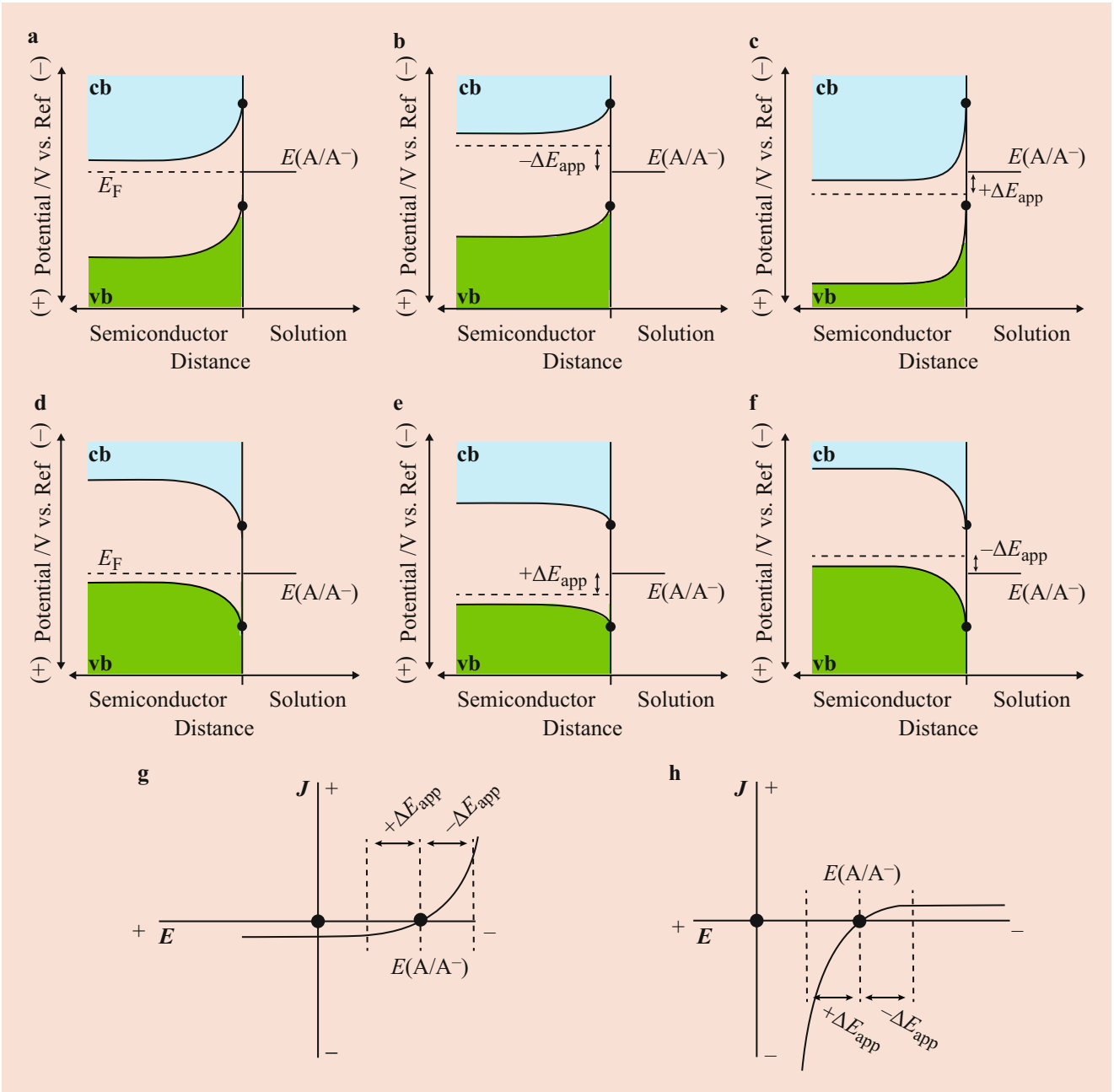

Fig. 27.2 Schematic depictions of the energy band diagrams for (**a**–**c**) n- and (**d**, **e**) p-type semiconductors immersed in liquid solutions containing both halves of dissolved redox couple, A/A^-, at various applied potentials, ΔE_{app}, in the absence of illumination. These images specifically describe the situation where the rate constant for minority charge carriers (k_{ht} for n-type and k_{et} for p-type semiconductors) is zero. A non-zero value for these rate constants would result in quasi-Fermi level splitting in the near surface region of the semiconductor but otherwise would not change the corresponding steady-state current-potential responses for n- and p-type semiconductors shown in (**g**) and (**h**), respectively

semiconductor electrode. The more negative ΔE_{app} is, the larger the net cathodic current. In principle, ΔE_{app} can be sufficiently negative that the original electron density in the depletion width is restored. This potential corresponds to the so-called flat band potential, E_{fb}. E_{fb} is a useful operating point because there is no electrostatic barrier for either electrons or holes to cross the interface at this value of E_F. Further, knowledge of E_{fb} then allows for easy determination of E_{cb} and E_{vb} through Eq. 27.2 using N_d as the value of n. Nevertheless, in the forward bias portion of the current-potential response, there is no prominent, characteristic feature for E_{fb}. In fact, mass transport of redox species from the

bulk solution to the semiconductor/solution interface most often limits the attainable current flux at potentials even less negative than flat band. Accordingly, other techniques beyond simple measurement of current-potential responses are needed to identify E_{fb} [39].

As indicated in Fig. 27.2c, when ΔE_{app} is positive, E_F of the semiconductor moves to more positive potentials. In this condition, even more electron density is removed from near surface region of the semiconductor, extending the depletion width and increasing the potential drop between the interior and surface of the semiconductor. The larger potential barrier means that even fewer electrons cross over from the semiconductor. In other words, the number of electrons available at the semiconductor surface to reduce A in solution is so small that the net current is dominated by the *opposite* process. In this case, A^- donates an electron to the semiconductor while being oxidized into A. For reasons enumerated later in this chapter, this process is independent of the applied potential and so the net current at more positive potentials reaches a small and constant current, as shown in Fig. 27.2g. This condition is typically referred to as "reverse bias".

Figures 27.2d–f show the corresponding energy band diagrams for a p-type semiconductor. Qualitatively, the general behavior is mirrored but with holes as the majority charge carriers. Notably, the current would still be 0 at $E(A/A^-)$ but now the current would become progressively more negative (anodic) at more positive potentials, i.e., when the semiconductor electrode is "forward biased" (Fig. 27.2h). Conversely, the current would be positive (cathodic) and reach a potential-independent value at more negative potentials, i.e., when the semiconductor electrode is in reverse bias.

Governing Equations

Unlike the equilibrium case, interpreting and predicting the specific current-potential behavior of a semiconductor electrode does depend on the values of the pertinent rate constants for charge transfer. In the ideal case, charge transfer in either direction at the semiconductor/solution interface occurs at the band edge potentials. Accordingly, the following kinetic description applies irrespective of n- or p-type character. The net rate, v_{net}, (equivalents s^{-1} cm^{-2}) of total charge transfer at the semiconductor/liquid interface can be understood by examining the rates of charge transfer through each band.

The total rate of electron transfer, v_{et}, into/from the conduction band edge is the sum of two processes. The rate of electron transfer from the conduction band edge to solution to reduce A to A^-, $v_{et,\rightarrow}$, is equal to the product of the forward rate constant for electron transfer, k_{et}, the concentration of electrons at the semiconductor surface, n_s, and the concentration of acceptors in solution at the semiconductor/solution interface, [A], in units of molecules cm^{-3}.

$$v_{et,\rightarrow} = k_{et} n_s [A] \tag{27.6}$$

Notably, k_{et} is a second order rate constant that has units of cm^4 s^{-1} since both the values of n_s and [A] are variable. Also, the value of [A] at the interface will be the same as the value of [A] in the bulk electrolyte solution so long as mass transfer from the bulk of solution to the electrode interface is sufficiently fast. When this is not true, a concentration overpotential develops [25] and this relation must be modified to indicate that [A] in the bulk solution and at the semiconductor/liquid interface are different. Conversely, the rate of back electron transfer from the solution into the conduction band is equal to the rate constant for back electron transfer, k_{et}^{-1} and the concentration of donors in solution, $[A^-]$,

$$v_{et,\leftarrow} = k_{et}^{-1} [A^-] \tag{27.7}$$

Notably, the units of k_{et}^{-1} have units of cm s^{-1} since the number of vacancies in the conduction band that can receive an electron from A^- is fixed (i.e., N_{cb}) and therefore this rate constant is first order overall. The net rate of electron transfer from/into the conduction band is then the difference between Eqs. 27.6 and 27.7,

$$v_{et} = v_{et,\rightarrow} - v_{et,\leftarrow} = k_{et} n_s [A] - k_{et}^{-1} [A^-] \tag{27.8}$$

Similarly, the total rate of hole transfer into/from the valence band edge, v_{ht}, is a function of two separate processes,

$$v_{ht,\rightarrow} = k_{ht} p_s [A^-] \tag{27.9}$$

$$v_{ht,\leftarrow} = k_{ht}^{-1} [A] \tag{27.10}$$

where p_s is the surface concentration of holes, k_{ht} is the second order rate constant for hole transfer (cm^4 s^{-1}), and k_{ht}^{-1} is the first order rate constant for back hole transfer (cm s^{-1}). Accordingly, the total rate of hole transfer between the valence band edge and solution is,

$$v_{ht} = v_{ht,\rightarrow} - v_{ht,\leftarrow} = k_{ht} p_s [A^-] - k_{ht}^{-1} [A] \tag{27.11}$$

The net rate of charge transfer across the semiconductor/solution interface is then the sum of v_{et} and v_{ht}, taking into consideration of the opposite signs of charge on electrons and holes,

$$\begin{aligned} v_{net} &= v_{et} - v_{ht} \\ &= k_{et} n_s [A] - k_{et}^{-1} [A^-] - k_{ht} p_s [A^-] + k_{ht}^{-1} [A] \end{aligned} \tag{27.12}$$

Since the net current density flowing across the semiconductor/solution interface, J_{net}, is directly proportional to v_{net} by q, the net current density is then simply,

$$J_{\text{net}} = qk_{\text{et}}n_{\text{s}}[\text{A}] - qk_{\text{et}}^{-1}[\text{A}^-] - qk_{\text{ht}}p_{\text{s}}[\text{A}^-] + qk_{\text{ht}}^{-1}[\text{A}] \tag{27.13}$$

In principle, Eq. 27.13 can describe the full current-potential response. However, two aspects complicate its use. First, superficially this expression contains four separate rate constants with different units that must be first determined. In practice, four independent measurements are not necessary since the forward and back rate constants can be related by the principle of detailed balance [40], i.e., at equilibrium the forward and back rates of elementary process must be equal. Simply stated, there can be no net charge transfer across either the conduction band edge or the valence band edge by definition at equilibrium. Accordingly, at equilibrium the forward and back rate expressions are equal to each other,

$$v_{\text{cb},\rightarrow} = v_{\text{cb},\leftarrow} = k_{\text{et}}n_{\text{s},0}[\text{A}] = k_{\text{et}}^{-1}[\text{A}^-] \tag{27.14a}$$

$$v_{\text{vb},\rightarrow} = v_{\text{vb},\leftarrow} = k_{\text{ht}}p_{\text{s},0}[\text{A}^-] = k_{\text{ht}}^{-1}[\text{A}] \tag{27.14b}$$

where $n_{\text{s},0}$ and $p_{\text{s},0}$ are specifically the surface concentrations of electrons and holes *at equilibrium*, respectively. From these relations, the values of the back rate constants are readily apparent,

$$k_{\text{et}}^{-1} = k_{\text{et}}n_{\text{s},0}\frac{[\text{A}]}{[\text{A}^-]} \tag{27.15a}$$

$$k_{\text{ht}}^{-1} = k_{\text{ht}}p_{\text{s},0}\frac{[\text{A}^-]}{[\text{A}]} \tag{27.15b}$$

Then, with these definitions for the back rate constants, the net current density is given by Eq. 27.16,

$$J_{\text{net}} = qk_{\text{et}}n_{\text{s}}[\text{A}] - qk_{\text{et}}n_{\text{s},0}[\text{A}] - qk_{\text{ht}}p_{\text{s}}[\text{A}^-] + qk_{\text{ht}}p_{\text{s},0}[\text{A}^-] \tag{27.16}$$

A slightly more convenient form of this same expression is as follows,

$$J_{\text{net}} = qk_{\text{et}}[\text{A}]n_{\text{s},0}\left(\frac{n_{\text{s}}}{n_{\text{s},0}} - 1\right) - qk_{\text{ht}}[\text{A}^-]p_{\text{s},0}\left(\frac{p_{\text{s}}}{p_{\text{s},0}} - 1\right) \tag{27.17}$$

where the terms outside the parentheses collectively have units of C s^{-1} cm^{-2}. The ratios "$n_s/n_{s,0}$" and "$p_s/p_{s,0}$" directly reflect the difference between the Fermi level and the solution redox potential.

$$\frac{n_{\text{s}}}{n_{\text{s},0}} = e^{\frac{-q}{k_{\text{B}}T}(E_{\text{F}} - E(\text{A}/\text{A}^-))} \tag{27.18a}$$

$$\frac{p_{\text{s}}}{p_{\text{s},0}} = e^{\frac{-q}{k_{\text{B}}T}(E(\text{A}/\text{A}^-) - E_{\text{F}})} \tag{27.18b}$$

Equations 27.18 highlight a second complication in predicting the current-potential responses in the dark. Simply, exact analysis of the current-potential responses requires tracking of both electron and hole transfer at the conduction and valence band edges, respectively. Thankfully, three aspects afford simplification without loss in accuracy. First, for even moderately doped semiconductors, the supply of the majority charge carrier greatly surpasses the supply of minority charge carriers. Accordingly, when the surface concentration of the majority charge carrier is small, the factor "n_s-$n_{s,0}$" is much larger than "p_s-$p_{s,0}$" for n-type semiconductors in forward bias and vice versa for p-type semiconductors in forward bias. Second, for reasons enumerated later in this chapter, k_{et} or k_{ht} can differ by several orders of magnitude. As a result, Eq. 27.17 can often be simplified into the following forms for n- and p-type semiconductors, respectively, by ignoring the portion involving the minority charge carrier.

$$J_{\text{net}} \approx qk_{\text{et}}[\text{A}]n_{\text{s},0}\left(\frac{n_{\text{s}}}{n_{\text{s},0}} - 1\right) \quad \text{for an n-type semiconductor electrode} \tag{27.19a}$$

$$J_{\text{net}} \approx -qk_{\text{ht}}[\text{A}^-]p_{\text{s},0}\left(\frac{p_{\text{s}}}{p_{\text{s},0}} - 1\right) \quad \text{for a p-type semiconductor electrode} \tag{27.19b}$$

The potential dependence of J_{net} arises solely from the potential dependence of the charge-carrier concentrations. When the applied potential drops solely across the depletion width of the semiconductor (i.e., the applied potential only changes E_{F}), Eqs. 27.2 hold and expressions for n_{s}, p_{s}, $n_{\text{s},0}$, and $p_{\text{s},0}$ are given below,

$$n_{\text{s}} = N_{\text{cb}}e^{\frac{q}{k_{\text{B}}T}(E_{\text{cb}} - E_{\text{F}})} \tag{27.20}$$

$$n_{\text{s},0} = N_{\text{cb}}e^{\frac{q}{k_{\text{B}}T}(E_{\text{cb}} - E(\text{A}/\text{A}^-))} \tag{27.21}$$

$$p_{\text{s}} = N_{\text{vb}}e^{\frac{q}{k_{\text{B}}T}(E_{\text{F}} - E_{\text{vb}})} \tag{27.22}$$

$$p_{\text{s},0} = N_{\text{vb}}e^{\frac{q}{k_{\text{B}}T}(E(\text{A}/\text{A}^-) - E_{\text{vb}})}. \tag{27.23}$$

Substitution of these expressions back into Eqs. 27.19 yields the explicit current-potential relations for n-type and p-type semiconductor electrodes, respectively,

$$J_{\text{net}} = qk_{\text{et}}[\text{A}]N_{\text{cb}}e^{\frac{q}{k_{\text{B}}T}(E_{\text{cb}} - E(\text{A}/\text{A}^-))}\left(e^{\frac{-q}{k_{\text{B}}T}(E_{\text{F}} - E(\text{A}/\text{A}^-))} - 1\right) \quad \text{for an n-type semiconductor electrode} \tag{27.24a}$$

$$J_{\text{net}} = -qk_{\text{ht}}[\text{A}^-]N_{\text{vb}}e^{\frac{q}{k_BT}(E(\text{A}/\text{A}^-)-E_{\text{vb}})}\left(e^{\frac{-q}{k_BT}(E(\text{A}/\text{A}^-)-E_F)} - 1\right)$$

for a p-type semiconductor electrode. (27.24b)

Equations 27.24 have the familiar form of the diode equation used for solid-state semiconductor Schottky heterojunctions [9, 10, 41]. The collective terms to the left of the parentheses in Eq. 27.24 represent the exchange current density, which depends explicitly on the relevant heterogeneous charge-transfer rate constant. Accordingly, while the general exponential form of the current-potential response is independent of k_{et} and k_{ht}, the values of these rate constants strongly affect the magnitude of the current when the semiconductor is perturbed away from the equilibrium potential (Fig. 27.3).

It is important to note that Eqs. 27.24 do not necessarily hold for semiconductor electrodes that are not "ideal" (as defined above) nor are they universally applicable even for "ideal" semiconductor electrodes. Electrode form factors other than flat, planar substrates change the governing rate equations. Accordingly, the current-potential responses of nanostructured semiconductor electrodes can differ significantly [42]. Another complication not treated here is the possibility of semiconductors with extremely small charge-carrier mobilities. As detailed elsewhere [43, 44], this scenario can lead to currents that are wholly independent of the concentrations of redox species and instead are dictated by the rates of charge carrier transport in the semiconductor [45]. Section 27.2.5 of this chapter separately describes the possible complications introduced by the presence of surface states. Some redox species strongly adsorb, affecting how charge is passed. Other redox species are not readily reduced/oxidized even at "ideal" electrodes, requiring the deliberate introduction of heterogeneous catalysts to augment the rates of charge transfer. These modified semiconductor/solution interfaces do not necessarily follow the presented governing rate equations [46–48]. Simply, analytical expressions such as Eq. 27.24 are not always tenable.

Despite the many possible confounding factors, there are still viable approaches for predicting and interpreting the current-potential responses at semiconductor/solution interfaces. The most common method is to discretize the semiconductor/solution system and calculate numerical solutions of the coupled Poisson-continuity equations [47, 49–51] for electron and hole transport in semiconductors [47, 52, 53]. This approach has the advantage of being very adaptable to all the aforementioned variations but is strongly dependent on the particular selection of boundary conditions [54]. Alternatively, for macroscopic, flat semiconductor electrodes, a one-dimensional Onsager model has been proposed [29, 55, 56] to describe more fully and naturally the current-potential responses of semiconductor/solution contacts. This model yields Eqs. 27.24 for the conditions defined above but allows for the possibility of understanding current-potential responses when conditions are not "ideal." Although relatively under-utilized, the Onsager approach has shown versatility in the types of semiconductor/liquid interfaces that can be quantitatively analyzed and has the capacity to differentiate between currents from thermalized and nonthermalized charge carriers [55–58].

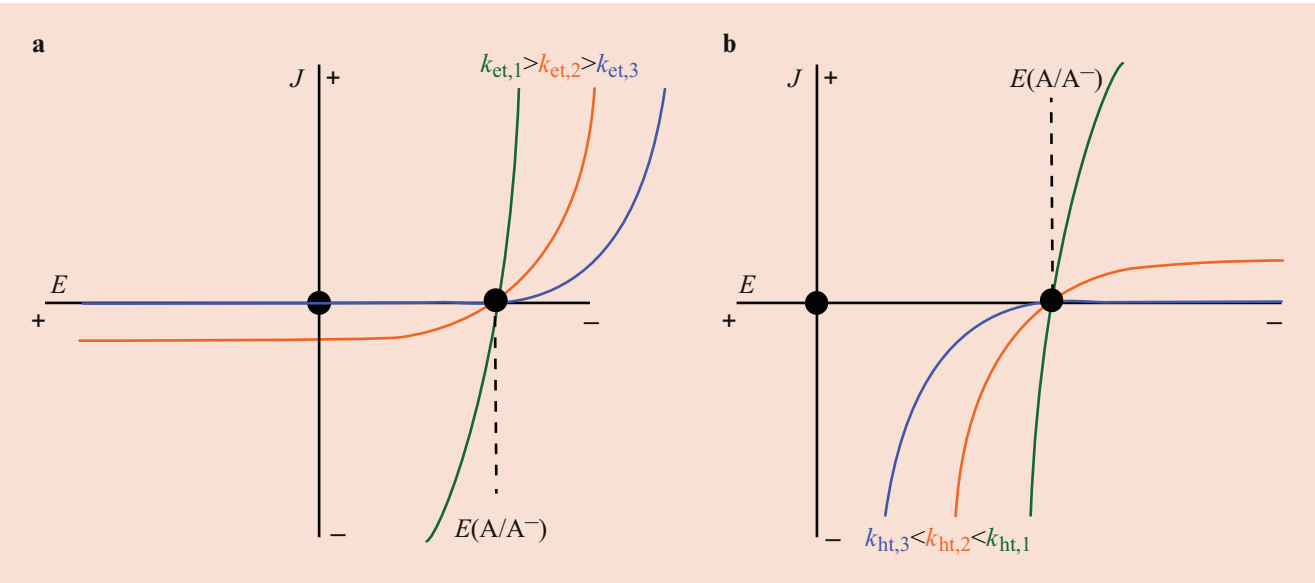

Fig. 27.3 Idealized depictions of the steady-state current-potential responses as a function of the rate constant for transfer of the majority charge-carrier into solution. The data are shown for (**a**) an n-type and (**b**) a p-type electrode in a poised solution containing both halves of a redox couple

27.2.3 Steady-State Condition of a Semiconductor Immersed in Liquid Solution Perturbed Away from Equilibrium by Suprabandgap Illumination

A fundamental tenet of semiconductor electrochemistry is semiconductor electrodes can also be perturbed away from equilibrium by the application of light. Specifically, when the illumination is comprised of photons with energies equal to or greater than E_g [59], then light absorption is possible that can change E_F. Light absorption results in the promotion of a delocalized electron from the valence band into the conduction band and a delocalized hole from the conduction band into the valence band. When photogeneration occurs in macroscopic semiconductor electrodes with photons with energy greater than E_g, the new charge carriers will quickly lose energy in excess of E_g by thermalization, i.e., the release of energy as heat. The photogenerated charge-carriers will then maintain the bandgap energy and populate the conduction band or valence band edges, respectively. The locations of light absorption and photogeneration depend strongly on the band structure of the semiconductor [60]. For semiconductors with a direct bandgap, light penetration and charge-carrier photogeneration occurs up to depths of 10^{-6} m. For semiconductors with an indirect bandgap, the relevant distance can be 10^{-4} m [61]. The effective distance photogenerated charge carriers can travel is proportional to the square root of the product between the lifetime of the charge carriers, τ, and the charge-carrier diffusion coefficient, D [61, 62].

Under constant illumination, carrier concentrations change because light absorbance introduces new mobile charge carriers. The following descriptions apply at steady-state,

$$n_s = n_{s,0} + \Delta n \tag{27.25a}$$

$$p_s = p_{s,0} + \Delta p \tag{27.25b}$$

where Δn and Δp are the new *net* carriers at the interface introduced by illumination. Importantly, the values of Δn and Δp reflect how the system has reached steady-state upon the application of constant light [63, 64]. As a result, the law of mass action is no longer valid in the semiconductor [50, 65],

$$n_i^2 < np \tag{27.26}$$

Several processes are possible that could facilitate recombination of the photogenerated charge carriers and thereby influence the values of Δn and Δp. Some of the most pertinent recombination processes are sketched in Fig. 27.4. Recombination of electrons and holes can occur throughout the semiconductor material, i.e., in the bulk and/or at the interface. In

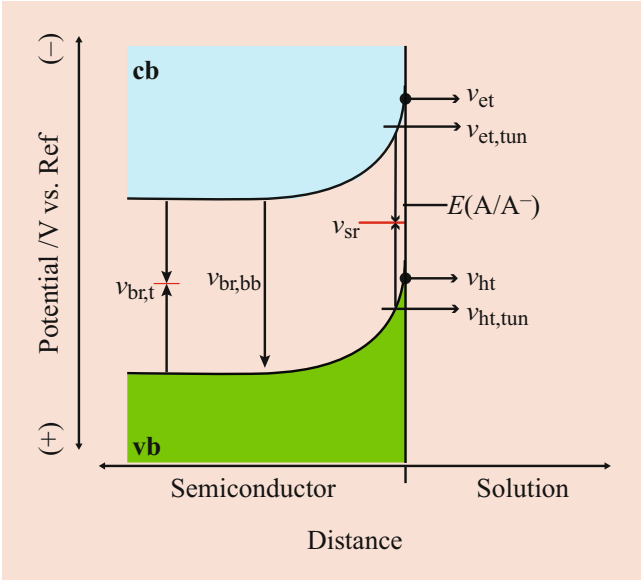

Fig. 27.4 Schematic depiction of the rates (v) of some charge-carrier recombination pathways including trap-mediated bulk recombination ($v_{br,t}$), band-to-band bulk recombination ($v_{br,bb}$), trap-mediated surface recombination (v_{sr}), electron transfer from the conduction band by tunneling through the depletion region ($v_{et,tun}$), electron transfer from the conduction band edge at the surface (v_{et}), hole transfer from the valence band by tunneling through the depletion region ($v_{ht,tun}$), and hole transfer from the valence band edge at the surface (v_{ht})

the bulk, band-to-band recombination can occur. This process is unavoidable and defines the limit of Δn and Δp values when all other recombination processes are mitigated. Charge-carrier recombination can also occur through discrete, localized states in the bandgap introduced by impurities or lattice defects. Notably, although such defects can and do exist inside the depletion width, the strong electric field helps physically separate electrons and holes so that the probability of recombining is low [66, 67]. For example, in an n-type semiconductor, electrons are driven away from the surface while holes are driven towards the surface [50]. This aspect is generally true in semiconductors where the charge carrier mobilities are large. In semiconductors with low charge carrier mobilities, the extent of recombination in the depletion width may be appreciable. Similar defects within the band gap are commonplace at the interface, where the outermost semiconductor atoms are necessarily under-coordinated and therefore subject to different bonding than atoms in the bulk. When both electrons and holes are used to drive both oxidations and reductions of the *same* redox couple, recombination of electrons and holes can also occur at the interface through heterogeneous charge transfer at the band edges, as described above, or through tunneling of carriers from within the semiconductor into solution.

Steady-state is achieved for Δn and Δp when the total rate of recombination of excess carriers is equal to the amount of

carriers being photogenerated, i.e., n and p are time invariant [68]. An important aspect to understand is that since n and p are no longer bound by the law of mass action, the concept of a single average energy ($\mathbf{E_F}$) that applies to all the charge-carriers in the semiconductor is no longer true. Rather, the average energies of electrons and holes must be considered separately through the concept of "quasi-Fermi levels" [61]. The implicit limitations of using equilibrium concepts under nonequilibrium conditions have been detailed [69] and must be recognized as not applicable at all times. Nevertheless, the concept that charge carrier populations can be described with an average value at steady-state has proven useful in understanding steady-state behaviors in semiconductor electrochemistry [64, 67, 70–79].

Figure 27.5 illustrates the energy band diagrams for an n-type semiconductor electrode immersed in the same solution as Fig. 27.1 and illuminated with a constant flux of suprabandgap illumination. In this scenario, no external bias is applied and no net current is drawn. Rather, the semiconductor is held at its open-circuit potential, which changes upon the application of light. The influence of light on a semiconductor electrode depends strongly on the duration and intensity of light, as well as the rates of all other competing/parallel processes that the photogenerated carriers could undergo. For these reasons, interpreting the precise photoresponse characteristics of a semiconductor electrode requires enumeration of several parameters. For simplicity, the following discussion assumes constant (i.e., time-invariant) illumination of an n-type semiconductor with high charge-carrier mobilities and the only recombination process at the surface is heterogeneous charge transfer at the band edges.

Perturbation away from equilibrium is possible by illumination with a light intensity (photons s^{-1} cm^{-2}), I_0. For reference, integration of the AM 1.5 solar spectrum out to 1050 nm at 1 Sun illumination amounts to ~10^{17} photons s^{-1} cm^{-2} [80]. Although no *net* current flows across this semiconductor/solution interface at open-circuit, photogenerated electrons and holes do both transfer into solution. Their respective rates are equal so as to effect no *net* change in solution. In this case, setting Eq. 27.17 equal to zero and using Eqs. 27.25 for n_s and p_s yields the following relation,

$$k_{et}\Delta n[A] = k_{ht}\Delta p[A^-]. \tag{27.27}$$

The values of Δn and Δp can then be understood by recognizing that the rate of charge-carrier loss must equal charge-carrier generation at steady-state. The rate of charge-carrier generation is dictated by the rate of photons being absorbed, which is the product of I_0 and fraction of incident photons that are absorbed, Φ (i.e., quantum yield). Thus, Δn and Δp at the interface are also bound by Eqs. 27.28,

$$k_{et}\Delta n[A] = \Phi I_0 \tag{27.28a}$$

$$k_{ht}\Delta p[A^-] = \Phi I_0. \tag{27.28b}$$

Combining Eqs. 27.25 and 27.28, the value of the charge carrier concentrations at the semiconductor/electrolyte interface are readily understood. As described above, the ratios of "$n_s/n_{s,0}$" and "$p/p_{s,0}$" are useful barometers of how far each carrier concentration is perturbed away from equilibrium. Accordingly, Eq. 27.28 can be rearranged into a slightly more convenient form,

$$\frac{n_s}{n_{s,0}} = \frac{\Phi I_0}{k_{et}[A]n_{s,0}} + 1 \tag{27.29a}$$

$$\frac{p_s}{p_{s,0}} = \frac{\Phi I_0}{k_{ht}[A^-]p_{s,0}} + 1. \tag{27.29b}$$

As evident in Eq. 27.29, under illumination, the concentrations of electrons and holes are not directly related to each other. Even if $p_{s,0}$ and $n_{s,0}$ were identical, the values of "$k_{et}[A]n_{s0}$" and "$k_{ht}[A^-]$ p_{s0}" separately influence how different the steady-state condition is from the equilibrium condition under a given level of illumination at open-circuit. This point is key to understanding how a semiconductor electrode ultimately performs work under illumination.

When "$k_{et}[A]n_{s0}$" and "$k_{ht}[A^-]p_{s,0}$" are both much larger than ΦI_0, n_s and p_s have essentially the same values as $n_{s.0}$ and $p_{s,0}$. Physically, the rate of photon absorption is too small to perturb the system appreciably away from equilibrium. In this instance, the amount of light is practically negligible and so Fig. 27.5a, which looks like the equilibrium case in the dark, would still essentially describe the system under this type of illumination.

Under more intense illumination, the situation changes. In Fig. 27.5b where both "$k_{et}[A]n_{s,0}$" and "$k_{ht}[A^-]p_{s,0}$" are small compared to ΦI_0, neither charge carrier type can readily transfer into solution. As a result, both electrons and holes accumulate at and near the surface. In effect, they are generated faster than they can be removed either by charge-transfer into solution or electrostatic drift into the interior of the semiconductor. The new net electrons replenish the depletion region, thereby lowering the potential drop between the bulk and surface of the semiconductor. Graphically, this facet is reflected as "unbending" of the bands. In addition, a single E_F is no longer sufficient to describe both electrons and holes. Strictly speaking, the concept "Fermi level" only has meaning at equilibrium. However, at steady-state, two "quasi-Fermi level" potentials, $E_{F,n}$ and $E_{F,p}$, can be ascribed to electrons and holes, respectively, since their concentrations are defined.

Combining Eqs. 27.18 and 27.29, the following expression applies,

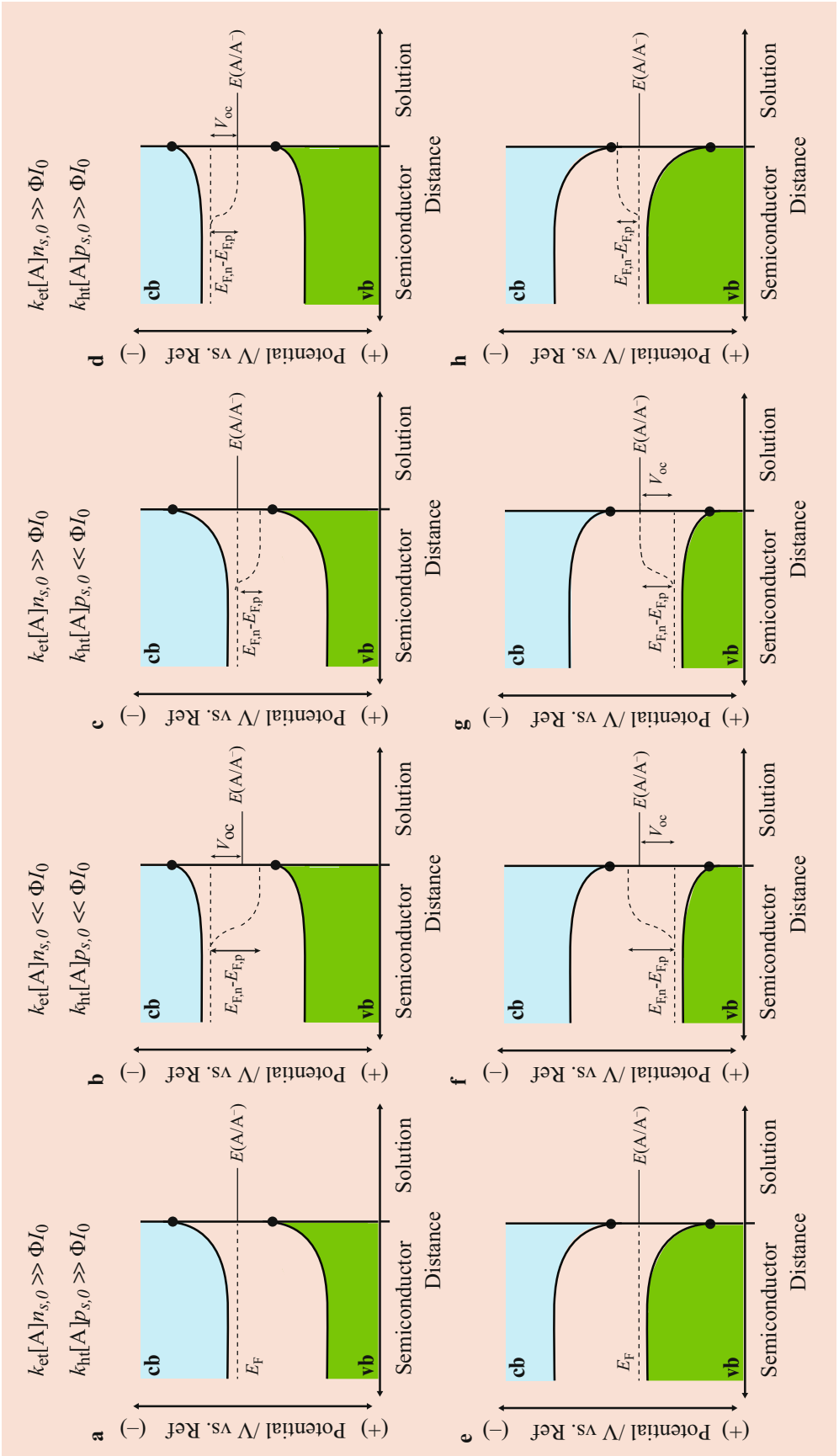

Fig. 27.5 Schematic depiction of the energy band diagrams for (top) n- and (bottom) p-type semiconductors at open-circuit while under various levels of constant, suprabandgap illumination defined by the value of the product of the quantum yield for absorption, Φ, and the light intensity, I_0, relative to the flux of charge-carrier emission from the band edges at equilibrium. (**a**, **e**) The illumination condition is so much less than the flux of charge-carrier emission from the band edges at equilibrium that the system resembles the equilibrium case. (**b**, **f**) The illumination condition is much greater than both fluxes of charge-carrier emission from the band edges at equilibrium, resulting in quasi-Fermi level splitting where both $E_{F,n}$ and $E_{F,p}$ are much different than E_F. (**c**, **g**) The illumination condition is much greater than the flux of hole emission from the valence band edge at equilibrium but less than the flux of electron emission from the conduction band edge at equilibrium, resulting in quasi-Fermi level splitting where $E_{F,n} = E_F$ and $E_{F,p} > E_F$. For the n-type electrode, the resultant quasi-Fermi level splitting results in no useful photovoltage. For the p-type electrode, the photovoltage is defined by $E_{F,p} - E(A/A^-)$. (**d**, **h**) The illumination condition is much greater than the flux of electron emission from the conduction band edge at equilibrium but less than the flux of hole emission from the valence band edge at equilibrium, resulting in quasi-Fermi level splitting where $E_{F,n} < E_F$ and $E_{F,p} = E_F$. For the n-type electrode, the photovoltage is defined by $E(A/A^-) - E_{F,n}$. For the p-type electrode, the resultant quasi-Fermi level splitting results in no useful photovoltage

$$E_{F,n} = -\frac{k_B T}{q} \ln\left(\frac{\Phi I_0}{k_{et}[A]n_{s,0}} + 1\right) + E(A/A^-). \quad (27.30)$$

Notably, the difference in the electron quasi-Fermi level at steady-state as compared to the Fermi level potential at equilibrium (i.e., $E_F = E(A/A^-)$) is described entirely by the natural log terms. Because electrons (and holes) are at thermal equilibrium and are highly delocalized (assuming large mobilities), their effective potential (or average energy) is thus uniform. For electrons in n-type semiconductors, this aspect is reflected by a flat quasi-Fermi level that spans the entire depicted material thickness. Notably, the value of $E_{F,n}$ is *uniformly* more negative than E_F at equilibrium (Fig. 27.5a). That is, the accumulation of electrons at the surface has made the potential of **all** electrons in the semiconductor more negative. The potential difference between $E_{F,n}$ and $E(A/A^-)$ reflects the electromotive force *available* to effect electrochemical reactions at the interface. This quantity is defined as the open-circuit photovoltage, V_{oc}, and is given by Eq. 27.31 for an n-type semiconductor electrode,

$$V_{oc} = -(E_{F,n} - E(A/A^-)). \quad (27.31)$$

Operationally, the larger V_{oc} is, the more uphill electrochemical transformations are possible. Accordingly, small "$k_{et}[A]n_{s,0}$"is desirable for an n-type photoelectrode.

Similarly, a small value of "$k_{ht}[A^-]p_{s,0}$" implies that p_s will be significantly larger than $p_{s,0}$. Accordingly, the quasi-Fermi level potential for holes shifts considerably more positive than $E(A/A^-)$. Notably, the more positive quasi-Fermi level potential for holes is flat only at and near the surface. In the bulk semiconductor, charge carrier recombination processes, in conjunction with fewer photon absorption events, limit the concentration of holes. Deep within the semiconductor, the law of mass action still holds and the two quasi-Fermi levels collapse back into one in the energy band diagrams. Notably, only the holes near/at the semiconductor interface have an effective potential sufficient to oxidize A^-. Holes far away from the semiconductor/solution interface are subject only to bulk recombination with electrons and therefore do not accumulate in excess. For the holes at the interface, the expression for their quasi-Fermi level value is analogous to Eq. 27.30,

$$E_{F,p} = \frac{k_B T}{q} \ln\left(\frac{\Phi I_0}{k_{ht}[A^-]p_{s,0}} + 1\right) + E(A/A^-). \quad (27.32)$$

In this case, the accumulation of holes (positive shift of $E_{F,p}$) does not result in added capacity for energy conversion. Rather, at the interface, the buildup of holes represents a penalty incurred to drive an oxidation reaction at the specific rate defined by the absorbed illumination intensity.

The value of "$E_{F,n} - E_{F,p}$" is proportional to the maximum internal potential difference generated by illumination, i.e., the numbers of electrons and holes at steady-state determine the free energy from the absorbed photons that can be utilized for energy conversion [64]. However, "$E_{F,n} - E_{F,p}$" is not necessarily related to V_{oc} since the value of $E_{F,p}$ has no bearing on V_{oc} (for an n-type semiconductor electrode). In this scenario, a fraction of the free energy from the absorbed photons is wasted. A further complication of "$E_{F,n} - E_{F,p}$" at a given level of illumination is that the maximum value is not unbound, as implied by Eqs. 27.30 and 27.32. That is, a naïve assumption might be that if "$k_{et}[A]n_{s0}$" and "$k_{ht}[A^-]p_{s,0}$" are progressively minimized (relative to ΦI_0), "$E_{F,n} - E_{F,p}$" can be indefinitely increased. This statement is tantamount to saying Eqs. 27.30 and 27.32 are operative at all times for the ideal semiconductor/solution interface being considered here. Such a statement is false because accumulation of both electrons and holes at the same location increases the probability for charge-carrier recombination by alternate processes [81, 82]. At some point, when "$k_{et}[A]n_{s0}$" and "$k_{ht}[A^-]p_{s,0}$" are small enough, bulk recombination becomes operative and limits how large n_s and p_s can be, i.e., the value of "$E_{F,n} - E_{F,p}$" is constrained. In such an instance, the value of $E_{F,n}$ is limited since "$E_{F,n} - E_{F,p}$" is bound, which ultimately hinders the attainable value of V_{oc}. This point caused confusion in the early semiconductor photoelectrochemistry literature [83–87] when the expectation was that a semiconductor/electrolyte system could be configured that would yield V_{oc} values as large as V_{bi} or even E_g. However, V_{oc} measurements were consistently both much smaller and independent of the kinetic features of the semiconductor/solution contact, even when the possibility of surface defects were eliminated [81, 82, 88].

A separate scenario to consider is depicted in Fig. 27.5c where "$k_{et}[A]n_{s0}$" is large but "$k_{ht}[A^-]p_{s,0}$" is small relative to ΦI_0. Here, n_s remains comparable to $n_{s,0}$ throughout the semiconductor and the quasi-Fermi level for electrons remains essentially unchanged relative to Fig. 27.5a. Effectively, electron transfer from the conduction band is so fast that no new net electrons are maintained under illumination. As a result, the semiconductor remains deficient in electrons in the depletion region and so the extent of "band bending" remains the same. The small value of "$k_{ht}[A^-]p_{s,0}$" does result in $p_s/p_{s,0} \gg 1$ and the hole quasi-Fermi level potential shifts considerably more positive than $E(A/A^-)$. However, as described above, this potential difference results in no added capacity to effect chemical transformations in solution. Hence, the V_{oc} for this junction would also be zero, as in Fig. 27.5a, even though "$E_{F,n} - E_{F,p}$" is not zero.

The final case to consider is summarized in Fig. 27.5d where "$k_{et}[A]n_{s,0}$" is small but "$k_{ht}[A^-]p_{s,0}$" is large relative to ΦI_0. These conditions ensure that $n_s/n_{s,0} \gg 1$ while $p_s/p_{s,0} \approx 1$. More pertinently, this case also represents the

ideal situation for realizing the largest values of V_{oc}. Because $E_{F,n}$ will shift to a more negative potential than $E(A/A^-)$ and since $E_{F,p}$ will not appreciably differ from $E(A/A^-)$, "$E_{F,n} - E_{F,p}$" is equivalent to "$E_{F,n} - E(A/A^-)$" and therefore defines V_{oc}. In this case, all of the internal free energy from the steady-state populations of electrons and holes is available to drive redox reactions in solution. This case is desirable from the perspective of systems that efficiently convert optical energy into stored chemical bond energy. For clarity, when the absorbed light intensity is much greater than "$k_{et}[A]n_{s,0}$," V_{oc} scales logarithmically with the light intensity over range of light intensities but not indefinitely. At high enough light intensities, the value of ΦI_0 may again become much larger than '$k_{et}[A]n_{s,0}$' and the system may revert to a state described by Fig. 27.5b. Alternatively, another complication arises at high light intensities. If light absorption results in enough new net electrons that there is no longer a depletion region, then there is no remaining potential drop within the semiconductor. Even if "$k_{ht}[A^-]p_{s,0}$" is still much larger than ΦI_0, a further increase in light intensity would not necessarily produce a larger V_{oc}. In this case, the capacity of the semiconductor to support an internal potential drop *of the opposite sign* is more limited. Although electrons still accumulate, they are confined much closer to the interface. As a result, $E_{F,n}$ shifts mostly because the potential drops at the interface. An alternative description would be the band edge potentials at the interface now are a function of the light intensity [89–91].

For completeness, Figs. 27.5e–h show the corresponding cases for a p-type semiconductor photoelectrode under illumination. The basic operational characteristics are the same, except now increasing "$k_{et}[A]n_{s0}$" while minimizing "$k_{ht}[A^-]p_{s,0}$" leads to the condition that yields the largest free energy gain without loss under illumination. In such p-type semiconductor electrodes, the accumulation of holes at the interface changes $E_{F,p}$ throughout the semiconductor and now "$E_{F,p} - E(A/A^-)$" defines V_{oc}.

27.2.4 Steady-State Condition of a Semiconductor Immersed in Liquid Solution Perturbed Away from Equilibrium by an Applied Potential and Suprabandgap Illumination

Predicting the full current-potential response of a semiconductor electrode that is perturbed both by an applied potential and illumination is complex. As noted above, even the simplest system configurations considered here behave quite differently depending on the experimental conditions. Hence, predicting a particular current-potential response requires a substantial amount of detail that applies to that specific case and is therefore beyond the scope of this chapter. For interested readers, numerical solutions that describe semiconductor electrode response characteristics under various illumination and bias conditions have been detailed [49, 51, 52, 54]. Still, for the purpose of this discussion, one operational point is worth discussing briefly.

The condition consisting of an applied potential to a semiconductor electrode that is being illuminated that exactly counteracts V_{oc} is called "short-circuit". The energy band diagrams for this specific case are indistinguishable from Fig. 27.5a and e for n-type and p-type semiconductor electrodes, respectively. The key point at the "short-circuit" condition is the quasi-Fermi level of the majority charge carrier is returned to $E(A/A^-)$ by applying an external potential, rendering either $\Delta n = 0$ (for an n-type semiconductor) or $\Delta p = 0$ (for a p-type semiconductor). Since the applied potential has no effect on the quasi-Fermi level of the minority charge carrier, the condition for the minority carrier at the surface remains unchanged. Correspondingly, at the "short-circuit" condition, a net photocurrent passes which arises solely from the transfer of the minority carrier from the semiconductor into solution [26]. For example, for an ideal n-type semiconductor, the photocurrent at the short-circuit condition, J_{sc}, is given by

$$J_{sc} = -qk_{ht}\Delta p[A^-] = q\Phi I_0. \tag{27.33}$$

Similarly, for an ideal p-type semiconductor, the photocurrent at the short-circuit condition is given by.

$$J_{sc} = qk_{et}\Delta n[A] = q\Phi I_0. \tag{27.34}$$

The photocurrent at short-circuit is directly proportional to the absorbed light intensity. If the light intensity is known with sufficient precision, the quantum yield for collection of photogenerated minority carriers is then readily identifiable. The energy band diagram for any other operational point in between the "open-circuit" and "short-circuit" conditions of a semiconductor photoelectrode would look like some intermediate of these respective band diagrams. For the operational point with the maximum energy conversion, the corresponding energy band diagram would describe the condition where the product of the available photovoltage and photocurrent is maximized. Since that condition obviously depends on many independent terms, the energy band diagram for this point is strongly system specific. Nevertheless, the more efficient semiconductor photoelectrodes will attain a maximum energy conversion when their energy band diagrams more closely resemble the "open-circuit" condition rather than the "short-circuit" condition.

A final general comment should be made regarding all of the diagrams in Fig. 27.5. Although they fully depict the primary qualitative features of each described scenario, they should not be considered as applicable at all times under all

experimental permutations. As mentioned above, when other recombination processes become appreciable relative to heterogeneous charge transfer, a limit is imposed on the magnitude of "$E_{F,n} - E_{F,p}$". Less obvious is a further complication that arises when appreciable charge accumulates under illumination. Specifically, in such cases, the potential may not drop solely within the semiconductor but instead may include an appreciable drop across the solution double layer. As described in the next section, such a scenario occurs when the capacity for the semiconductor to store charge matches or exceeds the ability to store charge in the double layer. A result would be a vertical shift of the semiconductor side of the energy band diagrams, with the direction depending on the sign of the accumulated surface charge.

27.2.5 Effect of Surface States on the Operation of a Semiconductor Electrode

In the preceding text, charge transfer was only considered at the conduction and valence band edges at the interface without influence from any other surface process. It is possible, however, for states with energies within the bandgap to have profound influences on the (photo)electrochemical behavior of semiconductors in contact with electrolytes [53, 83–85, 87, 92–97]. Commonly referred to as trap or defect states, surface states can have densities, N_{ss}, (units of cm^{-2}) approaching zero for an ideal interface and as large as the atomic density of the surface ($\sim 10^{15}$ cm^{-2}) [86, 98, 99]. There is no singular, general, or universal way that surface states affect the observable current-potential responses, as their specific influence depends on the magnitudes of several system parameters. Nevertheless, this section will highlight the principal two aspects that surface states complicate in the interpretation of current flow across a semiconductor/solution interface.

First, the manner in which an applied potential alters the charge-carrier concentrations at the semiconductor surface is not intuitive [38]. For the ideal case devoid of surface states, the assumption is that all the applied potential is dropped entirely across the depletion width. This assumption can be rationalized by considering the depletion width of the semiconductor and the double layer of charges aligned in solution at the solid/liquid interface as capacitive elements where charge can be stored. By definition, the capacitance, C, of any element describes the amount of charge (Q) stored per potential drop across that element. If the capacitances for the depletion region and the double layer in solution are known and if they occur in series (i.e., a charge from the bulk of the semiconductor must traverse the depletion region in order to transfer into solution at the semiconductor/solution interface), the fractions of the total applied potential distributed across each region are readily calculable. Since capacitive elements in series add reciprocally [38, 43, 100], the following relation applies for an ideal semiconductor/solution interface devoid of surface states,

$$\frac{1}{C_{tot}} = \frac{1}{C_{dr}} + \frac{1}{C_{dl}} \tag{27.35}$$

The corresponding total applied potential drop across the interface, ΔE_{app}, can be written as the sum of the sequential potential drops across the depletion region of the semiconductor, ΔE_{dr}, and the double layer in solution, ΔE_{dl}, by Eq. 27.36.

$$\Delta E_{app} = \Delta E_{dr} + \Delta E_{dl}. \tag{27.36}$$

Equations 27.35 and 27.36 are slight over simplifications, as the potential dropped in solution can further be partitioned into the potential drops across the Helmholtz and diffuse layers [43, 100]. Still, this analysis is sufficiently accurate for the context of this discussion. The depletion region capacitance is a complex function of V_{bi} [101] but can be approximated by Eq. 27.37 when the semiconductor is moderately doped and E_F is at least $3k_BT/q$ away from either band edge [101],

$$C_{dr} = \left(\frac{qN_d\varepsilon\varepsilon_0\sigma}{2}\right)^{1/2}\left(V_{bi} - \frac{k_BT}{q}\right)^{-1/2} \tag{27.37}$$

where σ is the contact area between the semiconductor and solution. C_{dl} is typically on the order of 10^{-6} F cm^{-2} and generally much larger than C_{dr} when Eq. 27.37 is valid. Hence, the total capacitance is dominated by capacitance of the depletion region and the applied potential predominantly drops across the depletion region of the semiconductor. As a result, the applied potential only changes V_{bi} (i.e., the extent of "band bending" within the depletion region). Accordingly, when conditions are appropriate for use of Eq. 27.36, $\Delta E_{app} \approx \Delta E_{dr}$.

Whenever a non-zero fraction of the applied potential drops across C_{dl}, the values of E_{cb} and E_{vb} change (i.e., the band edges at the interface are "unpinned" by that amount) [100]. Determining precisely how an applied potential is partitioned, even for ideal semiconductor/solution contacts, requires iterative quantitative analyses. Such approaches have been described by several groups previously [38, 100]. When surface states are operative, the potential distribution at the interface is further complicated. Surface states effectively add additional capacitive elements to the aforementioned analysis because they also can store/release charge carriers as a function of potential [16]. That is, the capacitance of any population of surfaces state can be described by Eq. 27.38,

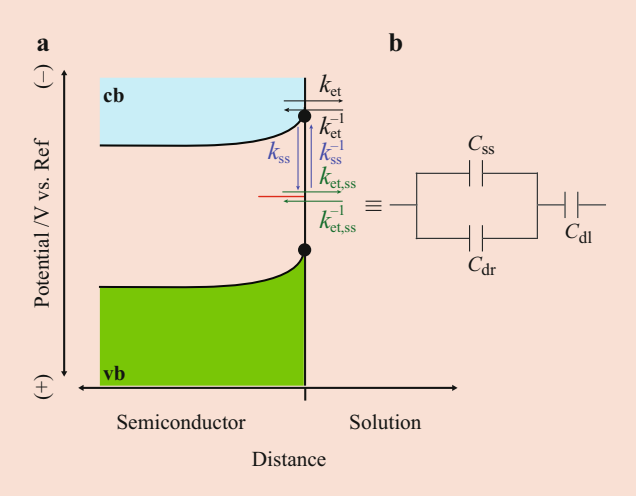

Fig. 27.6 (**a**) Schematic depiction of the various kinetic processes possible for electron transfer at an n-type electrode featuring surface states within the bandgap at the potential indicated by the red line. The rate constants are denoted for the emission and return of electrons at the conduction band edge to/from solution (k_{et} and k_{et}^{-1}, respectively), the transfer of electrons from/to the conduction band edge to/from the surface state (k_{ss} and k_{ss}^{-1}, respectively), and the emission and return of electrons at the surface sate to/from solution ($k_{et,ss}$ and $k_{et,ss}^{-1}$). (**b**) An equivalent circuit representation for the capacitances of surface states (C_{ss}), the depletion region (C_{dr}), and the double layer in solution (C_{dl})

$$C_{ss} = q\sigma N_{ss}\frac{\Delta f}{\Delta E_{ss}} \tag{27.38}$$

where $\frac{df}{dE_{app}}$ is the change in the fraction, f, of occupied surface states, N_{ss}, by the storage/release of electrons resulting from the applied potential dropped across the surface states. Assuming a single population of surface states exist at the interface, a charge carrier that reaches the surface could either transfer into solution directly from the band edge potentials or transfer into a surface state and then into solution (Fig. 27.6). Accordingly, the C_{dr} and C_{ss} elements act in parallel but are still collectively in series with C_{dl} [102]. The total capacitance is then given by Eq. 27.39,

$$\frac{1}{C_{tot}} = \frac{1}{C_{dr}+C_{ss}} + \frac{1}{C_{dl}} \tag{27.39}$$

Although outside the scope of this chapter, it is possible to formulate alternate equivalent circuits that describe semiconductor/solution interfaces with multiple, different populations of surface states [86, 93, 94, 103–105]. Nevertheless, the expression shown here in Eq. 27.39 is sufficient to make the following point. Since the capacitance of the surface states adds directly to the capacitance of the depletion region, if there is a high enough density that the sum capacitance is comparable to (or even greater than) the capacitance of the double layer in solution, then the applied potential will no longer just change the band bending within the semiconductor as with the ideal semiconductor/solution interface. Instead, an appreciable potential drop across the double layer will necessarily alter E_{cb} and E_{vb}. This result could be observed as the band edges apparently changing with different applied biases, effectively behaving as though they were "unpinned" [43]. Such a scenario considerably alters the energetics of the interface, potentially even changing the apparent values of k_{et} and k_{ht} (in a manner described in Sect. 27.3 of this chapter). Clearly, even if no charge passes from the surface states, their ability to store charge could significantly and non-intuitively distort the observed current-potential response both in the dark and under illumination.

The more overt influence of surface states on a semiconductor/solution contact is direct charge-transfer from/into solution. For an n-type semiconductor electrode in the dark, an energy band diagram including surface states is shown in Fig. 27.6. Even with no appreciable hole-transfer through the valence band-edge, there are now multiple inter-related charge-transfer processes in this system [98]. First, as in the ideal case, electron transfer can occur from the conduction band edge to an acceptor species in solution as described above and as governed by k_{et}. Second, electrons from the conduction band edge could alternatively transfer into/out of the surface states at rates governed by the density of surface states and the rate constants k_{ss} for capture of electrons and k_{ss}^{-1} for the emission of electrons by the surface state. Third, electrons in surface states can transfer into/from solution at rates governed by the concentrations of redox species in solution and the rate constants $k_{et,ss}$ ($cm^3\ s^{-1}$) for electron transfer into acceptors and $k_{et,ss}^{-1}$ ($cm^3\ s^{-1}$) for electron transfer from donors. Accordingly, the rate of electrons flowing into solution is no longer given by Eq. 27.6. Instead, the rate of electron transfer into solution, $v_{et\rightarrow}$, (assuming charge-transfer from/into the valence band is negligible) depends on the occupancy of the surface states,

$$v_{et\rightarrow} = k_{et}[A]n_s + k_{et,ss}[A]N_{ss}f \tag{27.40}$$

where the product $N_{ss}f$ is the explicit density of occupied surface states at steady state. Similarly, the rate of electrons flowing from solution back into the semiconductor, $v_{et\leftarrow}$, can be determined by applying the principle of microscopic reversibility separately to the transfer of electrons into/from the conduction band (as in Sect. 27.2.2) and to the transfer of electrons into/from the surface states,

$$v_{et\leftarrow} = k_{et}[A]n_{s,0} + k_{et,ss}[A]N_{ss}(1-f)\left(\frac{f_0}{1-f_0}\right) \tag{27.41}$$

where f_0 is the value of f at equilibrium. Combining these last two expressions yields the net rate of electron transfer in analogy to Eq. 27.12,

$$v_{\text{net}} = k_{\text{et}}[\text{A}]n_{\text{s},0}\left(\frac{n_{\text{s}}}{n_{\text{s},0}} - 1\right) + k_{\text{et,ss}}[\text{A}]N_{\text{ss}}\left(\frac{f - f_0}{1 - f_0}\right) \tag{27.42}$$

Clearly, when N_{ss} is sufficiently small, the second term on the right disappears irrespective of the rate constants for surface-state-mediated electron transfer. That is, if the surface state density can be sufficiently minimized, the observable rate ($qv_{\text{net}} = J_{\text{net}}$) will be effectively first order with n_{s} and [A], i.e., the system response is ideal.

Although Eq. 27.42 has a relatively compact form, it still implicitly requires knowledge of all rate constants that describe processes where charge flow into/out of surface states. Specifically, the fractions of occupied surface states both at equilibrium and at steady-state, f and f_0, are defined by the ratios of the relevant kinetic processes [4, 43, 106],

$$f_0 = \frac{k_{\text{ss}}n_{\text{s},0} + k_{\text{et,ss}}^{-1}[\text{A}^-]}{k_{\text{ss}}n_{\text{s},0} + k_{\text{et,ss}}^{-1}[\text{A}^-] + k_{\text{ss}}^{-1}N_{\text{cb}}e^{\frac{q}{k_{\text{B}}T}(E_{\text{cb}} - E_{\text{ss}})} + k_{\text{et,ss}}[\text{A}]} \tag{27.43}$$

$$f = \frac{k_{\text{ss}}n_{\text{s}} + k_{\text{et,ss}}^{-1}[\text{A}^-]}{k_{\text{ss}}n_{\text{s}} + k_{\text{et,ss}}^{-1}[\text{A}^-] + k_{\text{ss}}^{-1}N_{\text{cb}}e^{\frac{q}{k_{\text{B}}T}(E_{\text{cb}} - E_{\text{ss}})} + k_{\text{et,ss}}[\text{A}]}. \tag{27.44}$$

where E_{ss} is the potential of the surface states. That is, Eqs. 27.43 and 27.44 state that the sum of all the rates of processes that place electrons into surface states divided by the sum of all rate processes involving surface states define the fraction of states occupied. However, with this definition of f, the values of k_{ss}^{-1} and $k_{\text{et,ss}}^{-1}$ cannot be re-expressed solely with k_{ss} and $k_{\text{et,ss}}$, respectively, (as was the case with k_{et} and k_{et}^{-1}, vide supra) without further information. Still, three limiting cases are illustrative of the possible effects when N_{ss} is not negligibly small.

First, when the rates of electron transfer between surface states and solution are much faster than the rate of electron transfer between the conduction band edge and the surface states, i.e., $k_{\text{et, ss}}[\text{A}]$ and $k_{\text{et,ss}}^{-1}[\text{A}^-] \gg k_{\text{ss}}n_{\text{s}}$ and $k_{\text{ss}}^{-1}N_{\text{cb}}e^{\frac{q}{kT}(E_{\text{cb}} - E_{\text{ss}})}$, f becomes independent of potential, i.e., $f = f_0$. That is, even with fast rates of charge transfer between the surface states and solution, there is no net effect on electron density at the surface. Accordingly, the current-potential behavior follows the response expected for an ideal semiconductor/solution interface, i.e., Eq. 27.19, even for comparatively large N_{ss} values.

Second, when the rate of electron transfer from the conduction band edge into surface states is much faster than all other process, i.e., $k_{\text{ss}}n_{\text{s}} \gg k_{\text{et, ss}}[\text{A}]$, $k_{\text{et,ss}}^{-1}[\text{A}^-]$, and $k_{\text{ss}}^{-1}N_{\text{cb}}e^{\frac{q}{kT}(E_{\text{cb}} - E_{\text{ss}})}$, then the surface states act as electron "traps". Using this condition for defining f and then substituting into Eq. 27.42, the rate law for net electron transfer is then given by Eq. 27.45,

$$v_{\text{net}} = k_{\text{et}}[\text{A}]n_{\text{s},0}\left(\frac{n_{\text{s}}}{n_{\text{s},0}} - 1\right) + k_{\text{et,ss}}[\text{A}]N_{\text{ss}} \tag{27.45}$$

where $k_{\text{et,ss}}$ is the rate limiting constant. In this scenario, the observed net rate of electron transfer has a constant, positive contribution of electron transfer from surface states into solution acceptors. The weight of this potential-independent contribution is dictated by the product of "$k_{\text{et, ss}}N_{\text{ss}}$" relative to the product of "$k_{\text{et}}n_{\text{s}}$". Clearly, the rate law deviates most from the ideal case when n_{s} is small (i.e., at a bias near or more positive than the equilibrium potential). Again, when N_{ss} is small, the surface-state contribution becomes less influential. However, now the explicit value of $k_{\text{et,ss}}$ defines when the magnitude of N_{ss} causes a perceptible deviation from the ideal case. Assuming a value of 10^{-13} cm^3 s^{-1} for $k_{\text{et,ss}}$ (as has been reported for surface states consisting of adsorbed dyes interacting with redox mediators in dye-sensitized photoelectrochemistry) [107] and a maximum density of surface traps (i.e., $N_{\text{ss}} = 10^{15}$ cm^{-2}), the velocity of electrons flowing through surface states could be as large as 10^2 cm s^{-1}. Even when the potential is moved far into forward bias so that $n_{\text{s}} \sim N_{\text{cb}}$ (ca. 10^{19} cm^{-3}), the rate constant for electron transfer into solution directly from the conduction band edge would have to be $>10^{-17}$ cm^4 s^{-1} so that $k_{\text{et}}n_{\text{s}} \geq 10^2$ cm s^{-1} to outpace the velocity of electrons flowing through surface states.

Third, when only the rate of electron transfer from surface states into acceptors in solution is much faster than the rate of electron transfer between the conduction band edge and the surface states, i.e., $k_{\text{et, ss}}[\text{A}] \gg k_{\text{ss}}n_{\text{s}}$, $k_{\text{et,ss}}^{-1}[\text{A}^-]$, and $k_{\text{ss}}^{-1}N_{\text{cb}}e^{\frac{q}{kT}(E_{\text{cb}} - E_{\text{ss}})}$, the net rate of electron transfer is given by Eq. 27.46,

$$v_{\text{net}} = k_{\text{et}}[\text{A}]n_{\text{s},0}\left(\frac{n_{\text{s}}}{n_{\text{s},0}} - 1\right) + k_{\text{ss}}N_{\text{ss}}n_{\text{s},0}\left(\frac{n_{\text{s}}}{n_{\text{s},0}} - 1\right). \tag{27.46}$$

In this scenario, the rate-limiting factor in electron transfer from surface states becomes just the filling of surface states with electrons. The contribution of surface-state-based electron transfer will have the same potential dependence as electron transfer from the conduction band edge since both are first order with respect to n_{s} but will have no dependence with [A]. In other words, unlike the preceding scenario, the interpretation of the current-potential response could be problematic in both reverse and forward bias. The product "$k_{\text{ss}}N_{\text{ss}}$" as compared to the product "k_{et}[A]" now determines which process contributes the

most to the total rate of electron transfer. Here, the rate constant k_{ss} reflects the probability of capturing an electron at a surface state. In solid-state nomenclature for charge-carrier traps, this probability is a function of the effective cross-section (size) and the velocity that carriers can move in the material [108]. Assuming an effective size of a surface state as comparable to that of a surface atom ($\sim 10^{-15}$ cm^2) and considering the thermal velocity of electrons in crystalline semiconductors is fast ($\sim 10^7$ cm s^{-1}) [10], k_{ss} could reasonably be $\sim 10^{-8}$ cm^3 s^{-1}. If the density of surface traps is on the ppm scale (i.e., $\sim 10^9$ cm^{-2}) and a solution with a high concentration (e.g., 6.022×10^{20} molecules cm^{-3}) of redox species is used, then k_{et} must be $>10^{-19}$ cm^4 s^{-1} to observe electron transfer predominantly from the conduction band edge. However, if N_{ss} is $\sim 10^{15}$ cm^{-2}, then k_{et} would have to be $>10^{-13}$ cm^4 s^{-1} to observe electron transfer predominantly from the conduction band edge in forward bias.

Clearly, as described in the latter two cases, the magnitude of k_{et} for n-type electrodes (and k_{ht} for p-type electrodes) strongly dictates whether the semiconductor/solution response behaves ideally in the presence of a non-zero density of surface states. Accordingly, an understanding of the factors that define the rate constants k_{et} and k_{ht} are central to the field of semiconductor electrochemistry. In the following section, a description of what defines and bounds the values of k_{et} and k_{ht} is given.

27.3 Rate Constants for Heterogeneous Charge Transfer at Semiconductor/Solution Interfaces

27.3.1 Historical Context

Although the field of semiconductor photoelectrochemistry began in 1839 with Becquerel's discovery of a photoelectrochemical response [109], more than 100 years passed before a detailed understanding of k_{et} and k_{ht} at semiconductor/solution interfaces took shape [67, 70–72, 110–113]. The first fundamental studies were motivated in part by the burgeoning development of the semiconductor industry, where electrochemistry proved essential in defining the characteristic properties of semiconductor heterojunctions [114, 115], and the concurrent development of theories for charge transfer at metal/solution interfaces and between molecules dissolved in the same solution [110].

Although several viewpoints on the essential aspects of charge transfer were proposed [116–118], a general consensus emerged on four aspects. (1) Charge-transfer is empirically an activated process and therefore k_{et} and k_{ht} should follow Arrhenius-Eyring [119] behavior, i.e., $k = k_{max} e^{-\Delta G^{\ddagger}/k_B T}$ ($\Delta G^{\ddagger}$ is the activation energy, and k_{max} is the rate constant when $\Delta G^{\ddagger} = 0$). (2) Charge transfer is thermoneutral, occurring at a single transition state with no change in free energy. (3) Charge transfer must occur at timescales much shorter than nuclear motion. That is, during electron exchange, atomic nuclei can be considered immobile (i.e., the Franck-Condon principle) [16]. (4) Unlike charge-transfer within a crystalline solid, the transfer of charge necessarily must induce a measurable change in the structure of the medium (solvent) and charge carriers (redox molecules) that relates to $\Delta G^{\ddagger}$.

27.3.2 Reorganization Energy

The qualitative nature of the physical changes associated with the injection/removal of 1e$^-$ can be readily understood by considering an elementary redox process where a generic species A gets reduced to A$^-$ [120]. The coordination sphere and the dipole orientation of the solvent shell of species A (i.e., the gray circle) are depicted at the bottom of Fig. 27.7. In this figure, the solvent dipoles are randomly organized around A but the configuration represents the average energy configuration of all species. If the *y*-axis of this figure represents the total energy of the system, then injection of 1e$^-$ into A can be understood by the first vertical line labeled "*1*". The reduction of A to A$^-$ necessarily raises the total energy of molecule A. However, since the reduction occurs much faster than the motion of solvent molecules, the environment around the redox molecule remains unchanged. The solvent polarization is still matched to the charge of A not A$^-$, i.e., the local environment and nuclei positions are not energy minimized. Accordingly, the total energy input to reach this condition is labeled $\mathbf{E_A}$, reflecting the transition started from the local structure appropriate for molecule A. Since A$^-$ has a net negative charge, the local solvent environment must polarize and the bonding of A$^-$ must change to accommodate the new charge to minimize the total free energy of the system by an amount $-\lambda_A$ (vertical line labeled "*2*"). Now consider a related but distinct pathway. Suppose the local molecular structure around molecule A were changed first. That is, solvent polarization and molecular structure of A would shift to reflect that for molecule A$^-$ without A yet undergoing charge transfer (vertical line *3*). The energy to effect this change would be $+\lambda_{A^-}$. Now, under this condition, adding 1e$^-$ to molecule A (vertical line *4*) so that the total energy of the system is minimized would require an additional input of energy, $\mathbf{E}_{A^-}$. Irrespective of which pathway is taken, the reduction of A to A$^-$ results in the system with the same total energy.

When $\lambda_{A^-} = \lambda_A = \lambda$, λ represents an energy requirement for molecular reorganization that necessarily must be satisfied for a reduction/oxidation event to occur. That is, the energy needed to change the oxidation state of A by ± 1

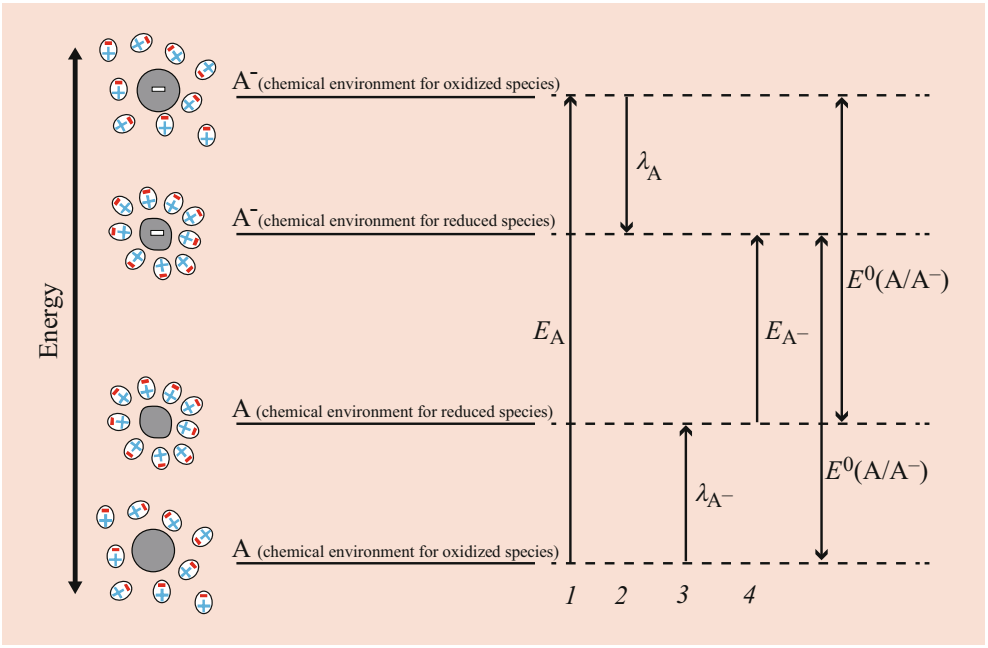

Fig. 27.7 A schematic depiction of the consequences of isoenergetic charge transfer at rates much faster than nuclear motions. Step 1 indicates the change in system energy, $\mathbf{E_A}$, when species **A** is reduced by 1 e^-. The local molecular structure cannot immediately respond, resulting in species $\mathbf{A}^-$ in a local molecular structure minimized for **A**. The local molecular structure must change to accommodate $\mathbf{A}^-$ to minimize the system energy, resulting in a loss of energy by an amount λ_A (Step 2). The same transition could be envisioned if the local molecular structure of **A** is first changed to that appropriate for $\mathbf{A}^-$ (Step 3). This requires an energy input of an amount λ_{A^-}. Species **A** can be reduced by 1 e^- to $\mathbf{A}^-$ by input of an additional energy $\mathbf{E}_{A^-}$

requires work beyond the thermodynamic driving force. From Fig. 27.7, the value of λ is,

$$\frac{\mathbf{E_A} - \mathbf{E_{A^-}}}{2} = \boldsymbol{\lambda}. \tag{27.47}$$

The quantitative value of the reorganization energy concept can be understood as a sum of two independent terms [116, 121, 122]. One component in the total reorganization energy describes the work needed specifically to rearrange the solvent shell. This component is explicitly depicted in Fig. 27.7 as the solvent dipole rearrangement and is often denoted as the outer reorganization energy, λ_o. It can be estimated by treating the solvent as a simple dielectric continuum that supports isolated, spherical charges [25, 121, 123]. For homogeneous electrochemical self-exchange reactions, the value of λ_o is given by Eq. 27.48,

$$\lambda_o = \frac{q^2}{4\pi\varepsilon_0}\left(\frac{1}{2a_A} + \frac{1}{2a_{A^-}} - \frac{1}{r}\right)\left(\frac{1}{\varepsilon_{op}} - \frac{1}{\varepsilon_s}\right) \tag{27.48}$$

where the a terms are the respective ionic radii, r is the mean distance between A and A^- during electron transfer, and ε_{op} & ε_s are the optical and static dielectric constants of the solvent medium. The dielectric constants reflect how the medium polarizes at short (~10^{-15} s) and long times (~10^{-11} – 10^{-14} s), respectively [124]. Equation 27.48 highlights that solvents with similar ε_{op} and ε_s necessarily afford smaller values of λ_o. Additionally, the first term in parentheses describes the change in volumes occupied between A and A^-. For the reduction of A at an electrode surface, Eq. 27.48 is not directly applicable since the reactants are A and an electron from the semiconductor. Several groups [125–127] have contributed to a related approach for estimating λ at the semiconductor/solution interface since the outer reorganization component is more nuanced. Ions in solution can generate an image potential within the near-surface of the semiconductor but not necessarily instantaneously [125]. The exact treatment is involved but an approximate expression has been developed that estimates the outer reorganization energy for a $1e^-$ reduction at a semiconductor/solution interface,

$$\lambda_{o,sc} = \frac{q^2}{4\pi\varepsilon_0}\left(\frac{1}{a_A}\left(\frac{1}{\varepsilon_{op}} - \frac{1}{\varepsilon_s}\right) - \frac{1}{2\delta}\left(\frac{1}{\varepsilon_{op}}\left(\frac{\varepsilon_{op,sc} - \varepsilon_{op}}{\varepsilon_{op,sc} + \varepsilon_{op}}\right) - \frac{1}{\varepsilon_s}\left(\frac{\varepsilon_{s,sc} - \varepsilon_s}{\varepsilon_{s,sc} + \varepsilon_s}\right)\right)\right) \tag{27.49}$$

where δ is the mean distance between the semiconductor surface and A during charge transfer and $\varepsilon_{op,sc}$ & $\varepsilon_{s,sc}$ are the optical and static dielectric constants of the semiconductor. The sum total value of λ for semiconductor/solution interfaces is typically on the order of 1 eV.

The other component of λ arises from the structural changes incurred by the redox molecule itself when it is reduced/oxidized. In Fig. 27.7, this reorganization energy, λ_i, is depicted simply as a change in the shape of A and A^-. For actual molecules, λ_i depends on the specific design of the redox molecule and can be estimated from the sum total bond length and angle increases/decreases that occur as the molecular structure responds to the change in oxidation state (Eq. 27.50) [25, 123],

$$\lambda_i = \sum_i \frac{k_{i,A} k_{i,A^-}}{k_{i,A} + k_{i,A^-}} \Delta x_i^2 \tag{27.50}$$

where the k_i terms are the force constants for specific bonds in A and A^- and Δx_i is the change in bond length before and after the redox event. The inner reorganization component for a homogeneous self-exchange reaction, e.g., $A + A^- \rightarrow A^- + A$, includes the total energy difference for two molecules. Since the number of participating molecules is halved in a heterogeneous electron transfer at a semiconductor/solution interface and since the electrode lattice is not substantially distorted by charge transfer [128], the inner reorganization energy for a heterogeneous reaction can just be estimated as half the value of the inner reorganization energy for the self-exchange reaction.

27.3.3 Fluctuating Energies of Redox Molecules in Solution and Models for Heterogeneous Charge Transfer at Semiconductor/Solution Interfaces

A key requirement for models of charge transfer is to relate λ to $\Delta G^{\ddagger}$ so that values of k_{et} and k_{ht} can be determined. A core premise in the models described in this chapter is that the fluctuations away from equilibrium in the free energies of the redox molecules in solution strongly factor into the cumulative rate of charge transfer. Since λ reports on the work needed to order/disorder the solvation shell and the molecular structure of redox species, λ is key to understanding the energy fluctuations.

Although quantum mechanics have been used extensively to detail energy fluctuations of species in solution [17, 122], the original fluctuating energy level concept developed by Marcus was classical in nature. A brief summary of the Marcus model is presented first, highlighting the basis of his 1990 Nobel prize in Chemistry [129]. Following, a related approach popularized by Gerischer is given [70–74], including both the commonalities and the two key distinctions. First, Gerischer formally connected the solution potential and the Fermi level of charge-carriers in semiconductors. Second, Gerischer used the fluctuating energy level concept to formulate a distribution of states for the redox molecules in solution analogous to the bands of a solid.

The classical version of the Marcus model of charge-transfer is represented in Fig. 27.8a. Treating the solvent as a dielectric continuum as described above, the Marcus model holds that a polar solvent has an energy minimized average orientation of its dipoles around a charged species. In order to inject (or remove) an electron from the ion, the solvent dipoles must first reorient. The timescale of these nuclear motions defines a (comparatively) slow first step in the charge transfer process of converting A to A^-. To polarize, the solvent must gain energy from the surrounding media through random collisions to attain a specific intermediate state. At this state, the local structure of the solvent shell and the coordination sphere of the redox species do not reflect the energy minimized structure for either A or A^-. Instead, the polarization of this intermediate state is such that the energies of the products and reactants are the same. Figure 27.8a displays this idea by depicting the system in terms of the relevant free energies along a reaction coordinate, where the intermediate state is the single point where the curves intersect [111, 130].

The dielectric continuum treatment of the solvent means that all the various possible molecular rearrangements are parametrized into one single variable (i.e., "q" in Fig. 27.8a). The free energies of the reactants (A & e^-) and the products (A^-) are then displayed as a function of this variable. The local molecular structure at this specific, non-equilibrium intermediate state specifically allows isoenergetic charge transfer on a fast timescale relative to nuclear motions. The probability that the system will attain this nonequilibrium configuration then is central to dictating the rate of charge transfer.

The free energy vs reaction coordinate profiles are shown in Fig. 27.8a as diabatic surfaces, i.e., the reactants/products exchange thermal energy with the surrounding medium. The reorganization energy is depicted in Fig. 27.8a as the vertical distance between the free energy minimum of the reactant curve at q_A and the free energy of the product curve at that same reaction coordinate. The difference in the vertical positions of each curve's minima defines the reaction driving force, ΔG^0. Assuming a parabolic form of the free energy curves of both the reactants and products along the reaction coordinate simplifies how λ, $\Delta G^{\ddagger}$, and ΔG^0 are related. In this view, the free energy of a species is proportional to the square of the reaction coordinate by λ (i.e., $G = \lambda q^2$). Setting the free energies of the two curves equal at $q^{\ddagger}$ yields the following relation between λ and $\Delta G^{\ddagger}$,

$$\Delta G^{\ddagger} = \frac{\lambda}{4}\left(\frac{\Delta G^0}{\lambda} + 1\right)^2 = \frac{\left(\Delta G^0 + \lambda\right)^2}{4\lambda} \tag{27.51}$$

Although compact and informative, the free energy vs reaction coordinate diagrams do not readily convey two

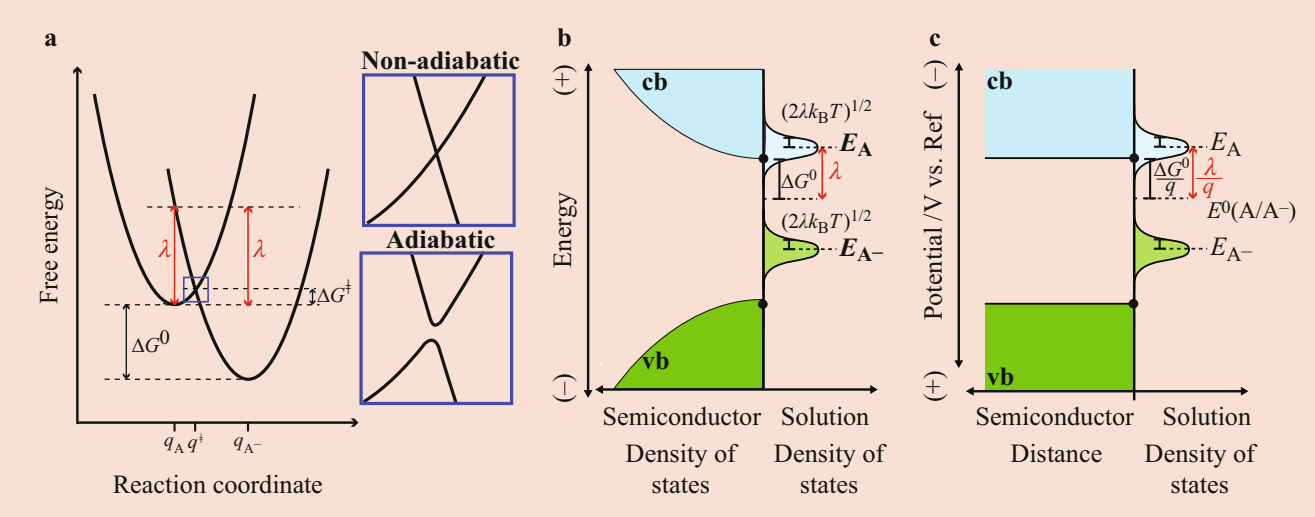

Fig. 27.8 (**a**) Free energy vs reaction coordinate diagrams of a spontaneous electron transfer event as described in the Marcus model. The reactant free energy curve is centered at q_A and the product free energy curve is centered at q_{A^-}. Charge transfer occurs when the reactant-product complex is formed at $q^{\ddagger}$. The values of λ and ΔG^0 are denoted. Insets: a magnified view of the transition state assuming either non-adiabatic or adiabatic charge transfer. (**b**) An energy band diagram plotted as a function of the density of states (increasing away from the interface). The "band structure" for a poised solution containing a dissolved redox couple as proposed by Gerischer is shown on the right side. The values of λ and ΔG^0 are denoted. (**c**) A hybrid energy band diagram where the left side represents the semiconductor band structure as a function of position and the right side represents the density of states of the solution "bands"

aspects pertinent to the semiconductor/solution interface. First, the specific energetics of the semiconductor electrode surface (E_{cb} and E_{vb}) are not obvious in this representation. Second, the diagrams do not readily describe the notion of concentration. Considering homogeneous chemical reactions as events between discrete molecules is natural and the typical way chemical mechanisms are discussed. However, the reactivity of charge carriers in semiconductor electrodes is more often understood from a perspective of carrier statistics [40, 64], where the concept of concentration changes is important to the concept of (quasi-)Fermi levels. Although the limits of the statistical viewpoint have been intently debated [131], practitioners in the semiconductor electrochemistry field generally have adopted it.

Figure 27.8b presents the perspective put forth by Gerischer. Here the interface between the semiconductor and solution are explicitly understood as the contact between two phases with defined densities of charge-carrier donors and acceptors. The extent of overlap between the bands is relevant in predicting the rate of charge transfer. Accordingly, the Gerischer model requires development of the concept of densities of acceptor and donor states in solution [35].

Consider an ensemble of molecules A in solution with an average energy of $\mathbf{E_A}$. As described above, this energy describes the average orientation of the solvent shell and molecular structure of A. Brief fluctuations in the ordering/disordering of the solvent dipoles and the molecular structures of A will slightly alter the individual energies of each molecule A. In the original description [70, 72], the energy fluctuations were not ascribed to specific vibrational modes of the solvent or A. Rather, the key criterion was that the fluctuations were random. Such fluctuations would be expected at all $T > 0$ K where the available thermal energy for perturbations is "k_BT". The fluctuations move the energy of some molecules A to a value of $\mathbf{E}$. To be clear, these random fluctuations cancel out over time and do not alter $\mathbf{E_A}$ as the average energy. However, the square of the energy fluctuations (i.e., $(\mathbf{E_A} - \mathbf{E})^2$) will have a non-zero value. If the fluctuations are random, this squared energy displacement will be proportional to k_BT and follow the behavior of a harmonic oscillator, i.e., $k_BT = \frac{1}{2}K((\mathbf{E_A} - \mathbf{E})^2)$, where K is a "solvent force constant". [74] The "2λ" factor shown above (Fig. 27.7) defines the interaction, ($K^{-1} = 2\lambda$) [132, 133] since it represents the energy required for the solvent shell and coordination sphere to change by ± 1 [16, 110],

$$(\mathbf{E_A} - \mathbf{E})^2 = 4\lambda k_BT. \tag{27.52}$$

The value of "$4\lambda k_BT$" is then the barometer for the magnitude of energy fluctuations, i.e., it is the mean square value of the energy fluctuations.

The probability of finding molecule A with energy $\mathbf{E}$, $P(\mathbf{E})$, within an ensemble of non-interacting A molecules is defined by the mean square value of the energy fluctuations [134]. The normalizing factor in this case is "$(4\pi\lambda k_BT)^{1/2}$" [134],

$$P(\mathbf{E}) = \frac{e^{\frac{-(\mathbf{E_A}-\mathbf{E})^2}{4\lambda k_B T}}}{\sqrt{4\pi\lambda k_B T}} = \frac{e^{\frac{-q^2(E-E_A)^2}{4\lambda k_B T}}}{\sqrt{4\pi\lambda k_B T}}. \quad (27.53)$$

The density of molecules A with a particular energy **E**, $D(\mathbf{E})$, is then given by Eq. 27.54,

$$D(\mathbf{E}) = [A]\frac{e^{\frac{-(\mathbf{E_A}-\mathbf{E})^2}{4\lambda k_B T}}}{\sqrt{4\pi\lambda k_B T}} = [A]\frac{e^{\frac{-q^2(E-E_A)^2}{4\lambda k_B T}}}{\sqrt{4\pi\lambda k_B T}}. \quad (27.54)$$

Similarly, the density of molecules A^- with a given energy is given by Eq. 27.55,

$$D(\mathbf{E}) = [A^-]\frac{e^{\frac{-(\mathbf{E}-\mathbf{E_{A^-}})^2}{4\lambda k_B T}}}{\sqrt{4\pi\lambda k_B T}} = [A^-]\frac{e^{\frac{-q^2(E_{A^-}-E)^2}{4\lambda k_B T}}}{\sqrt{4\pi\lambda k_B T}}. \quad (27.55)$$

The functional forms of these distributions are depicted explicitly in Fig. 27.8b, where these distribution functions define the "bands" in the solution. Each Gaussian is centered at $\mathbf{E_A}$ and $\mathbf{E_{A-}}$, respectively, with a full width at half maxima equal to "$(4\lambda k_B T)^{1/2}$" and is separated from the other Gaussian by a factor of "2λ".

To be clear, the analogy of Eqs. 27.54 and 27.55 as defining electronic density of states is not unlimited. Unlike in a crystalline lattice where formal electronic bands arise from the overlap of stable, fixed chemical bonds, the faux solution "conduction band" described by Eq. 27.54 and the faux solution "valence band" described by Eq. 27.55 are transient in nature. That is, the distributions of A and A^- are a product of the random, brief interactions between the solvent and the redox molecules. Therefore, this band description does not imply the possibility of optical excitations to interconvert A and A^- [17, 124]. It should also not be considered a unique outcome of the ensemble description of energy fluctuations. Equations 27.53, 27.54, and 27.55 would still follow from the Marcus picture of Fig. 27.8a. That is, the probability of a molecule having an arbitrary free energy assuming a classical, parabolic free energy curve follows Boltzmann statistics. In this case, the partition function that defines the pre-exponential term is "$(4\pi\lambda k_B T)^{1/2}$" [135]. Accordingly, the solution band concept as developed by Gerischer is not in conflict with any aspect of the Marcus approach but rather is a useful complement for describing semiconductor/solution interfaces.

The essence of the Gerischer model for describing the solution with a band structure is visualized in Fig. 27.8c [74]. This diagram shows the same semiconductor/solution interface but in a hybrid form. This perspective still explicitly incorporates the band structure of the semiconductor, as routinely done for solid-state heterojunctions, in the form shown earlier in this chapter (i.e., the y-ordinate is electrochemical potential and the x-ordinate is a physical distance normal to the surface plane) [10]. However, implicit in Fig. 27.8b and c is the relation between free energy and electrochemical potential. One concept that Gerischer specifically advanced is that the density functions of Eqs. 27.54 and 27.55 can also naturally be understood in terms of electrochemical potentials (rather than just absolute energies), arguing that a thermodynamic cycle can relate the ionization energies of species in the gas phase with electrochemical potential energies of redox chemistry in solution. The idea is that although the two quantities are not equal, they scale linearly and that $E(A/A^-)$ can be a characteristic reference point to relate the two [72]. The thermodynamic cycle arguments are sufficiently nuanced that interested readers are encouraged to review the original text. However, one important point is that thermodynamic cycle argument rigorously only holds when the semiconductor and solution are equilibrated with each other. Away from equilibrium, the connection between applied electrochemical potential and system energies do not necessarily hold for all conditions (e.g., $\Delta E_{dl} \neq 0$ in Sect. 27.2.5; "hot" electron/hole transfer in Sect. 27.3.6). Those conditions notwithstanding, the central point here is that Eqs. 27.53, 27.54, and 27.55 can be expressed on the electrochemical potential scale with no loss of accuracy or meaning.

The solution side of Fig. 27.8c still plots electrochemical potential on the *y*-axis but the *x*-axis on this side of the interface is the density of states, again appearing as Gaussians oriented normal to the semiconductor/solution interface, centered at E_A and E_A^-, respectively. Their values, with respect to the semiconductor band edge potentials at the interface, are now clear.

In Fig. 27.8c, the midpoint value between E_A and E_A^- is the standard reduction potential of the redox couple, $E^0(A/A^-)$,

$$\frac{(E_A - E_{A^-})}{2} = E_A + \frac{\lambda}{q} = E_{A^-} - \frac{\lambda}{q} = E^0(A/A^-) \quad (27.56)$$

where E_A and E_{A^-} are offset from $E^0(A/A^-)$ by $\pm\lambda/q$. Accordingly, the magnitude of the reorganization energy can be represented by the widths and separations of the two energy state distributions. The driving force for electron and hole transfers $\Delta G^0_{et} = -q(E_{cb} - E^{0'}(A/A^-))$ and $\Delta G^0_{ht} = -q(E^{0'}(A/A^-) - E_{vb})$ are still apparent in this depiction. Finally, since [A] and $[A^-]$ are explicitly included in Eqs. 27.54 and 27.55, the relative heights of the energy state distributions in solution are also readily communicated (Fig. 27.9a–c).

In this depiction, the consequences of isoenergetic charge transfer at the semiconductor/solution interface become apparent. Figure 27.9d shows a scenario where the density of states for the A/A^- redox couple and the conduction band

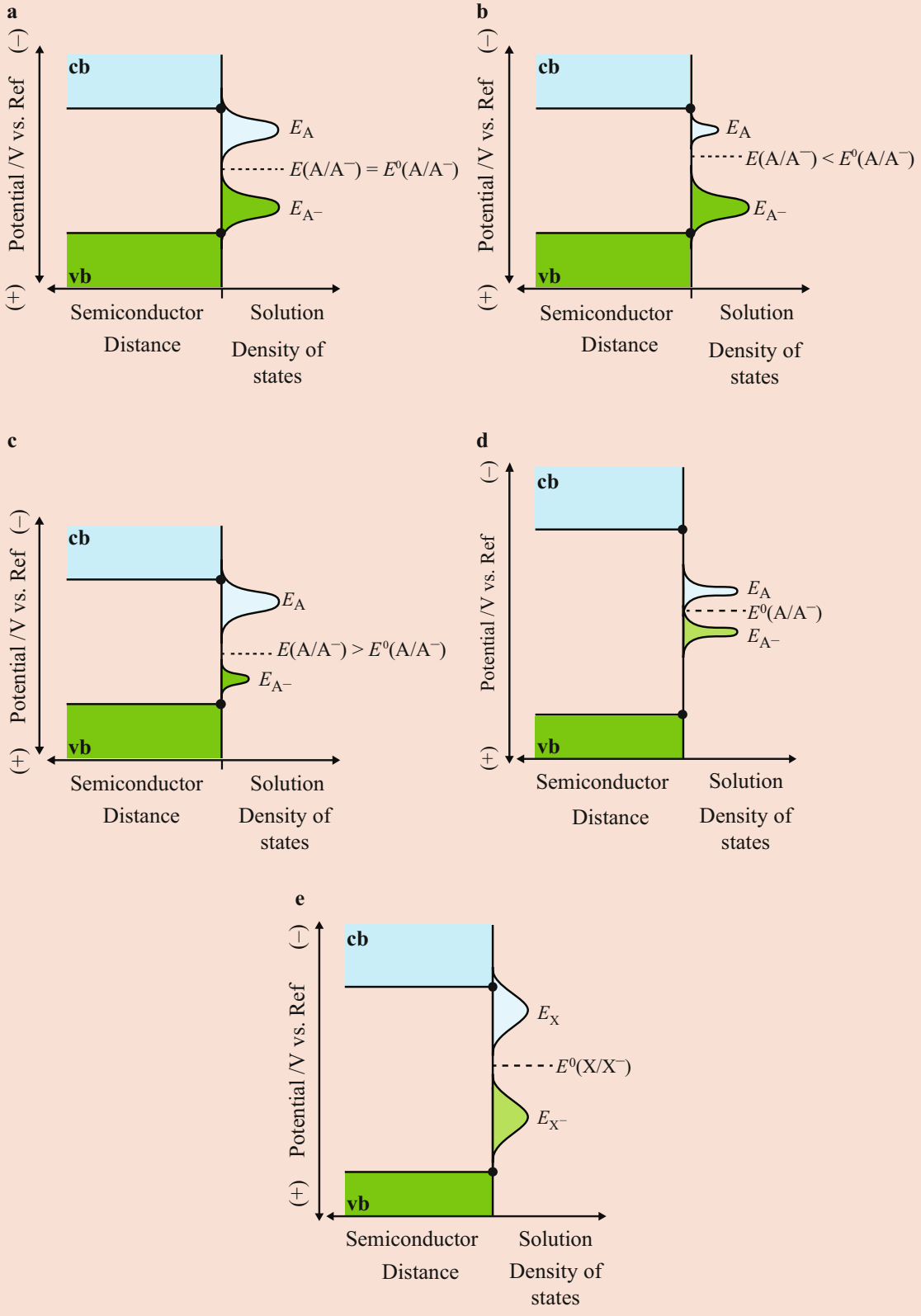

Fig. 27.9 (**a**–**c**) Schematic depictions using the Gerischer model of semiconductor/solution interfaces showing how the relative concentrations of A and A^- affect the "band structure" in solution. (**d**, **e**) Schematic depictions using the Gerischer model of semiconductor/solution interfaces with redox couples with either (**a**) small or (**b**) large values of λ but otherwise the same standard potential, $E^0(A/A^-)$

of the semiconductor exhibit negligible overlap, implying very slow electron transfer. Figure 27.9e shows the same semiconductor immersed in a solution where the X/X^- redox couple has the same standard potential but a larger reorganization energy. The larger λ widens and moves the distribution of potentials for molecules A to a more negative potential, leading to a faster rate of electron transfer from this semiconductor conduction band to molecules A in solution. However, since charge transfer can occur in parallel at every potential spanned by the conduction band, the observed rate is the sum of all of these individual rates. Correspondingly, interpreting the meaning of a single rate constant for the sum of many charge transfer events may not be obvious a priori and requires further development of the microscopic picture of charge transfer at semiconductor/solution interfaces.

27.3.4 Explicit Expressions for Electron and Hole Transfer at Semiconductor/Solution Interfaces

In their classical forms, both the Marcus and Gerischer perspectives are fundamentally similar. They both rely on the fluctuating energy concept to make equivalent predictions regarding the form of $\Delta G^{\ddagger}$ with respect to λ. Accordingly, both representations have been proven useful to the field of semiconductor electrochemistry. Still, in their simplest forms, both are best understood with the proviso that the actual charge transfer event is non-adiabatic. This concept is best described from the Marcus perspective and is captured in the insets of Fig. 27.8a. At the transition state, the diabatic curves intersect. For a non-adiabatic process, it is possible for the reactants to reach the transition state configuration but not undergo charge transfer. For an adiabatic process, the probability of conversion from the reactant state to the product state is unity, i.e., all energy fluctuations that effect the transition state will always result in charge transfer. This implies the reactants and product curves are strongly coupled. Specifically, the orbitals of the redox species interact with states in the semiconductor band, lowering the energy of the transition state by some amount relative to the non-adiabatic case. Quantitatively describing adiabatic reactions thus requires more details specific to each system. Assumption of non-adiabaticity simply means the error in the energy of the transition state is assumed to be small, i.e., it is at the intersection point of the two free energy curves.

In the Gerischer model, the forward electron transfer rate at potential E is proportional to the product of the density of electrons in the semiconductor at E, $\rho_n(E)$, and the density of molecules A at E,

$$v_{et,\rightarrow}(E) = \kappa_n(E) D_A(E) \rho_n(E), \tag{27.57}$$

where $\kappa_n(E)$ is a proportionality constant with units of $cm^4\ s^{-1}$. Similarly, the forward hole transfer rate at potential E is proportional to the product of the density of holes in the semiconductor at E, $\rho_p(E)$, and the density of molecules A^- at E,

$$v_{ht,\rightarrow}(E) = \kappa_p(E) D_{A^-}(E) \rho_p(E) \tag{27.58}$$

where $\kappa_p(E)$ is a proportionality constant with units of $cm^4\ s^{-1}$. These relations can be expanded, using Eqs. 27.54 and 27.55 for the $D(E)$ terms, and the definitions of $\rho_n(E)$ and $\rho_n(E)$ [10],

$$\rho_n(E) = N_n(E) F(E) = N_n(E) \frac{1}{1 + e^{\frac{q}{k_B T}(E_F - E)}} \tag{27.59}$$

$$\begin{aligned} \rho_p(E) &= N_p(E)(1 - F(E)) \\ &= N_p(E) \frac{e^{\frac{q}{k_B T}(E_F - E)}}{1 + e^{\frac{q}{k_B T}(E_F - E)}} \end{aligned} \tag{27.60}$$

where $N_n(E)$ is the number of total states occupied by an electron at potential E, $N_p(E)$ is the number of states occupied by a hole at potential E, and $F(E)$ is the Fermi function that defines the occupancy of states at E_F. The total rate of electron transfer from the semiconductor conduction band into solution can then be understood by summing up the individual rates at all potential values,

$$\begin{aligned} v_{et,\rightarrow} = \int_{\infty}^{-\infty} \kappa_n(E)[A] \frac{e^{\frac{-q^2(E-E_A)^2}{4\lambda k_B T}}}{\sqrt{4\pi\lambda k_B T}} N_n(E) \\ \times \frac{1}{1 + e^{\frac{q}{k_B T}(E_F - E)}} dE. \end{aligned} \tag{27.61}$$

The total rate of hole transfer from the semiconductor valence band into solution can be similarly expressed as,

$$\begin{aligned} v_{ht,\rightarrow} = \int_{\infty}^{-\infty} \kappa_p(E)[A^-] \frac{e^{\frac{-q^2(E_{A^-}-E)^2}{4\lambda k_B T}}}{\sqrt{4\pi\lambda k_B T}} N_p(E) \\ \times \frac{e^{\frac{q}{k_B T}(E_F - E)}}{1 + e^{\frac{q}{k_B T}(E_F - E)}} dE. \end{aligned} \tag{27.62}$$

Several aspects can simplify Eqs. 27.61 and 27.62. First, in Figs. 27.8 and 27.9, current flow across the semiconductor/solution interface can visually be understood as not occurring at potentials more positive than E_{cb} because there is no electron density in the semiconductor at more positive potentials. Accordingly, since the integral is zero for $E > E_{cb}$, the bounds for integration can be simplified to $E = E_{cb}$ to $E = -\infty$. Second,

if charge-carriers are thermalized, then the only appreciable rates for charge-transfer will occur at potentials near the band edges. For electron transfer from the semiconductor conduction band, the relevant potential range then spans just from E_{cb} to "$E_{cb} - 2k_BT$" and for hole transfer from the semiconductor valence band, the relevant potential range spans from E_{vb} to "$E_{vb} + 2k_BT$". Over this potential range, the value of the exponential term for the density of molecules is roughly constant and can be pulled out of the integral, with E set explicitly to either E_{cb} or E_{vb}, respectively. Similarly, the values of $\kappa(E)$ over this small range can be considered constant and so these κ terms can be moved outside of the integral (with units of eV cm^4 s^{-1}). Third, the remaining integrals in Eqs. 27.61 and 27.62 represent the total electron and hole concentrations at the surface, n_s and p_s, respectively (i.e., $\int_{E_{cb}}^{-\infty} N_n(E) \frac{1}{1+e^{\frac{q}{k_BT}(E_F-E)}} dE \equiv n_s$; $\int_{\infty}^{E_{vb}} N_p(E) \frac{e^{\frac{q}{k_BT}(E_F-E)}}{1+e^{\frac{q}{k_BT}(E_F-E)}} dE \equiv p_s$). When E_F is within the semiconductor bandgap, then the solutions to these integrals are the Boltzmann expressions of Eqs. 27.2. Accordingly, the rate expressions for electron and hole transfer from the semiconductor into solution are simplified,

$$v_{et,\rightarrow} = \kappa_n[A] \frac{e^{\frac{-q^2(E_{cb}-E_A)^2}{4\lambda k_BT}}}{\sqrt{4\pi\lambda k_BT}} n_s \tag{27.63}$$

$$v_{ht,\rightarrow} = \kappa_p[A^-] \frac{e^{\frac{-q^2(E_{A^-}-E_{vb})^2}{4\lambda k_BT}}}{\sqrt{4\pi\lambda k_BT}} p_s. \tag{27.64}$$

Comparison of Eqs. 27.63 and 27.64 with Eqs. 27.6 and 27.9 show the explicit terms that constitute k_{et} and k_{ht},

$$k_{et} = \frac{\kappa_n}{\sqrt{4\pi\lambda k_BT}} e^{\frac{-q^2(E_{cb}-E_A)^2}{4\lambda k_BT}} \tag{27.65}$$

$$k_{ht} = \frac{\kappa_p}{\sqrt{4\pi\lambda k_BT}} e^{\frac{-q^2(E_{A^-}-E_{vb})^2}{4\lambda k_BT}} \tag{27.66}$$

where the Arrhenius-Eyring form is evident.

27.3.5 Franck-Condon Factor and the Inverted Region

In one sense, the assumption that the solution density-of-states term is energy independent is just a further expression of the Franck-Condon principle. Only the local molecular structures around A (for electron transfer) and A$^-$ (for hole transfer) at the band edge potentials are relevant since the charge transfer events occur predominantly just at the band edge potentials. In fact, the exponential term is often referred to as the nuclear or Franck-Condon factor [136–138]. However, this assumption also has a more profound consequence on the values of k_{et} and k_{ht}. The Franck-Condon term satisfies the Arrhenius condition, where the rate constant is proportional to an activation energy defined by the exponent. However, the form of the activation energy in charge-transfer reactions is different than activation energies in other chemical reaction rate constants.

As written, the activation energies for k_{et} and k_{ht} are given in terms of E_A and E_{A^-}. Since these potentials are not directly measurable quantities, the activation energies can be recast in terms of the readily observable term $E^0(A/A^-)$ using the equalities in Eq. 27.56,

$$\begin{aligned} k_{et} &= \frac{\kappa_n}{\sqrt{4\pi\lambda k_BT}} e^{\frac{-q^2\left(E_{cb}-E^0(A/A^-)+\frac{\lambda}{q}\right)^2}{4\lambda k_BT}} \\ &= \frac{\kappa_n}{\sqrt{4\pi\lambda k_BT}} e^{\frac{-\left(\Delta G^0_{et}+\lambda\right)^2}{4\lambda k_BT}} \end{aligned} \tag{27.67}$$

$$\begin{aligned} k_{ht} &= \frac{\kappa_p}{\sqrt{4\pi\lambda k_BT}} e^{\frac{-q^2\left(E^0(A/A^-)-E_{vb}+\frac{\lambda}{q}\right)^2}{4\lambda k_BT}} \\ &= \frac{\kappa_p}{\sqrt{4\pi\lambda k_BT}} e^{\frac{-\left(\Delta G^0_{ht}+\lambda\right)^2}{4\lambda k_BT}}. \end{aligned} \tag{27.68}$$

Here the activation energies are now readily understood from experimental observables. Specifically, the difference between the measured band edge potentials and the standard potential of the redox couple define the charge transfer driving forces (vide infra).

The expressions in Eqs. 27.67 and 27.68 identify one of the most unique and consequential aspects of the Marcus and Gerischer models for semiconductor/solution interfaces: the values of k_{et} and k_{ht} are **not** monotonic with respect to the reaction driving force. Instead, they have a maximum value when $\Delta G^0 = -\lambda$. At this specific condition of optimal exoergicity, the activation barrier is zero. The rate constants attain a maximum value since only the pre-exponential term remains. At any other value of the reaction driving force, the maximum rate constant value is attenuated by the exponential term. This unusual functional dependence was controversial. Although in retrospect multiple charge-transfer models predict such behavior [117, 139, 140], models based on the fluctuating energy level concept have been the most convincing on this point [110, 111, 141–143].

Since the reorganization energy and band edge potentials are clear in the Gerischer depiction of semiconductor/solution interfaces, the nonlinear dependences of k_{et} and k_{ht} with ΔG^0 can be readily understood graphically. Figure 27.10 depicts the Gerischer model for four different ideal semiconductor/

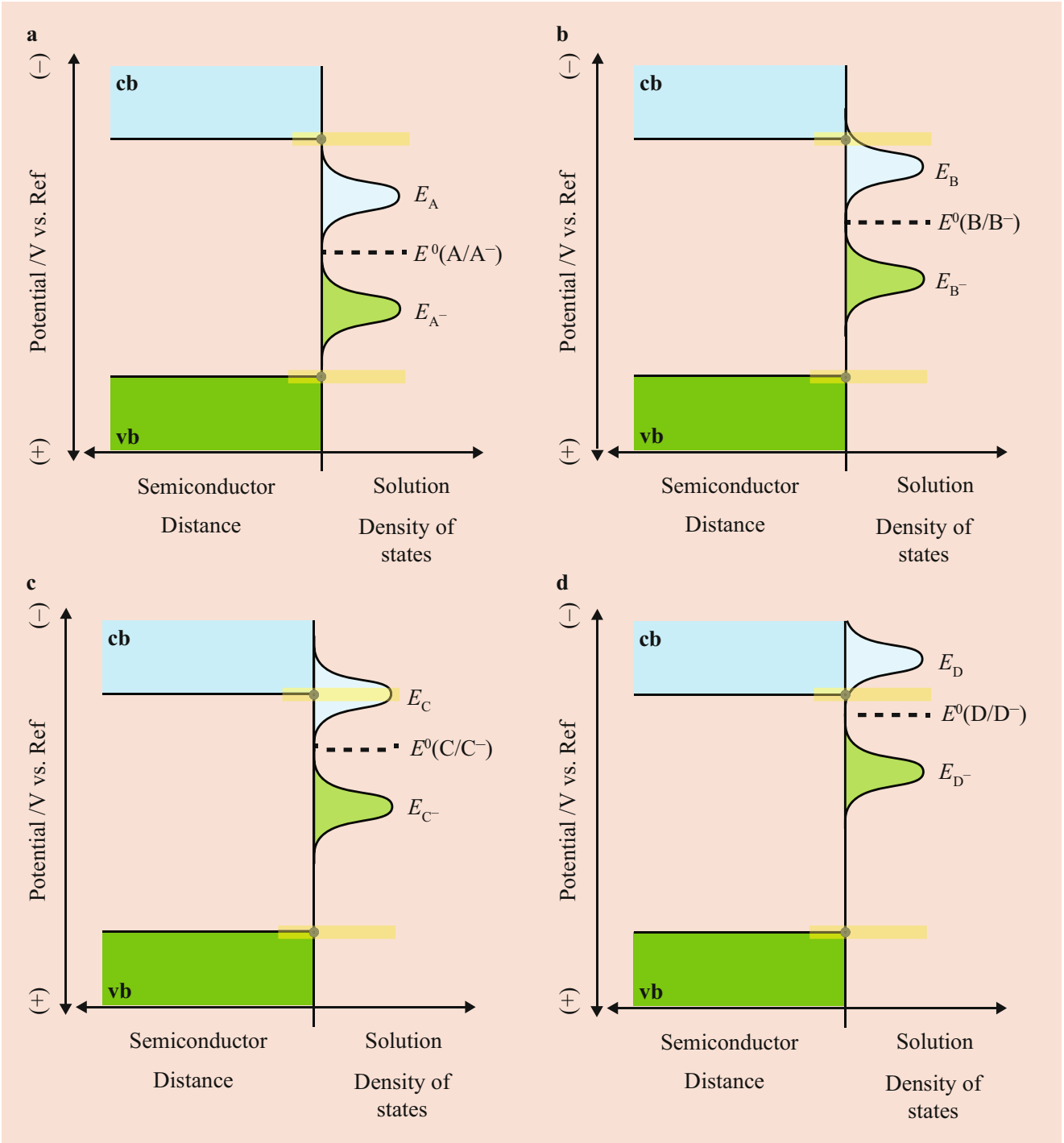

Fig. 27.10 Schematic depictions using the Gerischer model for four related semiconductor/solution interfaces, where the semiconductor is the same but the standard potential of the redox couples (A/A^-, B/B^-, C/C^-, and D/D^-) is progressively more negative. The yellow bars highlight the overlap between the semiconductor and solution bands at the band edge potentials. In this depiction, the C/C^- redox couple is expected to yield the largest k_{et} value since the overlap with the conduction band at the band edge is the greatest. The overlap with the valence band is minimal for all these redox couples, implying k_{ht} should be small for all

solution interfaces, where the properties of the semiconductor are kept constant and all three redox couples (A/A^-, B/B^-, C/C^-, D/D^-) have the same reorganization energy. In Fig. 27.10, the yellow bars highlight the overlap of the solution density of states at the band edge potentials. The redox couples only differ in their standard potentials, with $E^0(A/A^-) > E^0(B/B^-) > E^0(C/C^-) > E^0(D/D^-)$ but none are more negative than E_{cb}. For all these interfaces, the overlap between the

semiconductor valence band and the solution valence band is negligible. Accordingly, in all cases, only electron transfer from the semiconductor conduction band is operative. For the redox couple A/A^-, the overlap between the conduction bands at E_{cb} is small. Accordingly, the respective electron transfer rate constant is expected to be small. For redox couples B/B^- and C/C^-, the overlap gets progressively larger since these redox couples occur at increasingly more negative potentials. For the C/C^- redox couple, the overlap is maximized since $\Delta G^0 = -\lambda$. The further negative shift of the D/D^- redox couple acts to decrease the conduction band overlap. Thus, k_{et} for this redox couple will be proportionally smaller.

The diminution of k_{et} and k_{ht} when $\Delta G^0 < -\lambda$ is commonly described as "inverted" behavior [119, 144–147]. Although a natural consequence of the fluctuating energy level concept, the experimental observation of smaller rate constants when a large (relative to λ) reaction driving force is applied has historically proved difficult. For homogeneous charge transfer reactions, measuring rate constants under conditions approaching the "$\Delta G^0 = -\lambda$" criterion requires rate measurements typically much faster than the limit imposed by diffusion of reactants [148]. Accordingly, the apparent rate constant values often reach a limiting value as the reactions became more exoergic, exhibiting so-called Rehm-Weller behavior [149]. For heterogeneous charge transfer reactions at metal/solution interfaces, two problems are encountered. Again, the diffusion of redox species to the electrode surface can impose a limit on the fastest rates (currents) that can be measured. However, more profoundly, the continuum of available states in a metal ensures charge transfer is never slow at large reaction driving forces. Simply, at a metal, charge transfer will always be dominated by states below the Fermi level with optimal potential (energy) values. In this way, even in the absence of the diffusion limit, plots of the rate constant vs driving force are plateaued rather than parabolic [150–152].

In this regard, semiconductor electrochemistry has proven useful. Since (for an ideal semiconductor electrode) charge transfer occurs from only the band edges, the complication of a continuum of available states incurred with metal electrodes is not an issue with semiconductor electrodes. That is, irrespective of the applied potential, charge transfer occurs at the band edge (rather than at the quasi-Fermi level). Although the diffusion of species to the electrode surface is still problematic, it is not prohibitive for rate constant measurements since charge transfer occurs only at the band edge potentials (for an ideal semiconductor). A series of rate measurements were obtained by Morrison and co-workers that showed compelling evidence of "inverted" behavior for n-ZnO immersed in aqueous solutions with redox species possessing very positive standard potentials [153]. Current-potential responses collected at currents less than the mass-transport-limited current, when extrapolated to the potential where there is no band bending within the semiconductor, yielded data suggestive of smaller values of k_{et}. Unfortunately, the interpretation was complicated by large uncertainties in the reorganization energies of the employed redox couples. Nevertheless, these measurements were consistent with theory predictions and actually preceded the more-cited studies of tethered donor-acceptor molecules and solvated electron reactions [145, 154–157] that are credited for proving the existence of an "inverted region". Later measurements with n-Si in nonaqueous solvents [98, 158] and n-ZnO in aqueous solutions [128, 159, 160] further supported the observation of "inverted" behavior and reaffirmed the utility of semiconductor/solution interfaces for fundamental understanding of charge transfer processes.

To date, all the available current-potential data collected for semiconductor/solution contacts suggest that the shape of the "inverted region" for heterogeneous charge transfer reactions follows the classical form of the energy fluctuation model. Figure 27.11a depicts the semi-logarithmic plot of k_{et} (or k_{ht}) vs ΔG^0 assuming only classical mechanics, where the plot is symmetric and is centered at $\Delta G^0 = -\lambda$. In the classical case, there are no distinguishing features between reactions with small and large driving forces. Interestingly, the classical model has been demonstrated repeatedly as insufficient to describe the kinetic data of homogeneous charge-transfer reactions. Often asymmetric $\ln k$ vs $-\Delta G^0$ plots are observed, where the rate constant is larger than expected for strongly exoergic reactions [128, 159–161]. Based on compelling data [162], the prevailing rationale is when $-\Delta G^0 > \lambda$, the classical energy fluctuation concept does not accurately describe all real systems. Specifically, the high energy vibrational states of the reactants becomes relevant in dictating the rate of charge transfer. Quantum mechanical approaches [163] are necessary to describe the solvent/molecule environment. A general conclusion from such work is that large excess driving forces can facilitate nuclear tunneling between the reactant and product states. That is, specific molecular motions couple with electron transfer (i.e., "vibronic" states), lowering the effective activation energy for charge-transfer (Fig. 27.11b). The excess reactant driving force lowers the barrier for nuclear tunneling (i.e., electron transfer occurs along with a change along the reaction coordinate). This aspect facilitates larger charge transfer rate constants than the classical case with the same ΔG^0 [137, 148, 162, 164–167], resulting in a less steep "inverted" region in $\ln k$ vs ΔG^0 plot (Fig. 27.11a).

One practical reason why only classical behavior has been observed in semiconductor electrochemistry is that comparatively few semiconductor/solution interfaces have been sufficiently studied, particularly in the absence of complications. Beyond the complexities associated with interfacial surface states (Sect. 27.2.5), the uncertainty in rate constant measurements by the method of Morrison [153] and Gomes [168]

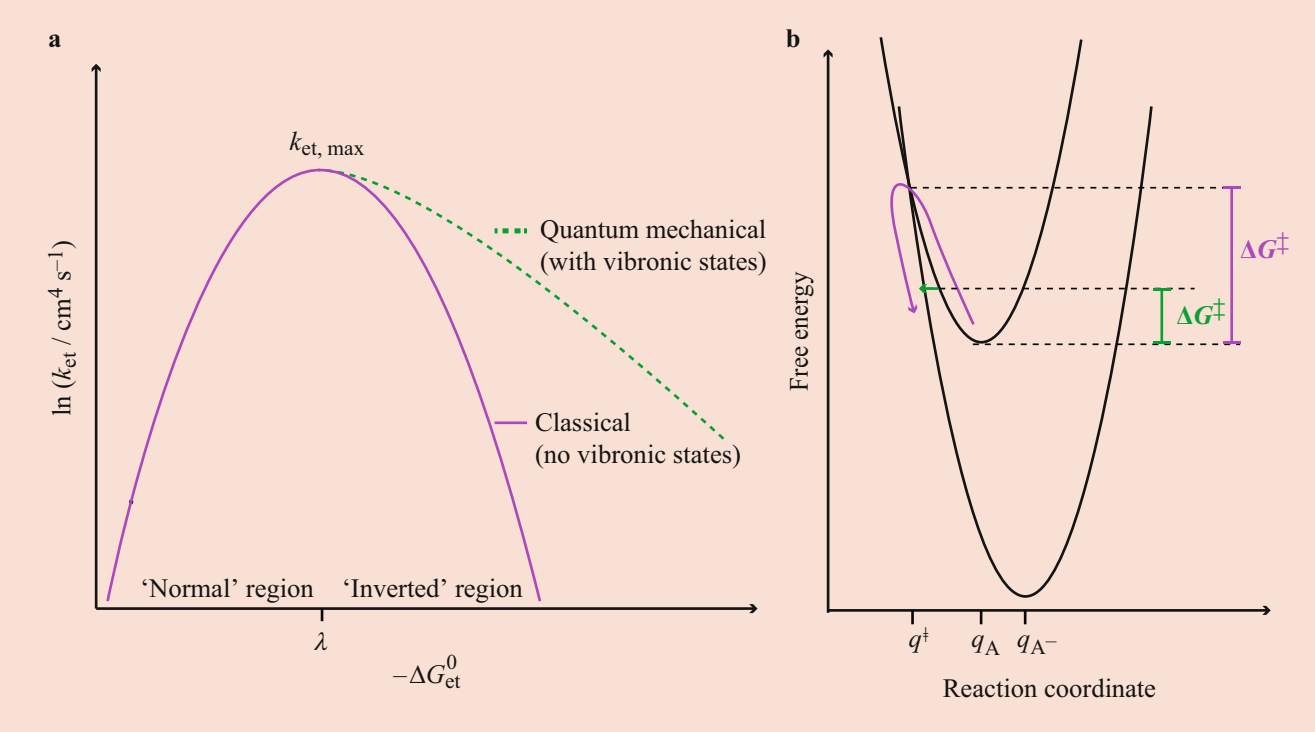

Fig. 27.11 (**a**) An idealized depiction of the expected dependence of k_{et} with $-\Delta G^0_{et}$. Models assuming classical interactions between the electrode and redox species predict parabolic plots of ln k_{et} vs $-\Delta G^0_{et}$. Models that incorporate the participation of vibronic states predict a shallower decrease in ln k_{et} at larger values of $-\Delta G^0$. (**b**) Free energy vs reaction coordinate diagrams of a spontaneous electron transfer event as described in the Marcus model occurring in the "inverted" region, i.e., $-\Delta G^0_{et} \gg \lambda$. The purple arrow represents the classical trajectory from the reactant diabatic surface to the transition state to the product diabatic surface, with $-\Delta G^{\ddagger}$ indicated. The green arrow represents a different trajectory from the reactant state to the product state where nuclear tunneling between diabatic curves occurs. The activation energy for this process is also indicated

may be large enough to mask the possibility of this aspect. Undoubtedly, the uncertainties in capacitive measurements of band edge potentials and in the reorganization energies of redox species decrease the precision in estimates of rate constants. Alternate approaches for making k_{et} and k_{ht} measurements would be valuable in this regard. One intriguing method is to fabricate semiconductor/solution contact areas small enough that the probability of the occurrence of a surface state becomes negligible and the possibility of larger numbers of repetitive measurements is greater [169]. Other reflectance spectroscopies for studying electrode interfaces may also prove useful in this regard [170].

A separate argument may be the observations are coincidental, i.e., classical models of charge transfer do not fully capture all relevant aspects of charge-transfer, even for putative outer-sphere redox processes. Work has been done to understand electron transfer at semiconductor electrodes without relying on any of the aforementioned assumptions and simplifications. For example, one study modeled n-type InP electrodes immersed in aqueous solutions of metal aquo complexes, using electronic structure calculations to determine $P(E)$ for the redox couple in solution [171–173]. Such calculations indicated that coupling between the electrolyte and the semiconductor through solvent is possible and suggested that the representation of the solution density of states as a Gaussian is inaccurate. More critically, these studies have argued that charge transfer at the semiconductor/solution interfaces intrinsically represents a transition between a discrete molecular state to a continuum of states in the semiconductor, an aspect that is not captured at all in the classical charge transfer models [174]. The modeling approaches advocated in these works have not been widely applied to other semiconductor/solution systems, have not shed light more generally on "inverted" behavior at semiconductor/solution interfaces, and remain to be supported by experimental observations. Nevertheless, such studies argue the dependences of k_{et} and k_{ht} on reaction driving force may not be simple to predict for all redox species.

27.3.6 Upper Bounds on Rate Constant Values

As described above, the Franck-Condon factor determines how the operative rate constants are attenuated when the conditions for charge transfer are not optimal. However, when $\Delta G^0 = -\lambda$, all charge transfer models based on the

fluctuating energy level concept, either classical or quantum mechanical, predict maximal rate constants for electron and hole transfer at semiconductor/solution interfaces. At this condition, charge transfer is activationless and only the electronic details of tunneling between reactants and products at the transition state dictate how fast charge is exchanged. The values of k_{et} and k_{ht} at the optimal exoergicity condition are explicitly the pre-exponential factors in Eqs. 27.67 and 27.68. Here, they are denoted as $k_{et,max}$ and $k_{ht,max}$,

$$k_{et,\,max} = \frac{\kappa_n}{\sqrt{4\pi\lambda k_B T}} \tag{27.69}$$

$$k_{ht,\,max} = \frac{\kappa_p}{\sqrt{4\pi\lambda k_B T}} \tag{27.70}$$

In the original Gerischer description of charge-transfer, the values of $k_{et,max}$ and $k_{ht,max}$ were not explicitly evaluated [19, 120]. Rather, the κ terms were cast as just quantum mechanical tunneling factors, representing the electronic coupling between the semiconductor and redox species [74]. Gerischer later advanced two approaches to describe $k_{et,max}$ and $k_{ht,max}$ in detail. One view held that the rate constants were simply the product of three separate terms [77]. The first component was a geometric factor, representing the number of pairs of charge-carriers and redox molecules close enough to react. This number was estimated from the product of the average distance between the redox species & the semiconductor surface ($\delta \sim 10^{-8}$ cm) and the hemispherical volume ($2/3\pi r^3 = 10^{-21}$ cm^3, where r is the maximum distance from the interface to which the wave function of an electron can interact with the redox species) within the semiconductor from which charge carriers interact with solution. The second term encompassed an attempt frequency for molecular motions along the reaction coordinate to reach the transition state configuration ($\sim 10^{13}$ s^{-1}) [175]. The third term is a unit-less fraction that describes the electronic overlap between the semiconductor and the redox species, using a Landau-Zener approximation for transfer between two discrete states [175]. A deficiency of this approach is the large uncertainty in both the interaction volume in the semiconductor and the values of the electronic factor, where the validity of the Landau-Zener approximation (i.e., the interaction of two discrete states) has been called in to question [173, 174]. The second approach to determine $k_{et,max}$ and $k_{ht,max}$ followed the formalism used to describe current flow across solid-state heterojunctions [3, 16, 74, 77]. Specifically, $k_{et,max}$ and $k_{ht,max}$ were cast as the product of the velocity of charge carriers inside the semiconductor ($\sim 10^7$ cm s^{-1}), the cross section of interaction (taken to be the area of an ion, $\sim 10^{-15}$ cm^2), and the average distance between the redox species and the semiconductor surface ($\delta \sim 10^{-8}$ cm). These two approaches both suggest that the maximum rate constants are $\sim 10^{-16}$ cm^4 s^{-1}.

Separate work on developing $k_{et,max}$ and $k_{ht,max}$ more explicitly using the Marcus description has been reported [3, 176]. The interaction between charge-carriers within a semiconductor and redox species in solution has been treated as analogous to charge transfer between molecules at the interface between immiscible liquids [3, 177]. In this way, an explicit expression originally developed by Marcus [177] could be adapted for k_{et} at semiconductor/solution interfaces,

$$k_{et,\,max} = \frac{2\pi f_{et}}{\beta^3}(r_A + r_e) \tag{27.71}$$

where r_A is the radius of A ($\sim 10^{-8}$ cm), r_e is the effective radius of an electron in the semiconductor (10^{-7} cm), f_{et} is the attempt frequency for reaching the transition state (10^{13} s^{-1}), and β is an attenuation factor for electron tunneling across a distance ($\sim 10^8$ cm^{-1}). Accordingly, the maximum rate constant value predicted by this model is 10^{-17} cm^4 s^{-1} [178–180]. This approach has the advantage that, aside from f, all the terms are explicitly measurable. A critical assumption is that electrons (and holes) can be treated as hard spheres, with no associated reorganization energy. The validity of the assumption of electrons as hard spheres and the ambiguity of the distance at closest approach in this model has been raised [181].

An alternative method for predicting k_{et} and k_{ht} based on quantum mechanics has been described [138, 182]. In this approach, the rate constant is estimated directly from the probability of a transition occurring between two states. This probability is explicitly given by the value of electronic coupling between the semiconductor and acceptor in solution (i.e., Fermi's golden rule [183]). For electron transfer, the value of $k_{et,max}$ is given by Eq. 27.72,

$$k_{et,\,max} = \frac{4\pi^2}{h\sqrt{4\lambda k_B T}} \frac{V}{\beta} \frac{l_{sc}}{d_{sc}^{2/3}\left(\frac{6}{\pi}\right)^{1/3}} \tag{27.72}$$

where h is Planck's constant, V is the matrix coupling element observed at the distance of charge transfer averaged over all states at each E and across the semiconductor surface ($\sim 10^{-2}$ eV^2 per state), l_{sc} is an effective coupling length between the semiconductor surface & acceptor ($\sim 10^{-8}$ cm), and d is the atomic density of the semiconductor. The appeal of this formalism is it can be applied also to metal/solution interfaces. Doing so affords quantitative comparison between the two types of solid/solution junctions, enabling specific estimates of charge transfer rates for semiconductor electrodes from measurements recorded with metal electrodes. Accordingly, the implications of Eq. 27.72 have been assessed in two distinct ways. In one report, $k_{et,max}$ was evaluated for specific semiconductor/solution systems by calculating explicit V values [178, 179]. In a separate study, Eq. 27.72 was assessed through comparisons with analogous expressions for metal

electrodes, where a greater abundance of experimental data exists [138]. Both studies indicated the Fermi Golden Rule approach is consistent with $k_{et,max} = 10^{-16} - 10^{-17}$ cm^4 s^{-1}.

The paucity of experimental data for k_{et} and k_{ht} at semiconductor/solution junctions makes fuller tests of these models difficult. In fact, the majority of data is focused only on k_{et} since measuring k_{ht} invariably incurs parallel corrosion processes [73, 184]. There are experimental reports that suggest the maximum rate constant values are larger than predicted [185–188]. However, such studies do not follow the predictions of rate measurements that are first order in [A] and n_s (i.e., Eq. 27.24). Within the subset of studies where the current-potential responses do comport with these conditions, the data appear to be globally consistent with the premise that $k_{et,max} \leq 10^{-16}$ cm^4 s^{-1} [98, 128, 158–160, 169, 176, 180, 189].

Several experimental challenges have contributed to the difficulty in accumulating unambiguous measurements of rate constants at semiconductor/solution interfaces. First, as described elsewhere in this chapter, the possible participation in heterogeneous charge transfer by surface states is difficult to avoid. This complexity can be appreciated by considering the number of available states at the band edges at the semiconductor/solution interface. For many semiconductors, the effective density of states at the band edge is ~10^{19} cm^{-3}. Assuming that the average coupling length between redox molecules in solution and the semiconductor surface (δ) is ~10^{-8} cm, a reasonable estimate of the surface density of states at the band edges is ~10^{11} cm^{-2} [178]. For surface atom densities of 10^{15} cm^2, this estimate suggests that surfaces with defect densities of 1 per 10,000 atoms or higher will have comparable or greater densities at the potential(s) of surface states than at the band edge potentials. The problem is even more severe for semiconductors with lower effective density of states (e.g., $N_{cb,InP} = 10^{17}$ cm^{-3}) [178], indicating for some systems the demands for effective surface passivation are steep before unambiguous rate measurements can be made. Second, the steady-state method of Morrison [16, 153] and Gomes [168] for rate studies at semiconductor/solution interfaces does not directly measure k_{et} (or k_{ht}). Rather, the rate constants are inferred through extrapolation back to the specific potential where the built-in potential is zero and $n_s = N_{cb}$ for n-type electrodes ($p_s = N_{vb}$ for p-type electrodes). As described above, precise current measurements at this potential are often limited by the rate of mass transport of solution species to the electrode surface and uncertainties in the extrapolation can propagate to large errors in k_{et} or k_{ht} estimates [190]. Third, time-dependent electrochemical measurements do not necessarily report on heterogeneous charge transfer, as they are often limited by the *RC* time constant of the electrode/solution interface and/or do not follow charge-transfer processes directly [3]. Fourth, even for ideal semiconductor/solution interfaces, the potential drop across the solution double layer is not necessarily negligible at the potentials required for unambiguous determination of k_{et} or k_{ht} [16, 38, 100]. Fifth, adsorption of the redox species on the electrode can severely complicate interpretation. Adsorption necessarily changes the effective concentration of redox species at the interface and likely the coupling between the semiconductor and solution species. Since adsorption puts the redox species in direct contact with the semiconductor, the assumption of weak coupling during charge-transfer may no longer be valid.

The possibility of adsorption has been cited as a source of uncertainty in a series of k_{et} measurements [188, 191, 192]. In fact, the premises that adsorption never occurs at the semiconductor/solution interface for putative outer-sphere redox species and that the non-adiabatic assumption is generally valid have been questioned [171–173, 181]. Abandoning these assumptions requires revisiting the validity of the Marcus and Gerischer equations presented above for estimating k_{et} [171–173]. Specifically, some work has been performed to replace the use of a single parameter (λ) to describe the interactions between the redox species, solvent, and semiconductor with a comprehensive, first principles approach based on molecular dynamics and extended Huckel theory [171]. This work suggests that the electronic coupling between semiconductor electrodes and redox molecules is dynamic and depends strongly on the orientation and position of the redox molecules relative to the interface. Doing so has led to noticeably larger predictions for $k_{et,max}$ ($\leq 10^{-14}$ cm^4 s^{-1}) [191], a prediction at odds with the models presented above but compatible with the Onsager model for charge transfer at semiconductor/solution interfaces [56]. Still, the use of such comprehensive tools for describing charge transfer at semiconductor/solution interfaces have not been widely adopted and no definitive experimental measurements have yet been collected to indicate conclusively that large values of k_{et} or k_{ht} are regularly incurred for putative outer-sphere redox species.

Even within the classical framework, the notion that a single λ value should be replaced with separate reorganization energies for the reduced and oxidized forms of some redox couples (i.e., $\lambda_A \neq \lambda_A$) has been discussed [111, 193–195]. Additionally, the idea that λ is affected by the specific nature of the semiconductor electrode surface morphology has been proposed [196], where the operative dielectric constant (as used in Eq. 27.49) is sensitive to variations in roughness at the nanoscale. Variations in the effective dielectric constant at the interface could accelerate or decelerate the observed rate of charge-transfer. It is presently unclear what role, if any, these aspects play in the rate measurements performed on semiconductor/liquid junctions to date.

To be clear, the possibility of extremely fast, non-adiabatic charge transfer reactions in semiconductor electrochemistry are not without precedent, even within the conventional Marcus and Gerischer frameworks. The most well-known cases of

ultra-fast charge transfer involve charge injection from excited vibrational modes of attached/adsorbed dyes into the conduction band of the semiconductor [197–204]. While charge transfer from semiconductors into molecules in solution has been discussed occurring only at potentials approximately $\pm 2k_BT/q$ of the band edge potential [74], the inverse process is not necessarily true in dye sensitized charge transfer [200]. Dye sensitization can occur through unoccupied states well above or below the conduction and valence band edges, respectively, from short-lived excited states of dye molecules (Fig. 27.12a). One recent example has shown with time-resolved spectroscopy that charge transfer between a photoexcited dye and a semiconductor [200, 205] can occur at short timescales (10^{-15} s), much faster than the timescale for intermolecular relaxations (10^{-13} s). To put in context, extremely rapid charge-transfer rates were previously thought to be hallmarks specifically of strongly coupled, adiabatic processes [206]. However, in this study evidence of vibronic coupling strongly indicated the process was non-adiabatic. This work, in conjunction with related sensitized studies [207], further suggests that purely classical models are insufficient for strongly driven, exoergic heterogeneous charge transfer reactions at semiconductor electrodes.

Time-resolved spectroscopic measurements are not the only instances of fast charge-transfer events (and by inference, large rate constants) semiconductor electrode interfaces. A specific study demonstrated plausible evidence for "hot" electron transfer from a semiconductor electrode into solution redox species [99, 208]. Figure 27.12b summarizes the premise, where photoexcitation of the p-type semiconductor generated excited electron/hole pairs. In doped semiconductors, the timescale for thermal relaxation of the "hot electron" to the band edge is ~10^{-11} s. For a moderately doped semiconductor, all photoexcited electrons thermalize (blue arrow) well before they reach the interface and are emitted from the band edge potential. However, for a heavily doped semiconductor where the depletion width is sufficiently thin, the thermalized electron could tunnel through the depletion region and react with solution species at a potential much more negative than the band edge. Indirect evidence for this scenario was observed for the reduction of a metal complex to zero valent metal clusters only occurring under the conditions of degenerate doping and illumination for the p-type electrode [99, 208]. These data suggest that the reduction process occurred with a rate constant different than k_{et}, as defined above but with a magnitude yet to be characterized or understood.

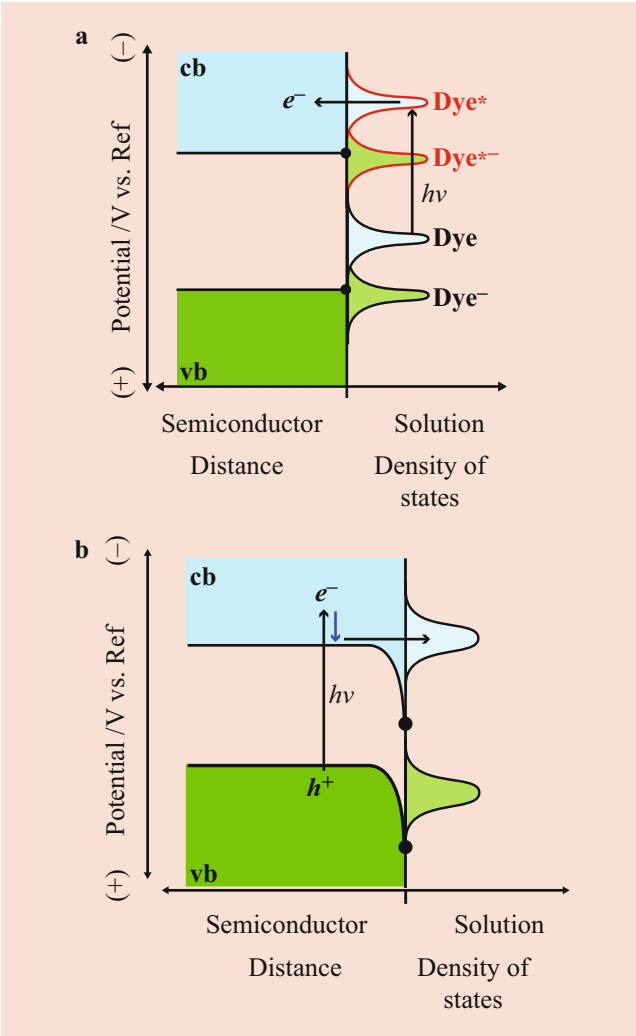

Fig. 27.12 (**a**) Idealized depiction of light stimulated, sensitized charge transfer from a dye molecule into the conduction band of a semiconductor at a potential more negative than the band edge. (**b**) Idealized depiction of the possibility of "hot" (i.e., unthermalized) electron transfer at a degenerately doped semiconductor electrode, where electron tunneling through the depletion region affords charge transfer at potentials more negative that the conduction band edge

27.4 Summary

This chapter summarized many of the basic ideas underpinning the operation of semiconductor electrodes immersed in electrolyte solutions. The text is not an exhaustive listing of the many careful and thought-provoking works on any of the presented topics, so readers are encouraged to consult the cited literature and references contained within for more detail. However, two important points to take from this overview are that even the most basic aspects of semiconductor electrochemistry have taken time to develop and that several unresolved questions still remain.

As has been the case for the past decade, a push in the field of semiconductor electrochemistry is to move away from "ideal" interfaces and instead develop non-ideal semiconductor/solution interfaces. Attaining "ideality" is not just difficult, but complex, non-ideal semiconductor electrode interfaces can actually offer many tangible, practical

advantages. For example, deliberately "complicating" the chemistry and composition of a semiconductor/solution interface can perhaps solve the longstanding issues in corrosion susceptibility [209–212]. Understanding the design principles of non-ideal semiconductor electrodes, however, requires understanding of even more diverse and nuanced concepts. With this in mind, it cannot be over-stated how enabling and useful a basic understanding of "simple," "ideal" semiconductor photoelectrochemistry is. Without the insight and appreciation of the operating principles, the probability of designing an optimal, non-ideal photoelectrochemical system will likely remain low, particularly for electrochemical transformations that involve more complexity than outer-sphere reactions. Accordingly, a deep understanding of how to manipulate k_{et} and k_{ht} purposely for practical electrochemical reactions of interest remains vital to drive semiconductor electrochemistry forward.

Acknowledgements
S.M. acknowledges the Department of Energy (DE-SC0006628) for support of this work. M.M. and S. H. acknowledge the National Science Foundation Graduate Research Fellowship Program.

References

1. Archer, M.D., Nozik, A.J. (eds.): Nanostructured and Photoelectrochemical Systems for Solar Photon Conversion, vol. 3. Imperial College Press, London (2008)
2. Khaselev, O., Turner, J.A.: A monolithic photovoltaic-photoelectrochemical device for hydrogen production via water splitting. Science. **280**, 425–427 (1998)
3. Lewis, N.S.: Charge transfer rate constants for semiconductor/liquid contacts. Sol. Energy Mater. Sol. Cells. **38**, 323–325 (1995)
4. Lewis, N.S.: Progress in understanding electron-transfer reactions at semiconductor/liquid interfaces. J. Phys. Chem. B. **102**, 4843–4855 (1998)
5. Tan, M.X., Laibinis, P.E., Nguyen, S.T., Kesselman, J.M., Stanton, C.E., Lewis, N.S.: Principles and applications of semiconductor photoelectrochemistry. Prog. Inorg. Chem. **41**, 21–144 (1994)
6. Uosaki, K., Kita, H.: Theoretical aspects of semiconductor electrochemistry. In: White, R.E., Bockris, J.O.M., Conway, B.E. (eds.) Modern Aspects of Electrochemistry, vol. 18. Plenum Press, New York and London (1986)
7. Lewerenz, H.-J.: Semiconductor electrodes. Edited by H. O. Finklea. Elsevier, Amsterdam 1988. xxii, 520 pp., bound, DFI. 340.00.—ISBN 0-444-42926-3. Adv. Mater. **1**, 96–97 (1989)
8. Snowden, C.M.: Semiconductor device modelling. Rep. Prog. Phys. **48**, 223–275 (1985)
9. Fonash, S.: Solar Cell Device Physics. Academic Press (2010)
10. Sze, S.M., Ng, K.K.: Physics of Semiconductor Devices, 3rd edn. Wiley, Hoboken (2007)
11. Hill, R., Archer, M.D.: Photoelectrochemical cells — a review of progress in the past 10 years. J. Photochem. Photobiol. A Chem. **51**, 45–54 (1990)
12. Sivula, K., van de Krol, R.: Semiconducting materials for photoelectrochemical energy conversion. Nat. Rev. Mater. **1**, 15010 (2016)
13. Peter, L.M.: Dynamic aspects of semiconductor photoelectrochemistry. Chem. Rev. **90**, 753–769 (1990)
14. Nozik, A.J., Memming, R.: Physical chemistry of semiconductor-liquid interfaces. J. Phys. Chem. **100**, 13061–13078 (1996)
15. Nozik, A.J.: Photoelectrochemistry: applications to solar energy conversion. Annu. Rev. Phys. Chem. **29**, 189–222 (1978)
16. Morrison, S.R.: Electrochemistry at Semiconductor and Oxidized Metal Electrodes. Plenum Press, New York (1980)
17. Memming, R.; 2nd ed.; Wiley-VCH, Verlag GmbH & Co. KGaA: Weinheim, 2015
18. Willig, F., Gundlach, L.: Redox processes at semiconductors-Gerischer model and beyond. In: Kreysa, G., Ota, K.-i., Savinell, R.F. (eds.) Encyclopedia of Applied Electrochemistry, pp. 1786–1798. Springer New York, New York (2014)
19. Wilson, R.H.: Electron transfer processes at the semiconductor-electrolyte interface. Crit. Rev. Solid State Mater. Sci. **10**, 1–41 (1980)
20. Gurnee, E.F.: Fundamental principles of semiconductors. J. Chem. Educ. **46**, 80–85 (1969)
21. Wurfel, P.: Physics of Solar Cells, 2nd edn. Wiley-VCH, Germany (2009)
22. Yu, P.Y., Cardona, M.: Fundamentals of Semiconductors, 4th edn. Springer (2010)
23. Blakemore, J.S.: Semiconductor Statistics. Pergamon Press, Oxford (1962)
24. Khan, S.U.M., Kainthia, R.C., Bockris, J.O.M.: The redox potential and the Femi level in solution. J. Phys. Chem. **91**, 5974–5977 (1987)
25. Bard, A.J., Faulkner, L.R.: Electrochemical Methods: Fundamentals and Applications, 2nd edn. Wiley, Hoboken (2001)
26. Uosaki, K., Kita, H.: Theoretical aspects of semiconductor electrochemistry. In: White, R.E., Bockris, J.O.M., Conway, B.E. (eds.) Modern Aspects of Electrochemistry, pp. 1–60. Springer US, Boston (1986)
27. Bicelli, L.P.: A review of photoelectrochemical methods for the utilization of solar energy. Surf. Technol. **20**, 357–381 (1983)
28. Conway, B.E.: Electrochemical Supecapacitors: Scientific Fundamentals and Technological Applications. Springer, New York (1999)
29. Goossens, A.: The space charge capacitance of non-degenerate semiconductors with shallow and deep impurity levels. J. Electroanal. Chem. Interfacial Electrochem. **317**, 27–42 (1991)
30. Boddy, P.J.: Oxygen evolution on semiconducting TiO_2. J. Electrochem. Soc. **115**, 199–203 (1968)
31. Garrett, C.G.B., Brattain, W.H.: Physical theory of semiconductor surfaces. Phys. Rev. **99**, 376–387 (1955)
32. Morrison, S.R.: Electrochemistry at Semiconductor and Oxidized Metal Electrodes / S. Roy Morrison. Plenum Press (1980)
33. Memming, R.: Charge transfer kinetics at semiconductor electrodes. Ber. Bunsenges. Phys. Chem. **91**, 353–361 (1987)
34. This discussion assumes that the macroscopic semiconductor is re-configured as an electrode in the following ways. At least one interface of the semiconductor is in contact with the solution but at least one other interface is in contact with an electronic conductor. Ideally at this other interface (which is insulated from contact with the solution), the flow of electrons and/or holes is unimpeded, i.e., there is no barrier for transfer. This case would represent an ohmic contact that is used to connect the semiconductor to an external circuit. If the flow of electrons and/or holes is hindered in any way at this interface, the ability to affect the potential of the semiconductor is complicated and can affect the observable/attainable charge transfer at the semiconductor/liquid interface
35. Or equivalently, by the ergodic principle, the energy of a single molecule over an infinite time period
36. Elgrishi, N., Rountree, K.J., McCarthy, B.D., Rountree, E.S., Eisenhart, T.T., Dempsey, J.L.: A practical beginner's guide to cyclic voltammetry. J. Chem. Educ. **95**, 197–206 (2018)

37. In practice, the two types of plots can be inter converted by rotation of the figure by 180 degrees
38. Natarajan, A., Oskam, G., Searson, P.C.: The potential distribution at the semiconductor/solution interface. J. Phys. Chem. B. **102**, 7793–7799 (1998)
39. Degryse, R., Gomes, W.P., Cardon, F., Vennik, J.: On the interpretation of Mott-Schottky plots determined at semiconductor/electrolyte systems. J. Electrochem. Soc. **122**, 711–712 (1975)
40. Shreve, G.A., Lewis, N.S.: An analytical description of the consequences of abandoning the principles of detailed balance and microscopic reversibility in semiconductor photoelectrochemistry. J. Electrochem. Soc. **142**, 112–119 (1995)
41. Kumar, A., Wilisch, W.C.A., Lewis, N.S.: The electrical properties of semiconductor/metal, semiconductor/liquid, and semiconductor/conducting polymer contacts. Crit. Rev. Solid State Mater. Sci. **18**, 327–353 (1993)
42. Foley, J.M., Price, M.J., Feldblyum, J.I., Maldonado, S.: Analysis of the operation of thin nanowire photoelectrodes for solar energy conversion. Energy Environ. Sci. **5**, 5203–5220 (2012)
43. Hamnett, A.: Chapter 2 Semiconductor electrochemistry. In: Compton, R.G. (ed.) Comprehensive Chemical Kinetics, vol. 27, pp. 61–246. Elsevier, Amsterdam (1988)
44. Ullman, D.L.: Current limited by transport through the space-charge region of a semiconductor electrode. J. Electrochem. Soc. **128**, 1269–1273 (1981)
45. Vandermolen, J., Gomes, W.P., Cardon, F.: Investigation on the kinetics of electroreduction processes at dark TiO_2 and $SrTiO_3$ single crystal semiconductor electrodes. J. Electrochem. Soc. **127**, 324–328 (1980)
46. Lin, F., Boettcher, S.W.: Adaptive semiconductor/electrocatalyst junctions in water-splitting photoanodes. Nat. Mater. **13**, 81–86 (2013)
47. Mills, T.J., Lin, F., Boettcher, S.W.: Theory and simulations of electrocatalyst-coated semiconductor electrodes for solar water splitting. Phys. Rev. Lett. **112**, 148304 (2014)
48. Nellist, M.R., Laskowski, F.A.L., Lin, F.D., Mills, T.J., Boettcher, S.W.: Semiconductor-electrocatalyst interfaces: theory, experiment, and applications in photoelectrochemical water splitting. Acc. Chem. Res. **49**, 733–740 (2016)
49. Reiss, H.: Photocharacteristics for electrolyte-semiconductor junctions. J. Electrochem. Soc. **125**, 937–949 (1978)
50. Reichman, J.: The current-voltage characteristics of semiconductor-electrolyte junction photovoltaic cells. Appl. Phys. Lett. **36**, 574–577 (1980)
51. Cendula, P., Tilley, S.D., Gimenez, S., Bisquert, J., Schmid, M., Grätzel, M., Schumacher, J.O.: Calculation of the energy band diagram of a photoelectrochemical water splitting cell. J. Phys. Chem. C. **118**, 29599–29607 (2014)
52. Chitambar, M., Wang, Z., Liu, Y., Rockett, A., Maldonado, S.: Dye-sensitized photocathodes: efficient light-stimulated hole injection into p-GaP under depletion conditions. J. Am. Chem. Soc. **134**, 10670–10681 (2012)
53. Anz, S.J., Lewis, N.S.: Simulations of the steady-state current density vs. potential characteristics of semiconducting electrodes. J. Phys. Chem. B. **103**, 3908–3915 (1999)
54. Iqbal, A., Bevan, K.H.: The impact of boundary conditions on calculated photovoltages and photocurrents at photocatalytic interfaces. MRS Commun. **8**, 466–473 (2018)
55. Spitler, M.T.: One dimensional onsager model for dye sensitized charge injection into semiconductors. J. Electroanal. Chem. Interfacial Electrochem. **228**, 69–76 (1987)
56. Spitler, M.T.: Exact expression for cathodic current flow at an n-type semiconductor electrode. Z. Phys. Chem. **212**, 173–178 (1999)
57. Watkins, K.J., Parkinson, B.A., Spitler, M.T.: Physical models for charge transfer at single crystal oxide semiconductor surfaces as revealed by the doping density dependence of the collection efficiency of dye sensitized photocurrents. J. Phys. Chem. B. **119**, 7579–7588 (2015)
58. Watkins, K.J., Parkinson, B.A., Spitler, M.T.: Fundamental aspects of photoinduced charge flow at a quantum-dot-sensitized single-crystal TiO_2 semiconductor interface. J. Phys. Chem. C. **122**, 13608–13616 (2018)
59. Butler, M.A.: Photoelectrolysis and physical properties of the semiconducting electrode WO2. J. Appl. Phys. **48**, 1914–1920 (1977)
60. Anderson, T.J., Ansara, I.: The Ga-In (gallium-indium) system. J. Phase Equilib. **12**, 64–72 (1991)
61. Chiarenzelli, R.V., Brown, O.L.I.: The mercury-indium equilibrium diagram. J. Chem. Engin. Data. **7**, 477–478 (1962)
62. Peter, L.M., Li, J., Peat, R.: Surface recombination at semiconductor electrodes: part I. transient and steady-state photocurrents. J. Electroanal. Chem. Interfacial Electrochem. **165**, 29–40 (1984)
63. van de Krol, R.: Principles of photoelectrochemical cells. In: van de Krol, R., Grätzel, M. (eds.) Photoelectrochemical Hydrogen Production, pp. 13–67. Springer US, Boston (2012)
64. Gerischer, H.: Electrochemical behavior of semiconductors under illumination. J. Electrochem. Soc. **113**, 1174–1182 (1966)
65. Memming, R.: Electron transfer theories. In: Semiconductor Electrochemistry, 2nd edn, pp. 127–168. Wiley-VCH, Germany (2015)
66. Vanmaekelbergh, D., Erné, B.H., Cheung, C.W., Tjerkstra, R.W.: On the increase of the photocurrent quantum efficiency of GaP photoanodes due to (photo)anodic pretreatments. Electrochim. Acta. **40**, 689–698 (1995)
67. Gerischer, H.: The impact of semiconductors on the concepts of electrochemistry. Electrochim. Acta. **35**, 1677–1699 (1990)
68. Gerischer, H. Semiconductor Electrochemistry. Lawrence Radiation Laboratory Berkeley, California (1968)
69. Wurfel, P.: Is an illuminated semiconductor far from thermodynamic-equilibrium? Sol. Energy Mater. Sol. Cells. **38**, 23–28 (1995)
70. Gerischer, H.: Über den Ablauf von Redoxreaktionen an Metallen und an Halbleitern. II. Metall-Elektroden. Z. Phys. Chem. Neue Fol. **26**, 325–338 (1960)
71. Gerischer, H.: Metal and semiconductor electrode processes. In: Surface Chemistry of Metals and Semiconductors, a Symposium, pp. 177–204 (1960)
72. Gerischer, H.: Über den Ablauf von Redoxreaktionen an Metallen und an Halbleitern. I. Allgemeines zum Elektronenübergang zwischen einem Festkörper und einem Redoxelektrolyten. Z. Phys. Chem. Neue Fol. **26**, 223–247 (1960)
73. Gerischer, H.: On role of electrons and holes in surface reactions on semiconductors. Surf. Sci. **13**, 265–278 (1969)
74. Gerischer, H.: Charge transfer processes at semiconductor-electrolyte interfaces in connection with problems of catalysis. Surf. Sci. **18**, 97–122 (1969)
75. Gerischer, H.: Electrochemical techniques for study of photosensitization. Photochem. Photobiol. **16**, 243–260 (1972)
76. Gerischer, H.: Solar photoelectrolysis with semiconductor electrodes. In: Seraphin, B.O. (ed.) Solar Energy Conversion: Solid-State Physics Aspects, vol. 31. Springer, New York (1979)
77. Gerischer, H.: Electron-transfer kinetics of redox reactions at the semiconductor electrolyte contact - a new approach. J. Phys. Chem. **95**, 1356–1359 (1991)
78. Kautek, W., Gerischer, H., Tributsch, H.: Role of surface orientation in the photoelectrochemical behavior of layer type d-band semiconductors. Berichte Der Bunsen-Gesellschaft-Phys. Chem. Chem. Phys. **83**, 1000–1008 (1979)
79. Tributsch, H., Gerischer, H.: The use of semiconductor electrodes in the study of photochemical reactions. Berichte Der Bunsen-Gesellschaft Fur Physikalische Chemie. **73**, 850–854 (1969)
80. Bird, R.E., Hulstrom, R.L.: Terrestrial solar spectral data sets. Sol. Energy. **30**, 563–573 (1983)

81. Lewis, N.S.: Mechanistic studies of light-induced charge separation at semiconductor/liquid interfaces. Acc. Chem. Res. **23**, 176–183 (1990)
82. Lewis, N.S.: A quantitative investigation of the open-circuit photovoltage at the semiconductor/liquid interface. J. Electrochem. Soc. **131**, 2496–2503 (1984)
83. Bard, A.J., Bocarsly, A.B.., Fan, F.R.F., Walton, E.G., Wrighton, M.S.: The concept of Fermi level pinning at semiconductor/liquid junctions. Consequences for energy-conversion efficiency and selection of useful solution redox couples in solar devices. J. Am. Chem. Soc. **102**, 3671–3677 (1980)
84. Bocarsly, A.B.., Bookbinder, D.C., Dominey, R.N., Lewis, N.S., Wrighton, M.S.: Photo-reduction at illuminated p-type semiconducting silicon photoelectrodes - evidence for Fermi level pinning. J. Am. Chem. Soc. **102**, 3683–3688 (1980)
85. Dominey, R.N., Lewis, N.S., Wrighton, M.S.: Fermi level pinning of p-type semiconducting indium phosphide contacting liquid electrolyte solutions: rationale for efficient photoelectrochemical energy-conversion. J. Am. Chem. Soc. **103**, 1261–1263 (1981)
86. Nagasubramanian, G., Wheeler, B.L., Bard, A.J.: Semiconductor electrodes .49. Evidence for Fermi level pinning and ssurface-state distributions from impedance measurements in acetonitrile solutions with various redox couples. J. Electrochem. Soc. **130**, 1680–1688 (1983)
87. Nagasubramanian, G., Wheeler, B.L., Fan, F.R.F., Bard, A.J.: Semiconductor electrodes .42. Evidence for Fermi level pinning from shifts in the flat-band potential of p-type silicon in acetonitrile solutions with different redox couples. J. Electrochem. Soc. **129**, 1742–1745 (1982)
88. Baglio, J.A., Calabrese, G.S., Harrison, D.J., Kamieniecki, E., Ricco, A.J., Wrighton, M.S., Zoski, G.D.: Elechtrochemical characterization of p-type semiconducting tungsten disulfide photocathodes: efficient photoreduction processes at semiconductor/liquid electrolyte interfaces. J. Am. Chem. Soc. **105**, 2246–2256 (1983)
89. Kelly, J.J., Memming, R.: The influence of surface recombination and trapping on the cathodic photocurrent at p-type III-V electrodes. J. Electrochem. Soc. **129**, 730–738 (1982)
90. McEvoy, A.J., Etman, M., Hemming, M.: Interface charging and intercalations effects on d-band transition metal diselenide photoelectrodes. J. Electroanal. Chem. Interfacial Electrochem. **190**, 225–241 (1985)
91. Kühne, H.M., Tributsch, H.: Energetics and dynamics of the interface of RuS2 and implications for photoelectrolysis of water. J. Electroanal. Chem. Interfacial Electrochem. **201**, 263–282 (1986)
92. Lieber, C.M., Gronet, C.M., Lewis, N.S.: Evidence against surface-state limitations on efficiency of p-Si/Ch3n junctions. Nature. **307**, 533–534 (1984)
93. Klahr, B., Gimenez, S., Fabregat-Santiago, F., Hamann, T., Bisquert, J.: Water oxidation at hematite photoelectrodes: the role of surface states. J. Am. Chem. Soc. **134**, 4294–4302 (2012)
94. Chazalviel, J.N.: Electrochemical transfer via surface-states - a new formulation for the semiconductor electrolyte interface. J. Electrochem. Soc. **129**, 963–969 (1982)
95. Leng, W.H., Zhang, Z., Zhang, J.Q., Cao, C.N.: Investigation of the kinetics of a TiO_2 photoelectrocatalytic reaction involving charge transfer and recombination through surface states by electrochemical impedance spectroscopy. J. Phys. Chem. B. **109**, 15008–15023 (2005)
96. Allongue, P., Cachet, H.: Surface-charges at the aqueous N-Gaas electrolyte interface under illumination. Vide. **40**, 155–155 (1985)
97. Lincot, D., Vedel, J.: Recombination and charge-transfer at the illuminated n-CdTe electrolyte interface - simplified kinetic-model. J. Electroanal. Chem. **220**, 179–200 (1987)
98. Fajardo, A.M., Lewis, N.S.: Free-energy dependence of electron-transfer rate constants at Si/liquid interfaces. J. Phys. Chem. B. **101**, 11136–11151 (1997)
99. Howard, J.N., Koval, C.A.: Kinetics of reduction of dimethylferrocenium ion in acetonitrile at nearly ideal regions of n-tungsten diselenide electrodes. Anal. Chem. **66**, 4525–4531 (1994)
100. Royea, W.J., Kruger, O., Lewis, N.S.: Frumkin corrections for heterogeneous rate constants at semiconducting electrodes. J. Electroanal. Chem. **438**, 191–197 (1997)
101. Many, A., Goldstein, Y., Grover, N.B.: Semiconductor Surfaces. Wiley, Amsterdam (1965)
102. Dewald, J.F.: The charge distribution at the zinc oxide-electrolyte interface. J. Phys. Chem. Solids. **14**, 155–161 (1960)
103. Gomes, W.P., Vanmaekelbergh, D.: Impedance spectroscopy at semiconductor electrodes: review and recent developments. Electrochim. Acta. **41**, 967–973 (1996)
104. Hens, Z., Gomes, W.P.: The electrochemical impedance of one-equivalent electrode processes at dark semiconductor/redox electrodes involving charge transfer through surface states. 2. The n-GaAs/Fe3+ system as an experimental example. J. Phys. Chem. B. **103**, 130–138 (1999)
105. Allongue, P., Cachet, H.: Band-edge shift and surface charges at illuminated n-GaAs/ aqueous electrolyte junctions - surface-state analysis and simulation of their occupation rate. J. Electrochem. Soc. **132**, 45–52 (1985)
106. Iqbal, A., Hossain, M.S., Bevan, K.H.: The role of relative rate constants in determining surface state phenomena at semiconductor–liquid interfaces. Phys. Chem. Chem. Phys. **18**, 29466–29477 (2016)
107. Kilså, K., Mayo, E.I., Kuciauskas, D., Villahermosa, R., Lewis, N. S., Winkler, J.R., Gray, H.B.: Effects of bridging ligands on the current−potential behavior and interfacial kinetics of ruthenium-sensitized nanocrystalline TiO_2 photoelectrodes. Chem. A Eur. J. **107**, 3379–3383 (2003)
108. Yablonovitch, E., Allara, D.L., Chang, C.C., Gmitter, T., Bright, T. B.: Unusually low surface-recombination velocity on silicon and germanium surfaces. Phys. Rev. Lett. **57**, 249–252 (1986)
109. Becquerel, A.E.: Memoire sur les effets électriques produits sous l'influence des rayons solaires. C. R. Acad. Sci. Paris. **9**, 561–567 (1839)
110. Marcus, R.A.: On the theory of oxidation-reduction reactions involving electron transfer. I. J. Chem. Phys. **24**, 966–978 (1956)
111. Marcus, R.A.: On the theory of electron-transfer reactions. VI. Unified treatment for homogeneous and electrode reactions. J. Chem. Phys. **43**, 679–701 (1965)
112. Marcus, R.A.: Electron transfer reactions in chemistry. Theory and experiment. Rev. Mod. Phys. **65**, 599–610 (1993)
113. Hush, N.S.: Adiabatic theory of outer sphere electron-transfer reactions in solution. T. Faraday Soc. **57**, 557–580 (1961)
114. Uhlir Jr., A.: Electrolytic shaping of germanium and silicon. Bell Syst. Tech. J. **35**, 333–347 (1956)
115. Brattain, W.H., Garrett, C.G.B.: Experiments on the interface between germanium and an electrolyte. Bell Syst. Tech. J. **34**, 129–176 (1955)
116. Marcus, R.A.: Chemical and electrochemical electron-transfer theory. Annu. Rev. Phys. Chem. **15**, 155–196 (1964)
117. Randles, J.E.B.: Kinetics of rapid electrode reactions. Part 2. Rate constants and activation energies of electrode reactions. Trans. Faraday Soc. **48**, 828–832 (1952)
118. Gurney, R.W., Fowler Ralph, H.: The quantum mechanics of electrochemistry.—II. Proc. Roy. Soc. Lond. Series A, Containing Papers of a Mathematical and Physical Character. **136**, 378–396 (1932)
119. Suppan, P.: The marcus inverted region. In: Mattay, J. (ed.) Photoinduced Electron Transfer IV, pp. 95–130. Springer Berlin Heidelberg, Berlin, Heidelberg (1992)

120. Gerischer, H.: In: Eyring, H., Hendeson, D., Jost, W. (eds.) Physical Chemistry, vol. 9A, pp. 463–488. Academic, New York (1970)
121. Dogonadze, R.R., Kuznetsov, A.M., Chernenko, A.A.: Theory of homogeneous and heterogeneous electronic processes in liquids. Russ. Chem. Rev. **34**, 759 (1965)
122. Christov, S.G.: Quantum theory of electron-transfer processes in solution. Ber. Bunsenges. Phys. Chem. **79**, 357–371 (1975)
123. Marcus, R.A.: On the theory of oxidation—reduction reactions involving electron transfer. V. Comparison and properties of electrochemical and chemical rate constants. J. Phys. Chem. **67**, 853–857 (1963)
124. Schmickler, W., Santos, E.: The semiconductor-electrolyte interface. In: Schmickler, W., Santos, E. (eds.) Interfacial Electrochemistry, pp. 117–131. Springer Berlin Heidelberg, Berlin, Heidelberg (2010)
125. Smith, B.B., Koval, C.A.: An investigation of the image potential at the semiconductor/electrolyte interface employing nonlocal electrostatics. J. Electroanal. Chem. Interfacial Electrochem. **277**, 43–72 (1990)
126. Kuciauskas, D., Freund, M.S., Gray, H.B., Winkler, J.R., Lewis, N.S.: Electron transfer dynamics in nanocrystalline titanium dioxide solar cells sensitized with ruthenium or osmium polypyridyl complexes. J. Phys. Chem. B. **105**, 392–403 (2001)
127. Marcus, R.A.: Reorganization free energy for electron transfers at liquid-liquid and dielectric semiconductor-liquid interfaces. J. Phys. Chem. **94**, 1050–1055 (1990)
128. Hamann, T.W., Gstrein, F., Brunschwig, B.S., Lewis, N.S.: Measurement of the dependence of interfacial charge-transfer rate constants on the reorganization energy of redox species at n-ZnO/H2O interfaces. J. Am. Chem. Soc. **127**, 13949–13954 (2005)
129. Marcus, R.A.: Electron transfer reactions in chemistry: theory and experiment (Nobel lecture). Angew. Chem. Int. Ed. Engl. **32**, 1111–1121 (1993)
130. Marcus, R.A.: Electron transfer reactions in chemistry: theory and experiment. J. Electroanal. Chem. **438**, 251–259 (1997)
131. Gregg, B.A., Nozik, A.J.: Existence of a light intensity threshold for photoconversion processes. J. Phys. Chem. **97**, 13441–13443 (1993)
132. Smith, B.B., Hynes, J.T.: Electronic friction and electron transfer rates at metallic electrodes. J. Chem. Phys. **99**, 6517–6530 (1993)
133. Carter, E.A., Hynes, J.T.: Solute-dependent solvent force constants for ion pairs and neutral pairs in a polar solvent. J. Phys. Chem. **93**, 2184–2187 (1989)
134. Landau, L.D., Lifshitz, E.M.: Statistical Physics. Butterworth-Heinemann, Oxford (1980)
135. Steiner, E.: The Chemistry Maths Book. Oxford Science Publications, Oxford (1996)
136. Bixon, M., Jortner, J.: Solvent relaxation dynamics and electron transfer. Chem. Phys. **176**, 467–481 (1993)
137. Chaudhuri, S., Hedstrom, S., Mendez-Hernandez, D.D., Hendrickson, H.P., Jung, K.A., Ho, J.M., Batista, V.S.: Electron transfer assisted by vibronic coupling from multiple modes. J. Chem. Theory Comput. **13**, 6000–6009 (2017)
138. Royea, W.J., Fajardo, A.M., Lewis, N.S.: Fermi golden rule approach to evaluating outer-sphere electron-transfer rate constants at semiconductor/liquid interfaces. J. Phys. Chem. B. **101**, 11152–11159 (1997)
139. Levich, V.G., Dogonadze, R.R.: The theory of non-radiaive electron transitions between ions in solution. Dokl. Akad. Nauk. **124**, 123–126 (1959)
140. Fletcher, S.: The theory of electron transfer. J. Solid State Electrochem. **14**, 705–739 (2010)
141. Hush, N.S.: Adiabatic theory of outer sphere electron-transfer reactions in solution. Trans. Faraday Soc. **57**, 557–580 (1961)
142. Marcus, R.A.: Exchange reactions and electron transfer reactions including isotopic exchange. Theory of oxidation-reduction reactions involving electron transfer. Part 4. A statistical-mechanical basis for treating contributions from solvent, ligands, and inert salt. Discuss. Faraday Soc. **29**, 21–31 (1960)
143. Marcus, R.A.: Theoretical relations among rate constants, barriers, and Broensted slopes of chemical reactions. J. Phys. Chem. **72**, 891–899 (1968)
144. Grampp, G.: The marcus inverted region from theory to experiment. Angew. Chem. Int. Ed. Engl. **32**, 691–693 (1993)
145. Irvine, M.P., Harrison, R.J., Beddard, G.S., Leighton, P., Sanders, J.K.M.: Detection of the inverted region in the photo-induced intramolecular electron transfer of capped porphyrins. Chem. Phys. **104**, 315–324 (1986)
146. Makita, H., Hastings, G.: Inverted-region electron transfer as a mechanism for enhancing photosynthetic solar energy conversion efficiency. Proc. Natl. Acad. Sci. U. S. A. **114**, 9267–9272 (2017)
147. Schmickler, W., Tao, N.J.: Measuring the inverted region of an electron transfer reaction with a scanning tunneling microscope. Electrochim. Acta. **42**, 2809–2815 (1997)
148. Siders, P., Marcus, R.A.: Quantum effects for electron-transfer reactions in the "inverted region". J. Am. Chem. Soc. **103**, 748–752 (1981)
149. Rehm, D., Weller, A.: Kinetics of fluorescence quenching by electron and H-atom transfer. Israel J. Chem. **8**, 259–271 (1970)
150. Chidsey, C.E.D.: Free-energy and temperature-dependence of electron-transfer at the metal-electrolyte interface. Science. **251**, 919–922 (1991)
151. Smalley, J.F., Feldberg, S.W., Chidsey, C.E.D., Linford, M.R., Newton, M.D., Liu, Y.-P.: The kinetics of electron transfer through ferrocene-terminated alkanethiol monolayers on gold. J. Phys. Chem. **99**, 13141–13149 (1995)
152. Richardson, J.N., Rowe, G.K., Carter, M.T., Tender, L.M., Curtin, L.S., Peck, S.R., Murray, R.W.: Electron transfer kinetics of self-assembled ferrocene (C12)Alkanethiol monolayers on gold electrodes from 125 K to 175 K. Electrochim. Acta. **40**, 1331–1338 (1995)
153. Morrison, S.R.: Electron capture by ions at the ZnO/solution interface. Surf. Sci. **15**, 363–379 (1969)
154. Miller, J.R., Beitz, J.V., Huddleston, R.K.: Effect of free energy on rates of electron transfer between molecules. J. Am. Chem. Soc. **106**, 5057–5068 (1984)
155. Closs, G.L., Miller, J.R.: Intramolecular long-distance electron transfer in organic molecules. Science. **240**, 440–447 (1988)
156. Fukuzumi, S., Ohkubo, K., Suenobu, T.: Long-lived charge separation and applications in artificial photosynthesis. Acc. Chem. Res. **47**, 1455–1464 (2014)
157. Wasielewski, M.R., Niemczyk, M.P., Svec, W.A., Pewitt, E.B.: Dependence of rate constants for photoinduced charge separation and dark charge recombination on the free energy of reaction in restricted-distance porphyrin-quinone molecules. J. Am. Chem. Soc. **107**, 1080–1082 (1985)
158. Farjardo, A.M., Lewis, N.S.: Rate constants for charge transfer across semiconductor-liquid interfaces. Science. **274**, 969–972 (1996)
159. Hamann, T.W., Gstrein, F., Brunschwig, B.S., Lewis, N.S.: Measurement of the free-energy dependence of interfacial charge-transfer rate constants using ZnO/H_2O semiconductor/liquid contacts. J. Am. Chem. Soc. **127**, 7815–7824 (2005)
160. Hamann, T.W., Gstrein, F., Brunschwig, B.S., Lewis, N.S.: Measurement of the driving force dependence of interfacial charge-transfer rate constants in response to pH changes at n-ZnO/H_2O interfaces. Chem. Phys. **326**, 15–23 (2006)
161. Kadhu, A.A.H., Salmon, G.A.: Reactivity of solvated electrons in tetrahydrofuran. J. Chem. Soc., Faraday Trans. 1. **82**, 2521–2530 (1986)
162. Lian, N., Miller, J.R., Closs, G.L.: Temperature-independet long-range electron transfer reactions in the Marcus inverted region. J. Am. Chem. Soc. **112** (1990)

163. Levich, R.R., Dogonadze, R.R.: An adiabatic theory of electron processes in solutions. Dokl. Akad. Nauk SSSR. **133**, 158–161 (1960)
164. Jortner, J., Bixon, M.: Intramolecular vibrational excitations accompanying solvent-controlled electron transfer reactions. J. Chem. Phys. **88**, 167–170 (1987)
165. Ulstrup, J., Jortner, J.: The effect of intramolecular quantum modes on free energy relationships for electron transfer reactions. J. Chem. Phys. **63**, 4358–4368 (1975)
166. Efrima, S., Bixon, M.: On the role of vibrational excitation in electron transfer reactions with large negative free energies. Chem. Phys. Lett. **25**, 34–37 (1974)
167. Miller, J.R., Calcaterra, L.T., Closs, G.L.: Intramolecular long-distance electron transfer in radical anions. The effects of free energy and solvent on the reaction rates. J. Am. Chem. Soc. **106**, 3047–3049 (1984)
168. Vanden Berghe, R.A.L., Cardon, F., Gomes, W.P.: On the electrochemical reactivity of the redox couple Fe(CN)63−/Fe(CN)64− at the single crystal zinc oxide electrode. Surf. Sci. **39**, 368–384 (1973)
169. Acharya, S., Lancaster, M., Maldonado, S.: Semiconductor ultramicroelectrodes: platforms for studying charge-transfer processes at semiconductor/liquid interfaces. Anal. Chem. **90**, 12261–12269 (2018)
170. Yang, Y., Gu, J., Young, J.L., Miller, E.M., Turner, J.A., Neale, N. R., Beard, M.C.: Semiconductor interfacial carrier dynamics via photoinduced electric fields. Science. **350**, 1061 (2015)
171. Smith, B.B., Nozik, A.J.: Study of electron transfer at semiconductor liquid interfaces addressing the full system electronic structure. Chem. Phys. **205**, 47–72 (1996)
172. Smith, B.B., Nozik, A.J.: Theoretical studies of electron transfer and electron localization at the semiconductor-liquid interface. J. Phys. Chem. B. **101**, 2459–2475 (1997)
173. Smith, B.B., Nozik, A.J.: A wave packet model for electron transfer and its implications for the semiconductor-liquid interface. J. Phys. Chem. B. **103**, 9915–9932 (1999)
174. Smith, B.B.: Electron wave packet propagation studies of etectron transfer at the semiconductor-liquid interface. Solid-Liquid Interface Theory; Am. Chem. Soc. **789**, 66–81 (2001)
175. Sutin, N., Brunschwig, B.: Electron transfer in weakly interacting systems. In: Rorabacher, D.B., Endicott, J.F. (eds.) Mechanistic Aspects of Inorganic Reactions ACS Symposium Series, vol. 198, ACS, United States of America, pp. 105–135 (1982)
176. Pomykal, K.E., Fajardo, A.M., Lewis, N.S.: Theoretical and experimental upper bounds on interfacial charge-transfer rate constants between semiconducting solids and outer-sphere redox couples. J. Phys. Chem. **100**, 3652–3664 (1996)
177. Marcus, R.A.: Theory of electron-transfer rates across liquid-liquid interfaces. 2. Relationships and application. J. Phys. Chem. **95**, 2010–2013 (1991)
178. Gao, Y.Q., Georgievskii, Y., Marcus, R.A.: On the theory of electron transfer reactions at semiconductor electrode/liquid interfaces. J. Chem. Phys. **112**, 3358–3369 (2000)
179. Gao, Y.Q., Marcus, R.A.: On the theory of electron transfer reactions at semiconductor/liquid interfaces. II. A free electron model. J. Chem. Phys. **113**, 6351–6360 (2000)
180. Kolasinski, K.W., Gogola, J.W., Barclay, W.B.: Test of Marcus theory predictions for electroless etching of silicon. J. Phys. Chem. C. **116**, 21472–21481 (2012)
181. Smith, B.B., Halley, J.W., Nozik, A.J.: On the Marcus model of electron transfer at immiscible liquid interfaces and its application to the semiconductor liquid interface. Chem. Phys. **205**, 245–267 (1996)
182. Tan, M.X., Lewis, N.S.: Charge transfer rate constants for the reduction of cobaltocenium at accumulated nSi electrodes. Inorg. Chim. Acta. **242**, 311–321 (1996)
183. Sun, X., Geva, E.: Equilibrium Fermi's golden rule charge transfer rate constants in the condensed phase: the linearized semiclassical method vs classical Marcus theory. Chem. A Eur. J. **120**, 2976–2990 (2016)
184. Gerischer, H.: The role of semiconductor structure and surface properties in photoelectrochemical processes. J. Electroanal. Chem. Interfacial Electrochem. **150**, 553–569 (1983)
185. Uhlendorf, I., Reineke-Koch, R., Memming, R.: Investigation of the kinetics of redox reactions at GaAs electrodes by impedance spectroscopy. J. Phys. Chem. **100**, 4930–4936 (1996)
186. Meier, A., Kocha, S.S., Hanna, M.C., Nozik, A.J., Siemoneit, K., Reineke Koch, R., Memming, R.: Electron transfer rate constants for majority electrons at GaAs and GaInP2 semiconductor-liquid interfaces. J. Phys. Chem. B. **101**, 7038–7042 (1997)
187. Meier, A., Kocha, S.S., Hanna, M.C., Nozik, A.J., Siemoneit, K., Reineke Koch, R., Memming, R.: Majority charge carrier transfer studies at n-type III-V semiconductor-liquid interfaces by impedance spectroscopy. Proc. Symp. Photoelectrochem. **97**, 161–171 (1997)
188. Siemoneit, K., Reineke-Koch, R., Meier, A., Memming, R.: Fast processes at semiconductor-liquid interfaces: reactions at GaAs electrodes. Electrochim. Acta. **45**, 4577–4589 (2000)
189. Groner, M.D., Koval, C.A.: Electron transfer at n-silicon|methanol interfaces: effects of ferricenium pretreatment and silicon dioxide overlayers. J. Electroanal. Chem. **498**, 201–208 (2001)
190. Rodman, S., Spitler, M.T.: Determination of rate constants for dark current reduction at semiconductor electrodes using ZnO single-crystal microelectrodes. J. Phys. Chem. B. **104**, 9438–9443 (2000)
191. Meier, A., Selmarten, D.C., Siemoneit, K., Smith, B.B., Nozik, A. J.: Fast electron transfer across semiconductor-molecule interfaces: GaAs/Co(Cp)(2)(+/0). J. Phys. Chem. B. **103**, 2122–2141 (1999)
192. Casagrande, L.G., Juang, A., Lewis, N.S.: Photoelectrochemical behavior of n-GaAs and n-AlxGa1-xAs in CH3CN. J. Phys. Chem. B. **104**, 5436–5447 (2000)
193. Henstridge, M.C., Laborda, E., Compton, R.G.: Asymmetric Marcus–Hush model of electron transfer kinetics: application to the voltammetry of surface-bound redox systems. J. Electroanal. Chem. **674**, 90–96 (2012)
194. Hupp, J.T., Weaver, M.J.: The driving-force dependence of electrochemical rate parameters: origins of anodic-cathodic asymmetries for metal-aquo redox couples. J. Phys. Chem. **88**, 6128–6135 (1984)
195. Zeng, Y., Bai, P., Smith, R.B., Bazant, M.Z.: Simple formula for asymmetric Marcus–Hush kinetics. J. Electroanal. Chem. **748**, 52–57 (2015)
196. Spitler, M.T.: Effect of nanometer-sized surface morphology upon electrochemical kinetics. Electrochim. Acta. **52**, 2294–2301 (2007)
197. Asbury, J.B., Ellingson, R.J., Ghosh, H.N., Ferrere, S., Nozik, A.J., Lian, T.Q.: Femtosecond IR study of excited-state relaxation and electron-injection dynamics of Ru(dcbpy)(2)(NCS)(2) in solution and on nanocrystalline TiO_2 and Al_2O_3 thin films. J. Phys. Chem. B. **103**, 3110–3119 (1999)
198. Asbury, J.B., Hao, E., Wang, Y.Q., Ghosh, H.N., Lian, T.Q.: Ultrafast electron transfer dynamics from molecular adsorbates to semiconductor nanocrystalline thin films. J. Phys. Chem. B. **105**, 4545–4557 (2001)

199. Benko, G., Kallioinen, J., Korppi-Tommola, J.E.I., Yartsev, A.P., Sundstrom, V.: Photoinduced ultrafast dye-to-semiconductor electron injection from nonthermalized and thermalized donor states. J. Am. Chem. Soc. **124**, 489–493 (2002)
200. Gundlach, L., Willig, F.: Ultrafast photoinduced electron transfer at electrodes: the general case of a heterogeneous electron-transfer reaction. ChemPhysChem. **13**, 2877–2881 (2012)
201. Huber, R., Moser, J.E., Gratzel, M., Wachtveitl, J.: Observation of photoinduced electron transfer in dye/semiconductor colloidal systems with different coupling strengths. Chem. Phys. **285**, 39–45 (2002)
202. Huber, R., Moser, J.E., Gratzel, M., Wachtveitl, J.: Real-time observation of photoinduced adiabatic electron transfer in strongly coupled dye/semiconductor colloidal systems with a 6 fs time constant. J. Phys. Chem. B. **106**, 6494–6499 (2002)
203. Kondov, I., Thoss, M., Wang, H.B.: Theoretical study of ultrafast heterogeneous electron transfer reactions at dye-semiconductor interfaces: Coumarin 343 at titanium oxide. J. Phys. Chem. A. **110**, 1364–1374 (2006)
204. Rehm, J.M., McLendon, G.L., Nagasawa, Y., Yoshihara, K., Moser, J., Gratzel, M.: Femtosecond electron-transfer dynamics at a sensitizing dye-semiconductor (TiO_2) interface. J. Phys. Chem. **100**, 9577–9578 (1996)
205. Gundlach, L., Burfeindt, B., Mahrt, J., Willig, F.: Dynamics of ultrafast photoinduced heterogeneous electron transfer, implications for recent solar energy conversion scenarios. Chem. Phys. Lett. **545**, 35–39 (2012)
206. Huber, R., Moser, J.-E., Grätzel, M., Wachtveitl, J.: Real-time observation of photoinduced adiabatic electron transfer in strongly coupled dye/semiconductor colloidal systems with a 6 fs time constant. J. Phys. Chem. B. **106**, 6494–6499 (2002)
207. Myahkostupov, M., Pagba, C.V., Gundlach, L., Piotrowiak, P.: Vibrational state dependence of interfacial electron transfer: hot electron injection from the S1 state of Azulene into TiO_2 nanoparticles. J. Phys. Chem. C. **117**, 20485–20493 (2013)
208. Koval, C.A., Segar, P.R.: Photoelectrochemical reduction of a copper(I) complex to copper metal by hot electrons at p-InP. J. Am. Chem. Soc. **111**, 2004–2010 (1989)
209. Guijarro, N., Prévot, M.S., Sivula, K.: Surface modification of semiconductor photoelectrodes. Phys. Chem. Chem. Phys. **17**, 15655–15674 (2015)
210. Liu, R., Zheng, Z., Spurgeon, J., Yang, X.: Enhanced photoelectrochemical water-splitting performance of semiconductors by surface passivation layers. Energy Environ. Sci. **7**, 2504–2517 (2014)
211. Hu, S., Shaner, M.R., Beardslee, J.A., Lichterman, M., Brunschwig, B.S., Lewis, N.S.: Amorphous TiO_2 coatings stabilize Si, GaAs, and GaP photoanodes for efficient water oxidation. Science. **344**, 1005 (2014)
212. Chen, Y.W., Prange, J.D., Dühnen, S., Park, Y., Gunji, M., Chidsey, C.E.D., McIntyre, P.C.: Atomic layer-deposited tunnel oxide stabilizes silicon photoanodes for water oxidation. Nat. Mater. **10**, 539 (2011)

Sofiya Hlynchuk obtained her B.S. in Chemistry at Rochestor Institute of Technology. She received her Ph.D. in Chemistry at the University of Michigan under Professor Stephen Maldonado. Her dissertation research focused on exploring heterogeneous reactions on semiconductor surfaces.

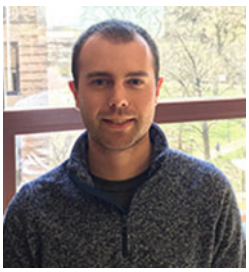

Mitchell Lancaster obtained his B.S. in Chemistry from the University of Minnesota before pursuing a Ph.D. in chemistry under the supervision of Professor Stephen Maldonado at the University of Michigan. His current research interests include investigation of charge transfer processes at semiconductor/electrolyte interfaces, low-temperature semiconductor electrodeposition, and stabilization of photoelectrodes for photoelectrochemical energy conversion.

Molly MacInnes obtained her B.A. in chemistry from Oberlin College in 2013. She then held a DAAD fellowship at BASF in Ludwigshafen, Germany, in 2014 where she synthesized new cross-linking hole transport materials for organic photovoltaics. She is currently completing her Ph.D. in chemistry as an NSF Graduate Research Fellow at the University of Michigan under the supervision of Professor Nicolai Lehnert and Professor Stephen Maldonado. Her research involves grafting molecular electrocatalysts to electrode and semiconductor surfaces.

Robert Vasquez obtained his B.S. in Chemistry from San Diego State University. He is currently a Ph.D. candidate in the Chemistry program at the University of Michigan in the Maldonado lab, where he was awarded the Rackham Merit Fellowship and the NSF Graduate Research Fellowship. His current researching involves the covalent passivation of redox couples on Group IV and III-V semiconductors to study charge transfer at dye-sensitized solar cell photocathodes.

Stephen Maldonado received his PhD from the University of Texas at Austin in 2006, studying advanced carbon electrode materials. From 2006–2008, he was a postdoc at Caltech, researching sensors, and semiconductor heterojunctions. Since 2008, he has been a Professor of Chemistry at the University of Michigan, working on the frontiers of semiconductor electrochemistry, solar energy, and electrodeposition.